DESIGN AND OPTIMIZATION OF A PLANAR CABLE ROBOT

by

Mohamad Hassan Kassem

A Thesis Presented to the Faculty of the
American University of Sharjah
College of Engineering
in Partial Fulfillment
of the Requirements
for the Degree of

Master of Science in
Mechatronics Engineering

Sharjah, United Arab Emirates

July 2020

## Declaration of Authorship

I declare that this thesis is my own work and, to the best of my knowledge and belief, it does not contain material published or written by a third party, except where permission has been obtained and/or appropriately cited through full and accurate referencing.

Signature ………Mohamad Kassem………………….

Date………………………26/07/2020….……………………………

**Approval Signatures**

We, the undersigned, approve the Master's Thesis of Mohamad Hassan Kassem

Thesis Title: Design and Optimization of a Planar Cable Robot

Date of Defense: 13-Jul-2020

| Name, Title and Affiliation | Signature |
|---|---|
| Dr. Lotfi Romdhane<br>Professor, Department of Mechanical Engineering<br>Thesis Advisor | |
| Dr. Mohammad Jaradat<br>Professor, Department of Mechanical Engineering<br>Thesis Co-Advisor | |
| Dr. Shayok Mukhopadhyay<br>Assistant Professor, Department of Electrical Engineering<br>Thesis Committee Member | |
| Dr. Bassam Abu-Nabah<br>Associate Professor, Department of Mechanical Engineering<br>Thesis Committee Member | |
| Dr. Mohamad Jaradat<br>Coordinator<br>Mechatronics Graduate Program | |
| Dr. Lotfi Romdhane<br>Associate Dean for Graduate Studies and Research<br>College of Engineering | |
| Dr. Sirin Tekinay<br>Dean<br>College of Engineering | |
| Dr. Mohamed El-Tarhuni<br>Vice Provost for Graduate Studies<br>Office of Graduate Studies | |

## Acknowledgement

Firstly, I would like to express my sincere gratitude to my advisors Dr. Lotfi Romdhane and Dr. Mohammad Jaradat for encouragement and guidance throughout each stage of this thesis. Their guidance, profound discussions and suggestions, sound analysis, and continuous assessments of my progress made all this possible.

I also feel obliged to extend my acknowledgment to every professor and member of the engineering department including lab assistants for their dedication and honest aid in every course taken.

And finally, a special thank you goes to Al Ghurair Foundation for Education, which is the main reason I was able to join the program. As a recipient of their fully funded scholarship, I feel deeply honored to be part of their community and their success story which brought me closer to my goals in life.

# Dedication

*I dedicate this achievement to my role model Mrs. Melek El Nimer and my beloved mother. I am greatly indebted to their tremendous support. Coming from humble beginnings, I never imagined I would be here today, pushing through another challenge, without their presence in my life.*

*Mrs. Melek: I know that there is no way to repay what you have done for all of us, but I know in my heart that our success is all you ask for, and for that, I will keep making you proud every step of the way.*

*Family in the UAE: You are my pillars and an example of passion and care.*

*Friends: Having you in my life made everything easier, I appreciate your mere presence.*

# Abstract

This thesis presents a new approach towards the design of Cable-Driven-Parallel Robots (CDPR). Typically, the design of such robots is not the main concern, whereas in this work, an optimization of the design is carried out to minimize the consumed energy during a given task. First, a simulation of a simple design, using a software called CASPR, is performed to serve as a validation of the developed model. This latter is then used in the optimization algorithm, where the objective function is the sum of the maximum tensions during the performance of the task. The primary goal is to determine the best design that requires the minimum resultant tensions in the cables while the end effector is following a random trajectory within the achievable workspace. The optimization algorithm aims at minimizing the objective function, based on the validated model, under constraints. The algorithm is implemented under Matlab. The positions of the centers of the different pulleys are the main variables of this problem. The optimum locations of the pulleys are the main results of the algorithm. To further validate the model, an experimental setup was built to test the CDDR to follow a simple trajectory. Preliminary experimental results were obtained showing the motion of the end-effector along the desired trajectory. Different tools were used to conduct the optimization and the results were compared. It is concluded that the obtained design is the best in minimizing the required tensions, for the selected tasks.

**Search Terms:** Cable-Direct-Driven Robot, CASPR, Optimization, Inverse kinematics

# Table of Contents

# List of Figures

## List of Tables

# List of Abbreviations

| | |
|------|------|
| 3-D | 3 Dimensional |
| CASPR | Cable-robot Analysis and Simulation Platform for Research |
| CDDR | Cable-Direct-Driven Robot |
| CDPR | Cable-Driven-Parallel Robots |
| DOF | Degree of Freedom |
| FAST | Five-hundred meters Aperture Spherical Telescope |
| WFW | Wrench Feasible Workspace |

# Chapter 1. Introduction

## 1.1. Overview

Mechanical systems such as parallel manipulators use a series of controlled links connected in parallel to an end-effector or a single platform which moves in a translational or rotary motion, also known as Degrees of Freedom (DOF). Cable-direct-driven robots (CDDRs) are one type of parallel manipulators. CDDRs are represented by an end-effector with a predefined configuration supported by n cables in parallel connected to n motors imposing tension through the cables on the end-effector to move it following a certain trajectory and maintaining a certain pose. There are several advantages to using parallel robots instead of serial robots, in addition, CDDRs are characterized by lower mass and lower stiffness compared to other parallel robots. On the other hand, CDDRs explicitly have workspace limitation resulting from the fact that the suspended robot is based on actuated cables. Nonetheless, the workspace is still considered to be larger than other serial robots such as cranes. Another limitation is the redundancy in the number of actuators compared to the number of DOFs such a robot offers. Achieving static equilibrium entails fully constraining the robot, hence creating a positive tension state through each time step in every instance in the cables to maintain this condition without losing control of the robot.

To overcome the fact that cable robots have only one basic structure whereas the cables are symmetric and attached to the edges of the platform, this study focuses on optimizing these attachment point creating a more efficient design.

## 1.2. Thesis objective

The main problem addressed in this thesis was to simulate a 3 DOF cable robot and optimize the attachment points of the pulleys on the main platform within a specified region. Such optimization aims to reduce the summations of all the tensions exerted by each cable for a particular trajectory. Then, a combined trajectory was created and compared with the default configuration, where all the cables are attached to the corner of the platform. Hence a predefined configuration resulted in less cumulative tensions for a given trajectory within the achievable workspace.

Such improvement can be used when a huge load is applied for more complicated trajectories, such as 3-D concrete printing where the goal is to build a

13

certain structure using a CDDR reducing the cost while utilizing a flexible and adaptable robot.

A comprehensive analysis across different configurations was carried out and the results were analyzed to conclude how and when this approach can be utilized.

## 1.3.   Research contribution

Based on the literature review and the best of my knowledge, all studies have been done focusing on one design to achieve a particular outcome. In this study, the focus has been shifted to creating a more agile design capable of minimizing the cost based on the sum of tensions in the cables when the end effector is following a trajectory within the achievable workspace. Hence the contributions can be summarized as follows:

- Comparing designs given an attachment point at the end-effector side and choose the most practical one based on the model
- Comparing results based on different optimization algorithms
- Optimize the attachment points within a specified region at the other end which is the base-frame

## 1.4.   Thesis Organization

The rest of the thesis is organized as follows: Chapter 2 provides a background about CDDR models and configurations studied from different approaches. Moreover, related works to this research are discussed. The method and approach to be used along with the algorithms and designs are discussed in Chapter 3. Chapter 4 presents the experimental setup used to run the CDDR to follow simple trajectories and Chapter 5 demonstrated the results providing a comprehensive analysis and comparisons between different designs and configurations. Finally, Chapter 6 concludes the thesis and outlines future work.

# Chapter 2.  Background and Literature Review

In this Chapter, several applications, ideas, methodologies, and studies are presented. First, most common applications of parallel manipulators are presented in the industrial and the medical field. Then the fundamentals of cable robots through theoretical studies have been demonstrated.

## 2.1.    Cable-Direct-Driven Robot Applications and Background

One of the earliest CDDRs is the Robocrane created by NIST found in [1]. The concept of parallel cable robot is relatively new and NIST experimented for many years to come up with this new concept relying on the Stewart platform like manipulators as shown in Figure 1.
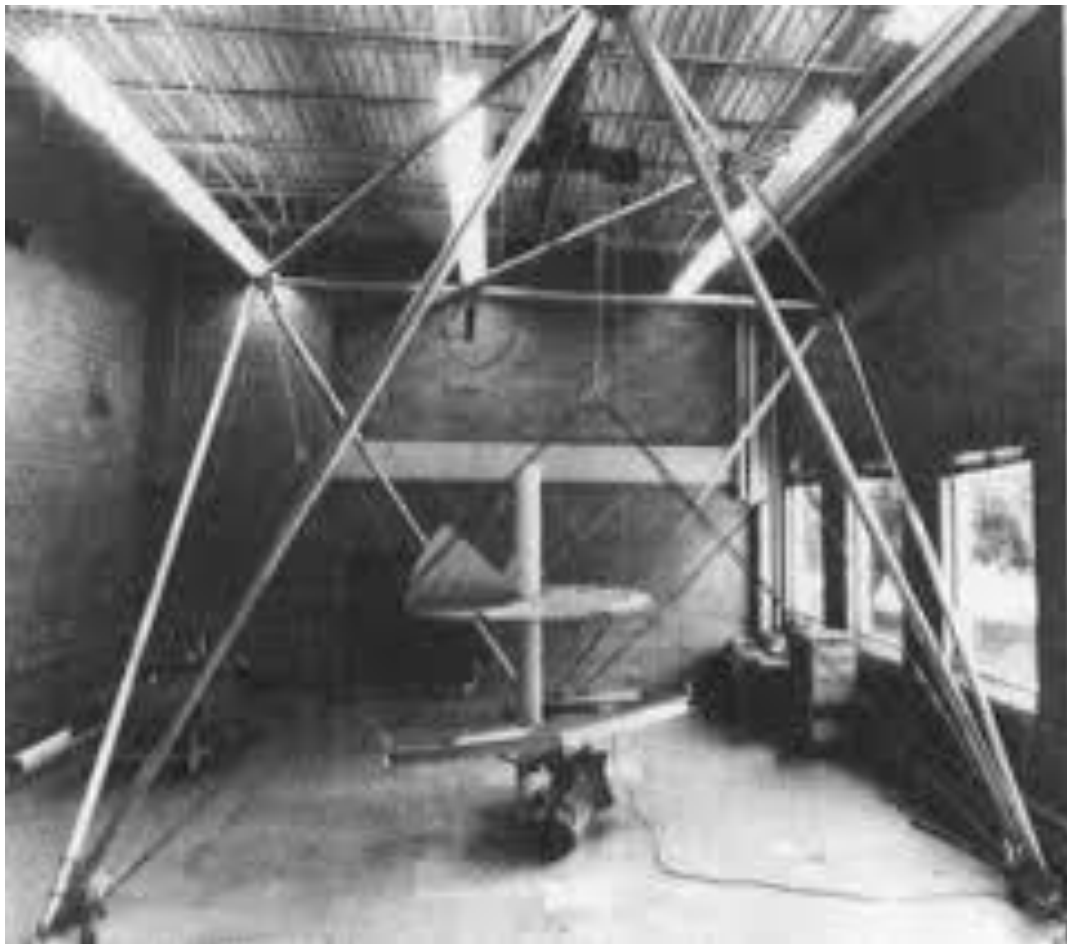


Figure 1. NIST Robocrane [1]

Another application of parallel manipulators and specifically CDDRs is as a flight simulator in the International Space Stations. Over the years, such simulations have improved to accommodate high and low gravity mediums [2].

Numerous applications have been studied and developed since then, for instance, rehabilitation robots in [3] were the fully-constrained robot is used as a gait training system or as lower limb rehabilitation robots [4] shown in Figure 2.
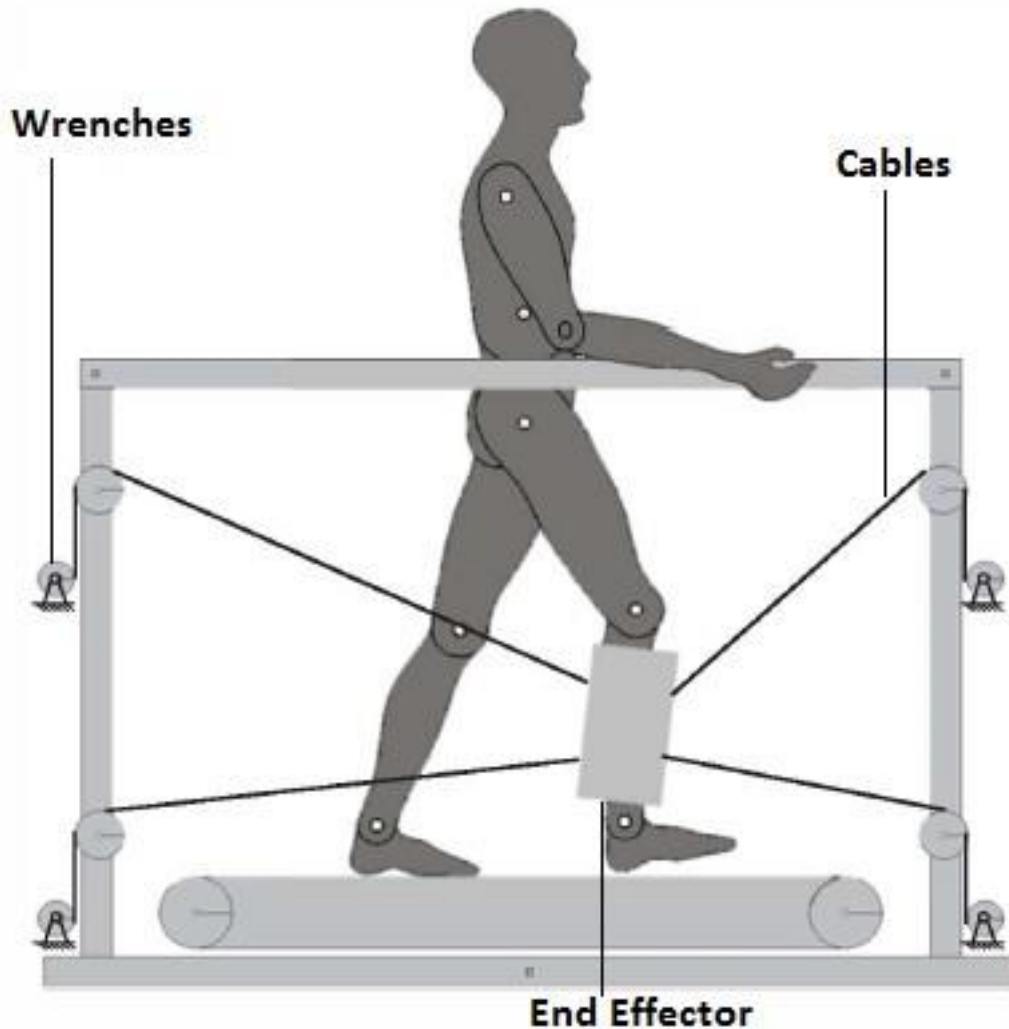


Figure 2. Gait rehabilitation system's diagram [3]

Radio telescopes and observatories have also utilized the concept of cable robots. One of the most known applications is the Five-hundred meters Aperture Spherical Telescope (FAST) [5], which became fully operational, after few years of testing, in January 2020 as shown in Figure 3. The Arecibo observatory shown in Figure 4 is another similar application. Other applications include shock vibration [6], tracking of focus cabin suspension [7] amongst many others.

Figure 3. FAST telescope [5]



Figure 4. Arecibo Observatory [5]

Other applications include Skycam [8] as shown in Figure 5, which is mainly used to record sports events carried out in a big field, and flight simulators [2] based on a large scale motion platforms as shown in Figure 6.



Figure 5. Skycam used in a sports field [8]
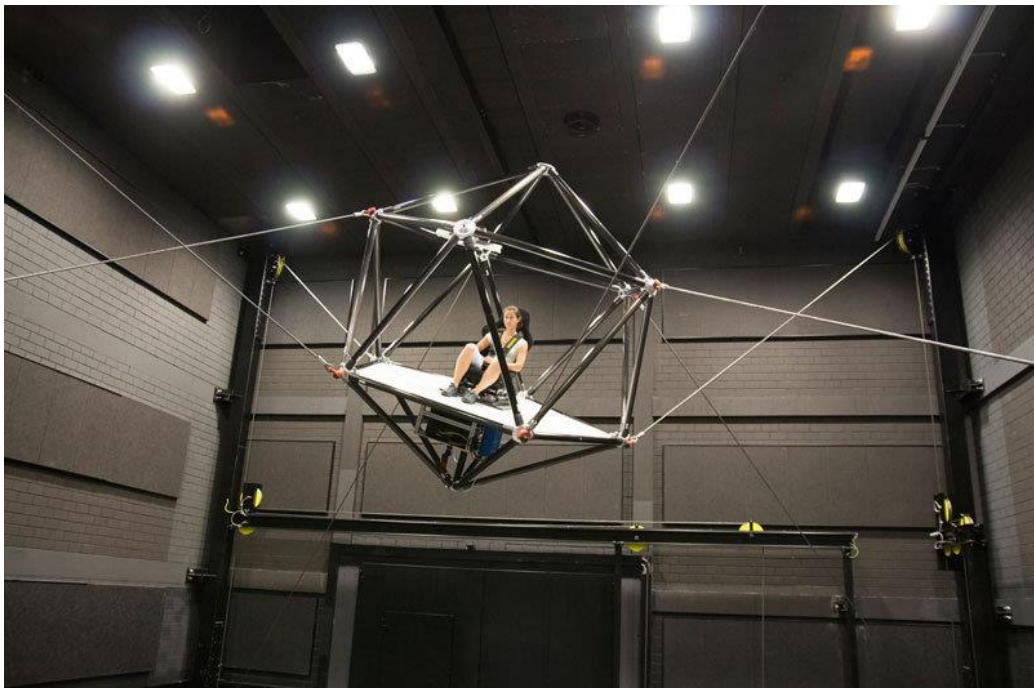


Figure 6. MPI flight simulator [9]

A more recent application of cable robots is 3-D printing, also called additive manufacturing, where a nozzle is attached to the end-effector, which is the feed mechanism supported by cables for positioning and control. Such application is still in its infancy. Figure 7 shows a 3-D printing mechanism based on a 6 DOF cable robot [10].
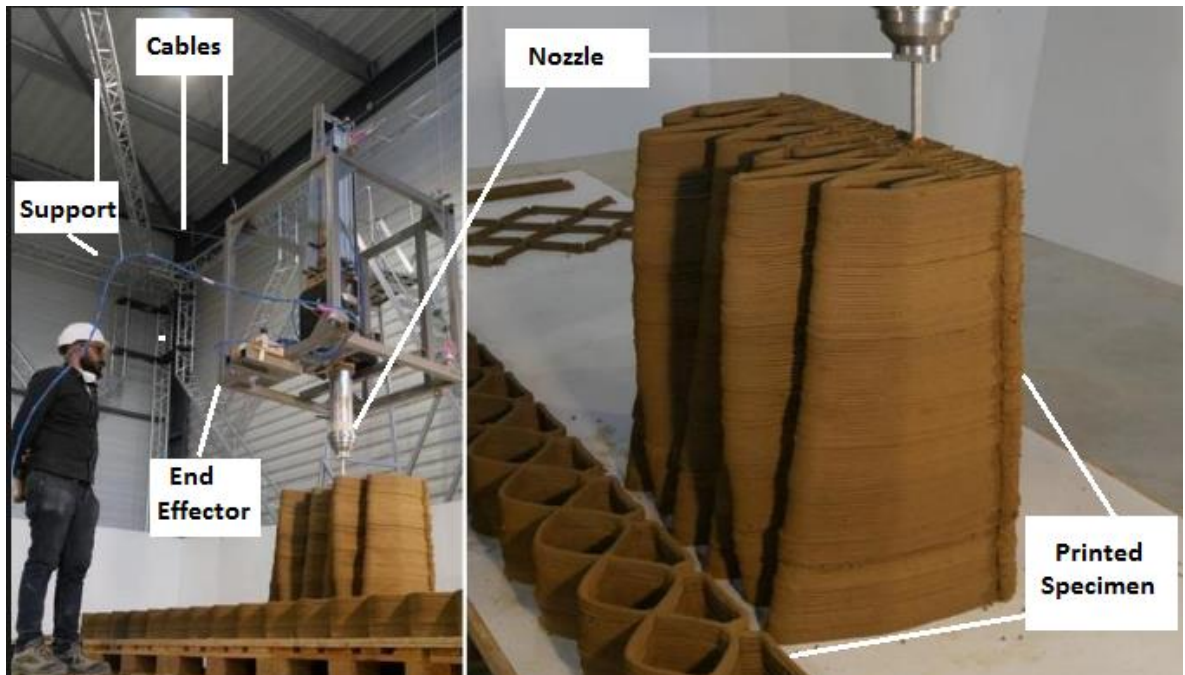


Figure 7. Additive manufacturing by Cogiro and Pylos using a 6 DOF CDDR [10]

## 2.2. Literature Review

Several researches have studied and discussed many aspects of the problem of cable robots. Researches focused on 3 main aspects of the problem. First, some studies targeted the workspace analysis, the authors of [11] established a relationship between the boundary of the workspace and the cable configurations of such robots and they solved the related optimization and motion planning problems. With valid configurations, the conditions were analyzed and the relationship involving the cable configuration, the workspace, and its motion state was established. Other researches focused on the wrench-feasible workspace (WFW). The authors of [12] use the net wrench set, which is the set of all wrenches that a cable robot can apply to its surrounding without violating tension limits in the cables, to calculate the boundaries of the WFW based on the geometric properties of the wrench set.

Other researches targeted the configuration and design analysis of CDPR [13]–[15]. These studies focused on the design criteria to model a climbing robot based on a CDPR. The authors of [13] presented a planar under-actuated cable-driven micro–macro robot. A hybrid system, which consists of two serial manipulators and a CDPR, was designed. Due to this combination, they focused on the design approach where these cables are configured in a way such that they avoid interference. The serial arm allows us to reach points close to the obstacles that would not be reachable by the cable robot alone due to cable–obstacle interference.

On the other hand, more researches focused on the modeling and mainly on the control part [4], [7], [13], [16]–[18]. In [5] the authors carried out a comprehensive comparison between a Five-Hundred Meter Aperture Spherical Radio Telescope FAST and the Arecibo observatory, which is meant to help astronomers in their scientific process, due to the controllability of the position of the CDPR with high accuracy. The dynamic and kinematic models of 6 cables translational CDPR were derived in [19]. The robust sliding mode control was utilized to control the translational CDPR under bounded disturbances. An adaptive control scheme for a cable suspended robot to handle uncertainties in mass and moments of inertia of the end effecter was presented in [20]. The studied controller was entirely independent on the physical specifications of the robot.

**2.2.1. Cable robot design and modeling.** Several researches focus on the modeling and design aspect of cable robots. Some focused mainly on the design as a novel contribution. In [14], a new reconfigurable CDDR has been designed eliminating collision between cables and the surrounding environment. An analytical method for the dynamic trajectory planning is introduced. Another novel design is presented in [21]. A 3 DOF pendulum-like CDDR where an online estimation technique of current pendulum phase is demonstrated. The underactuated robot shown in Figure 8 has been experimentally studied.

Modeling of cable robots is divided into two main parts, static and dynamic modeling. Using Lagrange's equations, the inverse dynamic model of a spatial CDDR was solved in [22]. The 6 DOFs cable robot rescaled from 500 meters to 5 meters based

on the FAST cable robot took other factors as disturbances into consideration, such as cable masses and wind effect on the configuration as shown in Figure 9.
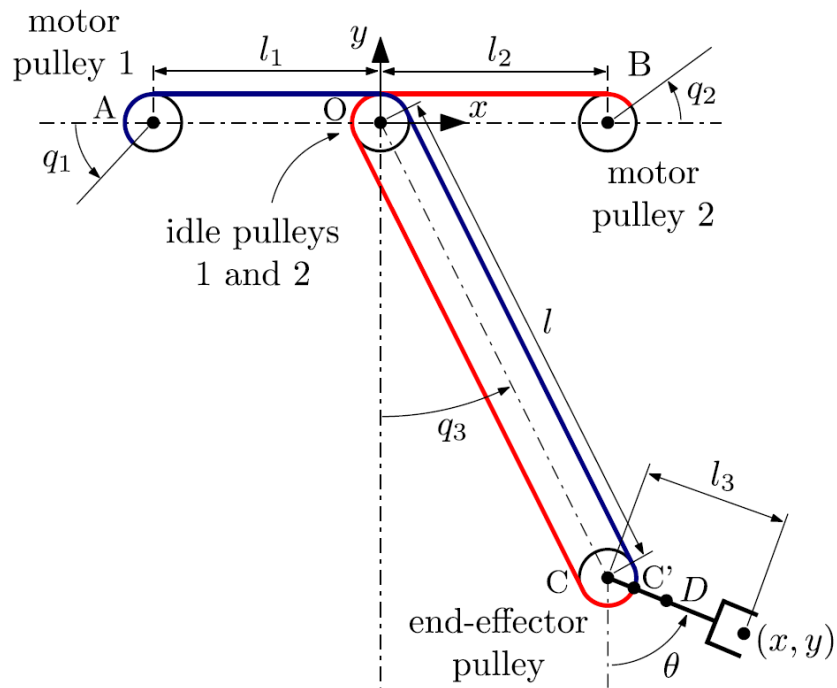


Figure 8. Pendulum-like manipulator kinematic diagram [21]
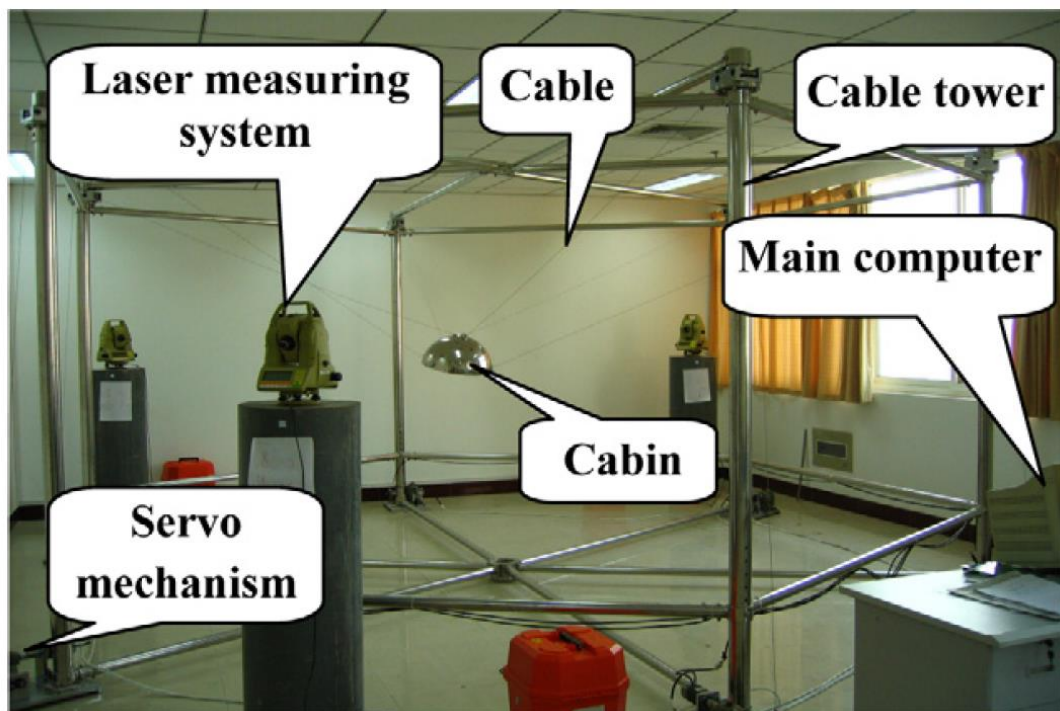


Figure 9. The model of feed support for 5 m FAST [22]

Since the rescaled model is representing the FAST CDDR, designing a hexagonal base-frame with 6 cables to provide the necessary degrees of freedom to control the motion of the end-effector. The number of cables does not determine the degrees of freedom by itself., the model and the configuration has to be taken into consideration.

A more detailed analysis of cable robot design in configuration was targeted in [23]. Three different configurations as shown in Figure 10 were studied. A relationship between the workspace area and the end-effector shape showed that the smaller the end-effector size is compared to that of the workspace, the less effect it will have on the model. In specific, the natural frequency resulted from a small end-effector size is almost negligible in this case.
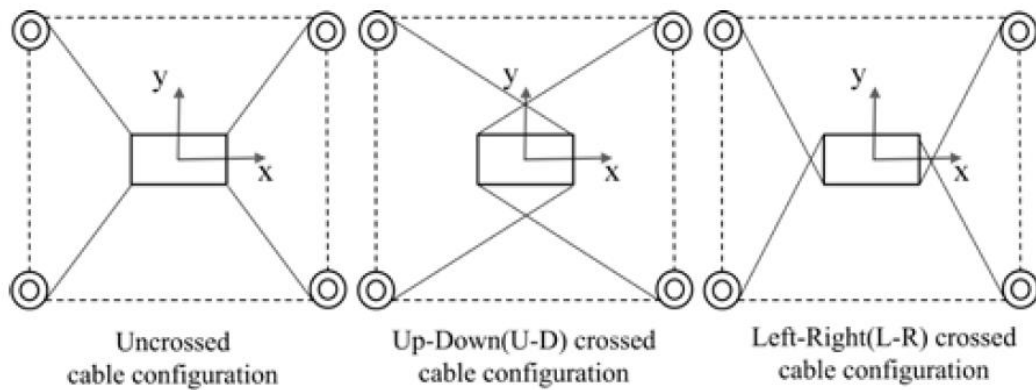


Figure 10. Cable configurations [23]

The modeling of every CDDR depends on the configuration of the robot as a main factor. Depending on the number of cables, their attachment points to the end-effector and the base-frame, the model can then be derived as well as the degrees of freedom can be specified. Figure 11 shows the workspace of the planar cable robot without rotation, in other words, it only has two degrees of freedoms in the x-y plane.

Another study accounted for the mass of the end-effector due to the effect of the gravitational force on the minimum tension exerted by the cables [24]. They proposed a method to calculate the "manipulability indices" to formulate the model of the end-effector.

**2.2.2. Workspace analysis.** Another focus is the workspace of CDDRs. Since the motion of the end-effector is affected by the number of cables, their connection to the base-frame and their overlap within the workspace when a certain trajectory is being achieved, such analysis is crucial to determine the feasible workspace the robot can attain which is not the same as the size of the base-frame. A planar and special CDDRs workspaces were studied in [25]. Furthermore, the workspace can be reduced when the rotational degree of freedom is introduced. Figure 11 shows the workspace when there is no rotation.
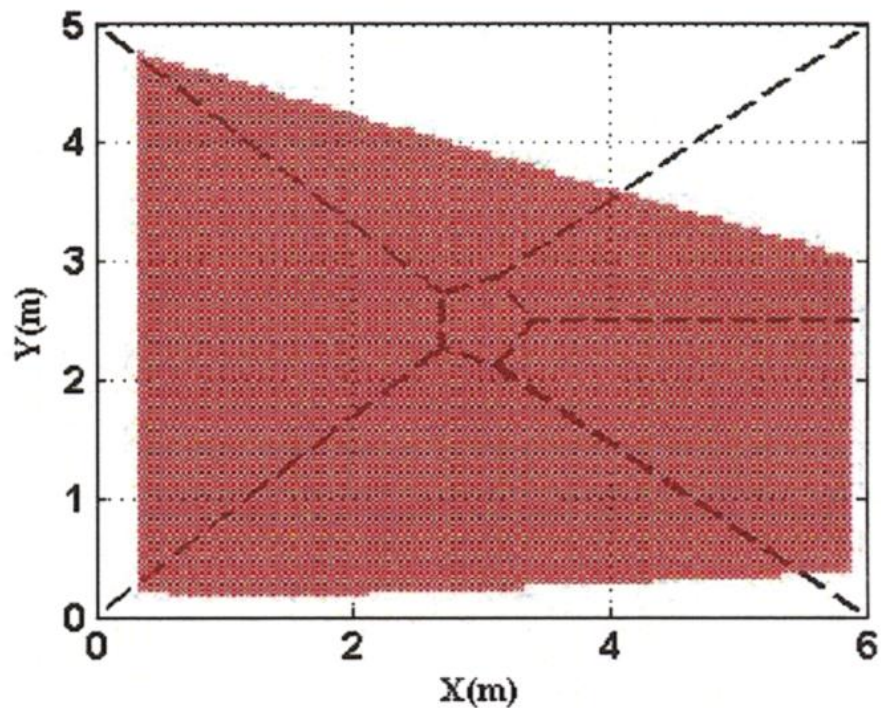


Figure 11. Workspace of a planar CDDR with no rotation [25]

To compare the difference when more DOFs are added, the special robot reduces the workspace within the x-y plane even further. Due to the limitation on the cables' motion when more cables are attached to the base-frame, it can be deduced that there is a direct relationship between the number of cables and their attachment points to the workspace limitations. As demonstrated in Figure 12, the workspace has been reduced when the planar model in Figure 11 became a spatial cable robot.

The workspace can also be influenced by other factors depending on its application. Not all applications require maximum achievable workspace.

Rehabilitation robots for instance have a specific and limited workspace since the motion of the end effector is connected to a human being limb and thus limiting the workspace to a certain region that allows the end effector to move the limb according to a certain motion. In these cases, the achievable workspace is not desired. The planar CDDR used for upper limb rehabilitation presents the workspace limitations clearly[26].
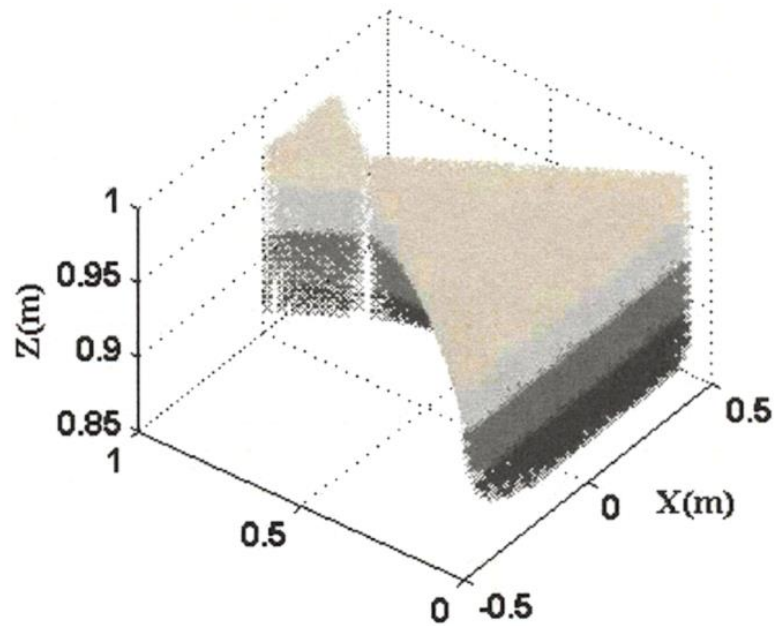


Figure 12. Workspace of a spatial CDDR [25]
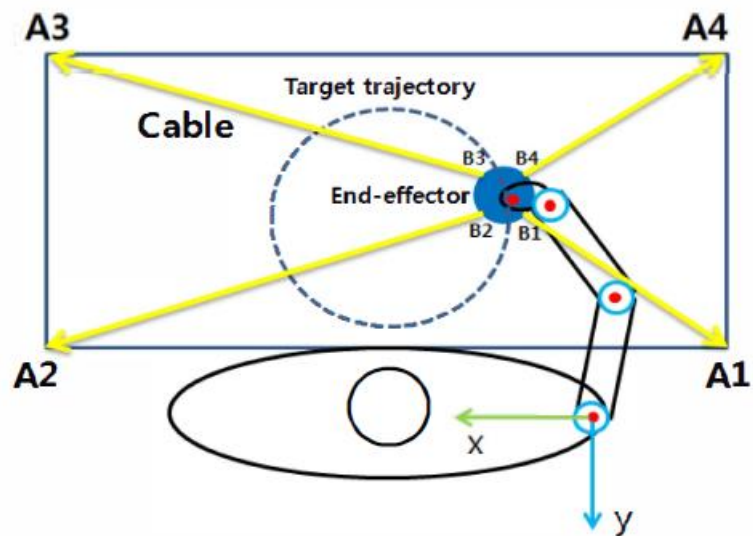


Figure 13. Workspace of upper limb rehabilitation robot [26]

In Figure 13, the workspace is limited to the target trajectory presented by a circle, whereas the Wrench Feasible Workspace (WFW) can extend further, but since the application limit the motion, the limb can only move in the shown target trajectory. A more accurate representation of such limitation can be seen in Figure 14.
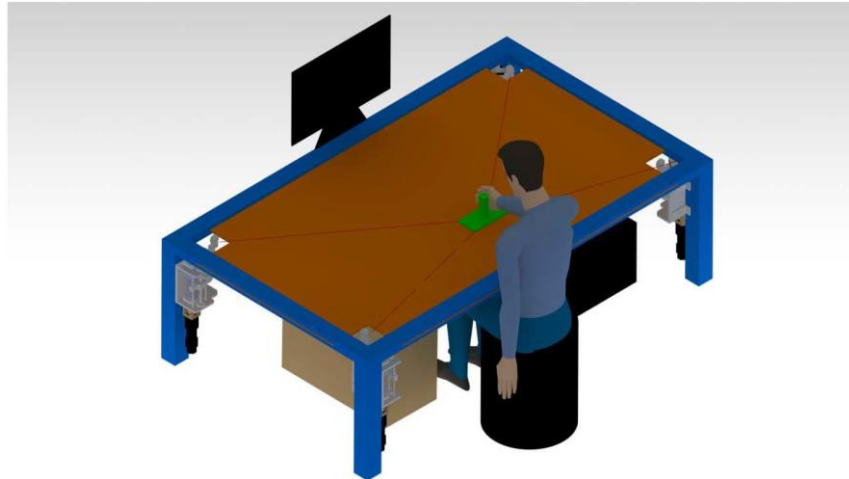


Figure 14. Workspace limitation of rehabilitation robot [26]

There is a big difference between the WFW created by the same number of cables but different degrees of freedom. In [12] the authors used 3 cables to create two different configurations of cable robot. A planar 2 DOF is formed using 3 cables attached as seen in Figure 15.
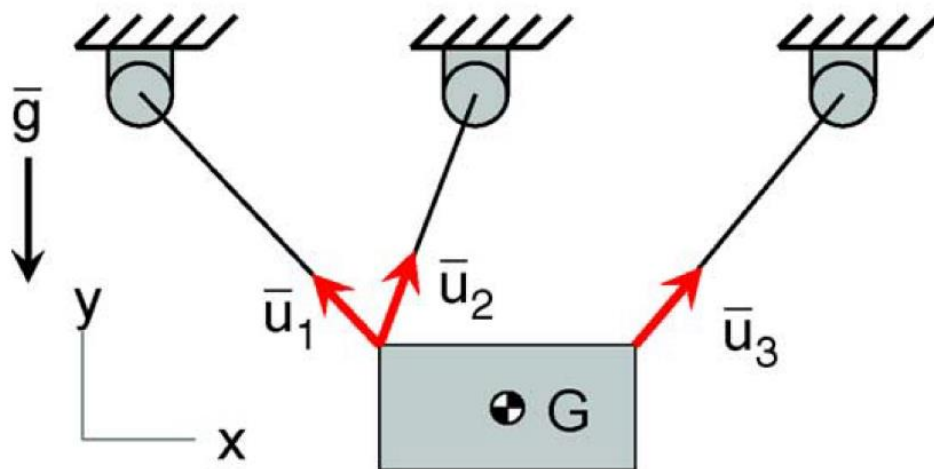


Figure 15. Planar Cable Robot [12]

The three cables are aligned on the upper bar and thus can only produce planar motion in the x-y plane shown in Figure 15. The mass of the end-effector generates a force in the y-axis which has to be encountered by a cumulative tension produced by the three cables to keep the end-effector in equilibrium and control its motion. Since all the cables always must stay in tension, the workspace generated by this configuration is limited.
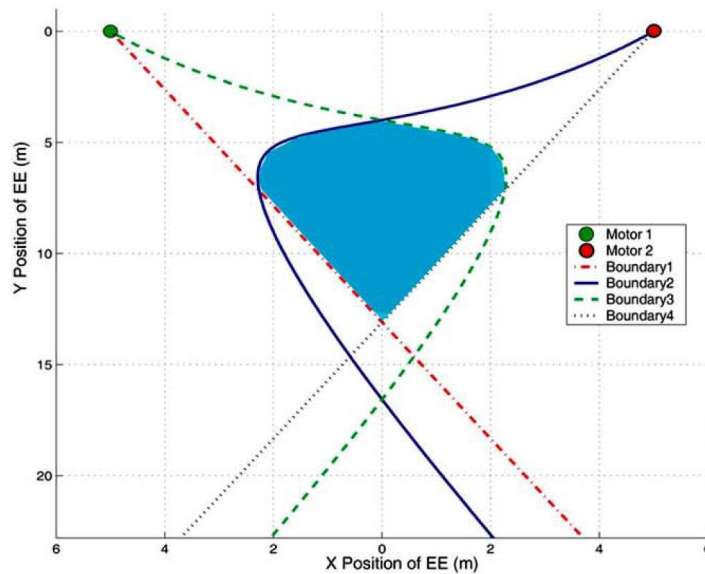


Figure 16. Wrench Feasible Workspace for a planar CDDR [12]

As can be seen in Figure 16, the workspace is very limited compared to Figure 11 which is also a planar CDDR. The main difference between the two is the number of cables, an over-constrained CDDR will have more flexibility and control over the motion and a larger workspace as a result.

Using the same number of cables to move in a spatial environment, the workspace is further reduced due to the under-constrained CDDR created. Such configuration is shown in Figure 17. In this case, the three cables are attached to the same point eliminating the rotational degree of freedom of the end-effector where the workspace is even reduced further.

To determine which configuration allows a more wrench feasible workspace, in addition to the previously studied cases, another study targeted this particular issue [27]. The attachment points at the end-effector side has been varied and the workspace as a

result was presented. The end-effector anchor points and configuration are represented in Figure 18 where *b* which is the distance between two anchor points is the varied parameter.
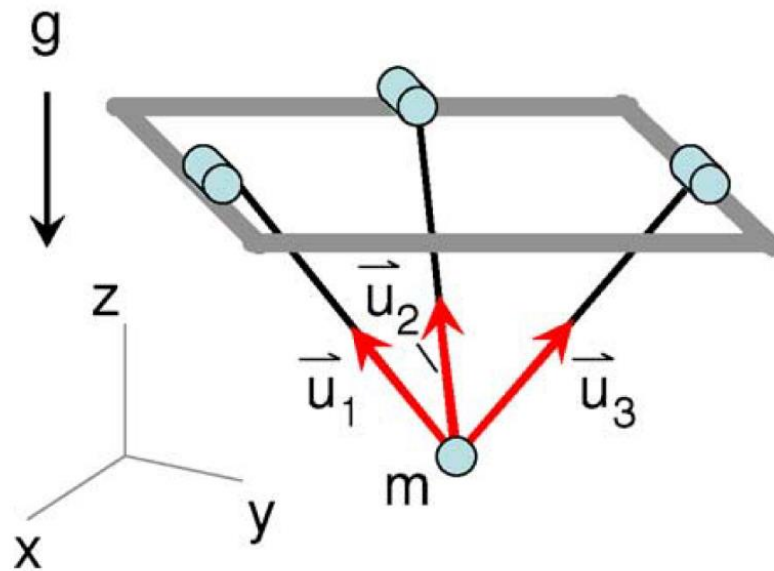


Figure 17. Point-mass CDDR [12]
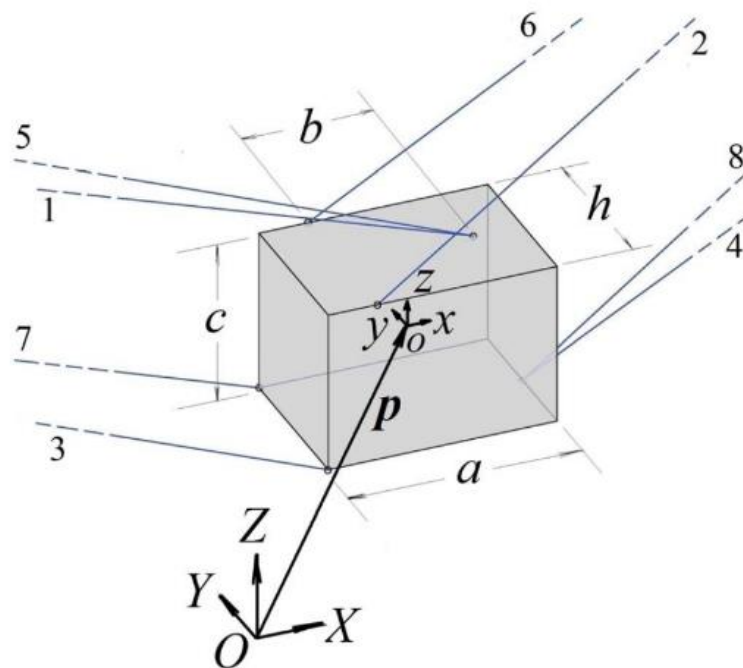


Figure 18. Parameters and anchor points at the end-effector[27]

As shown in Figure 18, $b$ is $-\frac{a}{2}$ where the cables are shown to be in a crossed pattern. When $b$ is positive, the cables are uncrossed and when $b$ is 0, the cables' anchor point have the same ordinate ($y$). The workspace resulting from these configurations are shown in Figure 19.
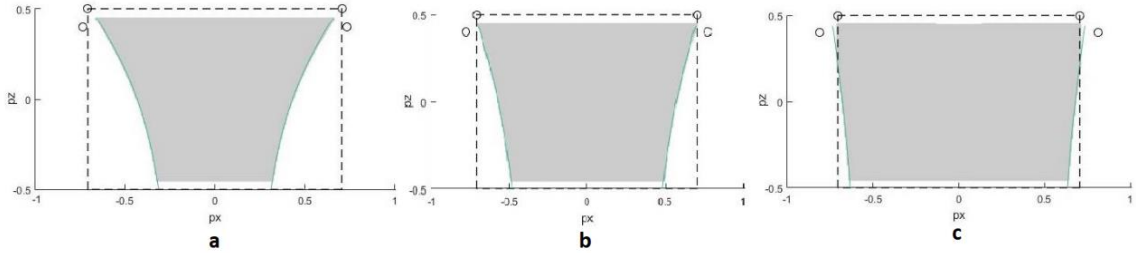


Figure 19. Workspace by varying anchor points based on parameter $b$ [27]

In Figure 19a, the anchor point selection was uncrossed, while in Figure 19b both anchor points had the same ordinate ($y$) where b=0, and in Figure 19c $b$ was $-\frac{a}{2}$ (uncrossed). Clearly, uncrossed configuration offers more flexibility and increases the workspace. For this study, the final optimized model was selected based on these findings to maximize the workspace and the controllability of the robot.

The number of cables can also affect the wrench feasible workspace. Having more cables will not always increase the workspace. Take for examples the two configurations presented in [28]. Two models with 3 DOF each are presented. The under-constrained model with 3 cables showed more flexibility than the over-constrained configuration with 4 cables. Figure 20 shows the WFW respectively. However, depending on the application, each workspace can reach different points while having a common region. This means that it can either be an advantage or a disadvantage. If the application targets a bigger workspace with no consideration of the exact location of the trajectory within the WFW, then 3 cables would be the choice. If however a specific pose is to be reached, then the selection of the configuration depends on the end-effector pose. Two different workspaces for each case is shown. A collision-free area (CFA) in blue and a collision-free force closure workspace (CFFCW) in red.

The CFA is, by definition, greater than the CFFCW since the forces are not taken into consideration. Furthermore, the orientation of the end-effector limits the

workspace even more. The rotation hence is limited and should not increase a certain limit based on the configuration of the end-effector. Having a crossed configuration will add more controllability and increase the maximum angle the CDDR can reach by rotation.
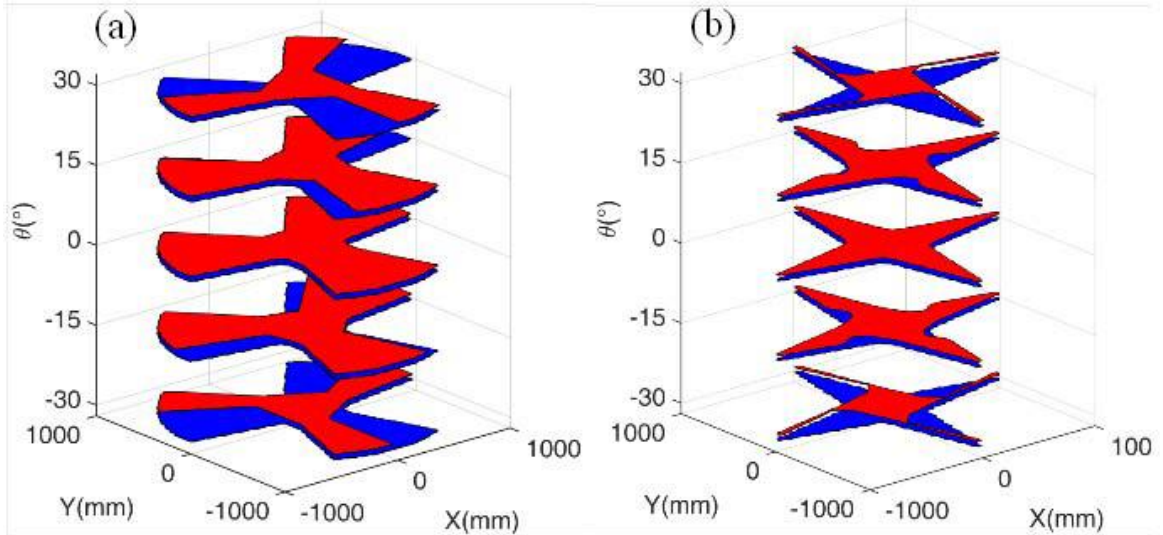


Figure 20. CFA and CFFCW of 3 cables and 4 cables models [28]

Another rehabilitation CDDR is studied in [29]. The workspace analysis is also limited not only to the WFW, but to the motion prescribed of the limb. Since the human shoulder can only move in a certain trajectory, the workspace of the robot is determined accordingly. High speed is also not required for obvious reasons.

**2.2.3. Trajectory and path planning.** CDDRs trajectories can be created using different techniques. A 2-D pendulum like CDDR point-to-point trajectory is investigated in [30]. Algebraic inequalities representing the constraints of the CDDR determine the feasibility of the planned trajectory. In this case, only two cables are attached to the end-effector creating an under-constrained cable robot where the motion is primarily relying on the mass of the end-effector creating opposing force to the tensions in the cables. Unlike over-constrained robots, this motion is approached differently since the suspended cable design can reach beyond the static workspace as shown Figure 21.

The attachment points are fixed on the base-frame. The forces balance on the point mass of the end-effector determine the dynamic model of the robot. Different

types of trajectories can be created, such as circular and cartesian trajectories from one point to another as shown in Figure 21.
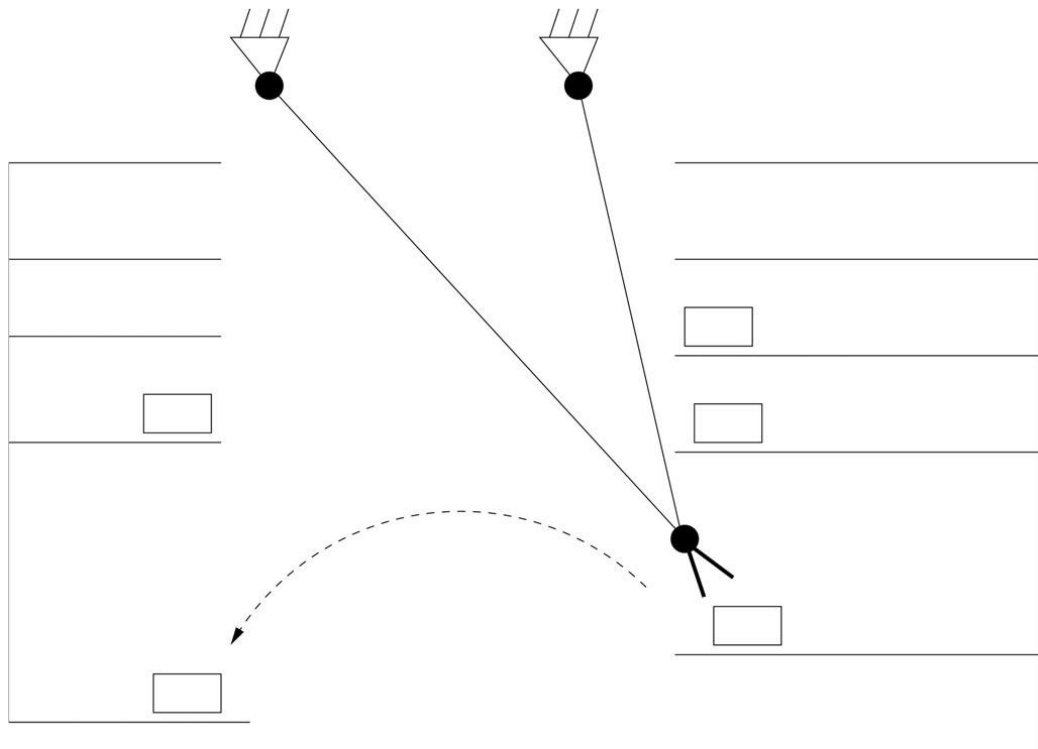


Figure 21. Planar two DOF suspended cable robot [30]

The derivation of the trajectories in Figure 22 and Figure 23 use the trigonometric, and the polynomial formulation of the circular and the point-to-point trajectory planning techniques accordingly. This kind of motion is different to over-constrained configurations since it is highly dependent on the forces balance in the vertical axis affected by the mass of the end-effector.

In an over-constrained configuration where the mass is also affecting the motion, i.e. the motion is in the vertical plane, different cases can be presented depending on the region where the motion is happening. [31] presented the aforementioned case with several regions of the trajectory. When the end-effector is moving inside the region III as shown in Figure 22, the mass of the end-effector should be accounted for since the motion is completely independent of it unlike all the other regions which extend beyond the conventional workspace. The trajectory formulation will vary from one region to another based on the symmetry of the design.
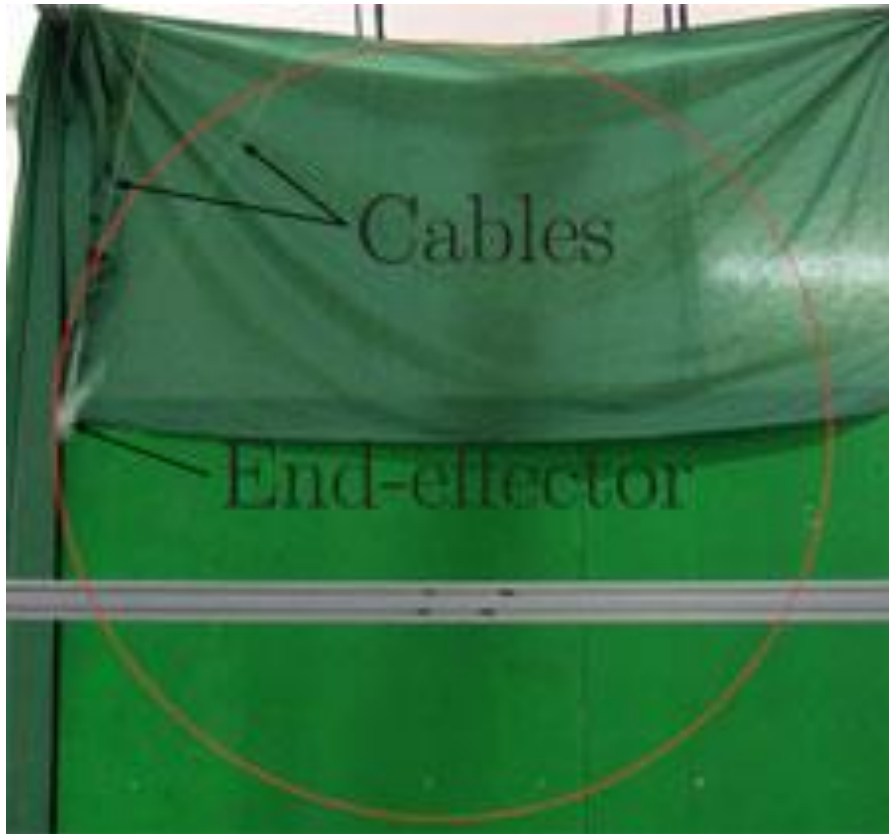
Figure 22. Circular trajectory of 2 DOF suspended CDDR [30]
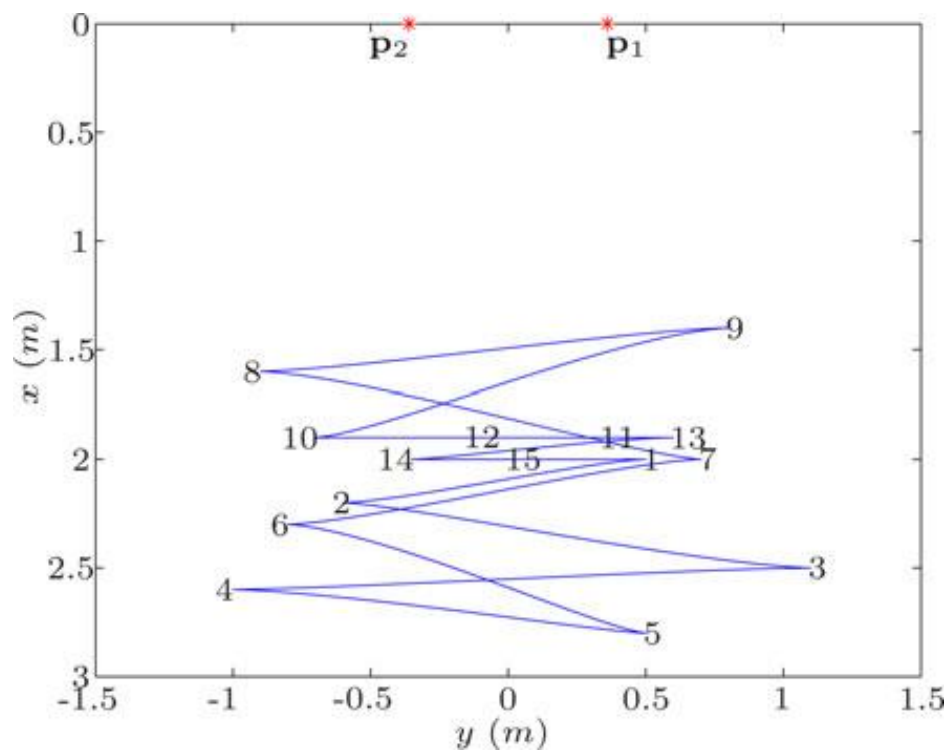


Figure 23. Target points and cartesian trajectory [30]
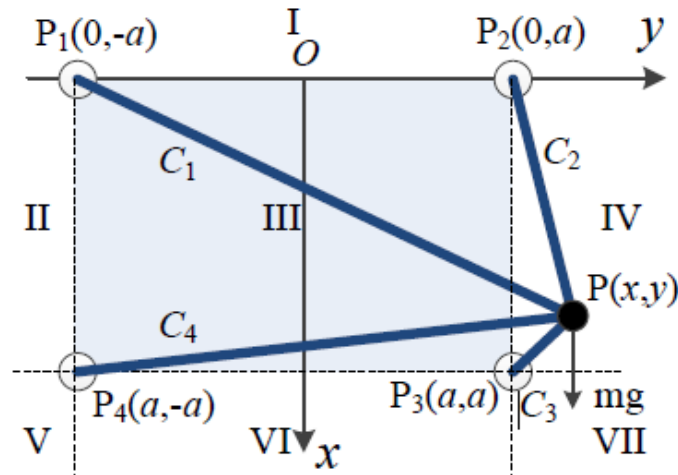
Figure 24. Redundantly actuated CDDR [32]

When the trajectory is outside region III, the case becomes similar to that in [30]. Those regions affect the motion of the end-effector since the mass cannot be disregarded by compensating its equivalent force in the cables' tensions. Thus, formulation of the trajectory becomes relatively similar.

Similar studies have targeted the trajectory planning aspect of the problem [33], [34]. All the studies in this section focused on a pendulum-like CDDR where the mass of the end-effector plays a role in its motion. A Cassino Low-Cost Wire Manipulator (CALOWI) was created in [35]. It is a planar over-constrained CDDR with 3 DOFs and 4 cables which was then used as a spatial model to move the end-effector in the force feasible workspace. The problem of collision-free path planning was investigated. Two path planning concepts were adopted, a depth search mode that is activated when the CDDR is far from the obstacle, and the second is width search mode that is active when the CDDR is near an obstacle which creates the appropriate condition to avoid the obstacle. The mechanism was put under experiment and results were analyzed. No matter how cluttered the environment is, the robot is able to reach the final pose and avoid obstacles but not necessarily following the shortest path. Another 3 DOF spatial CDDR with 3 cables is introduced in [36]. A linear interpolation method was introduced to reach the target point by adding intermediate points in the static workspace of the mechanism. To enhance the performance further, the trajectory was modified using quantic polynomials.

**2.2.4. Control schemes of cable robots**. The control part has been thoroughly studied in many researches. A PD controller was suggested in [37]. A Lyapunov and a feedback linearization-based controller were applied, and the steady state of the cable robot pose was analyzed. Due to the presence of friction, the steady state error existed with a small error, so an integral part was added to compensate for this error. A 3 DOF under-constrained rehabilitation cable robot was controlled using an admittance control approach [4]. Then results were compared with a PID controller. Based on the results, the admittance control was able recover faster to minimize the error unlike the PID controller which took more time when a disturbance is introduced into the system.

An adaptive controller was utilized in [18] to achieve the desired trajectory and obtain the estimated coefficients the planar CDDR using four cable with 2 DOFs. Using this type of controller, the error was reduced by 99% when no controller is used.
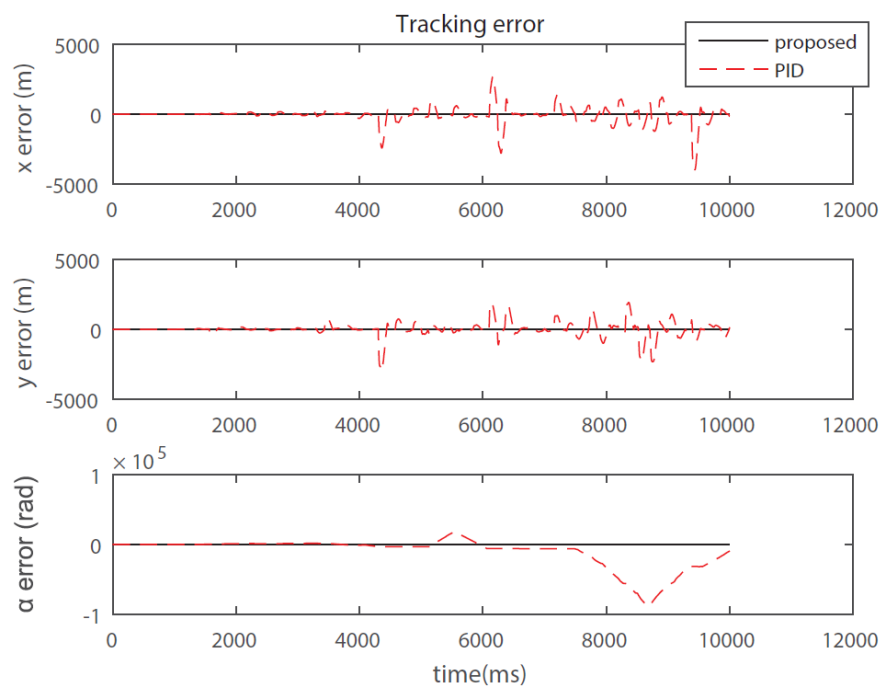


Figure 25. PID (red) vs Sliding mode (black) controllers [38]

Sliding mode controllers were also investigated in [19] and [38]. The tracking error 3 DOF translational cable robot, where the rotation was eliminated, was compared between two cases. One is without disturbances and the other is in the presence of

33

unknown disturbances. Another sliding mode controller was used in [38]. An over-constrained CDDR was modeled with elastic cables. Compared to a PID controller, the proposed sliding mode controller showed promising results reducing the error marginally as shown in Figure 25.

Other researches considered a discrete-time controlled [39] with a redundant 6 DOF cable robot, a vision-based controller [17] was implemented to attain the stability of a planar and a spatial CDDRs when there is and analytical model and experimental setup uncertainties existed. This approach is relatively new and not much research has been done in this field of control. Another application of cable suspended mechanism was introduced in [40]. In this study, cables were attached to packages to be transported from one location to another. It cannot be considered as a conventional CDDR since there is no fixed platform, instead, a drone was used to move the package with a cable attached to it on one end, and to the package on the other. A camera planted on the drone, also called aerial robot, was used to track the location of the package with an unknown mass while minimizing the cable-swing angle. It is similar to the pendulum-like CDDRs presented before but with only one cable and a moving drone instead of the fixed base-frame.

A more complex controller algorithm was investigated in [7]. A Stewart vibration control scheme is adopted which has the advantages of both PI controllers and Fuzzy controllers, such as, robustness, fast dynamic response, small overshoot, stability, and high dynamic tracking.

A Robust control scheme of a three dimensional CDDR was investigated in [41]. The $H_\infty$ controller guarantees the system stability when the trajectory is being tracked. Furthermore, the computational complexity of this particular controller is relatively less exhaustive on the system than most common robust and adaptive controllers. Accounting for the friction and inertia of the cable pulleys' uncertainty, it creates a more practical and applicable model. Three weighting functions are used to track the error, control the input and the output as shown in Figure 26. These weighting functions reduce the overshoot and minimize the settling time of the system.
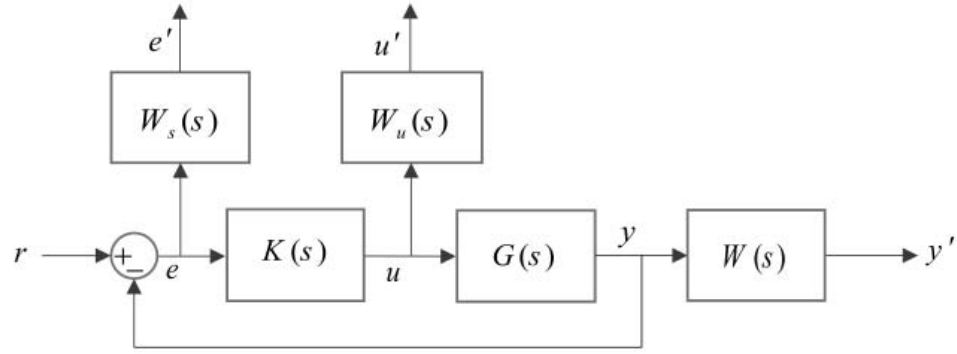
Figure 26. Schematic diagram of the $H_\infty$ controller with weighting functions [41]

A novel passive dynamic control approach targeted the velocity vector field [42] instead of the common time function adopted in most cases. Another study contained two-level controller, High-level and Low-level controllers [43] to track the force input of a bench press rehabilitation robot for astronauts. In [44], an ultrahigh speed CDDR force was controlled using an internal force controller using point-to-point controller with a linear PD scheme to reduce the vibration of the payload.

**2.2.5. Optimization of cable robots and related work.** Several studies focused on optimization of a certain aspect of either the configuration, the workspace, or the tension required to achieve certain trajectory. The optimum configuration is investigated for a redundant planar CDDR with four cables [45]. In this study, three different cases were investigated. An under-constrained CDDR 3 DOF planar CDDR with three cables, a similar over constrained CDDR with 4 cables with crossed configuration and the optimized configuration all shown Figure 27.
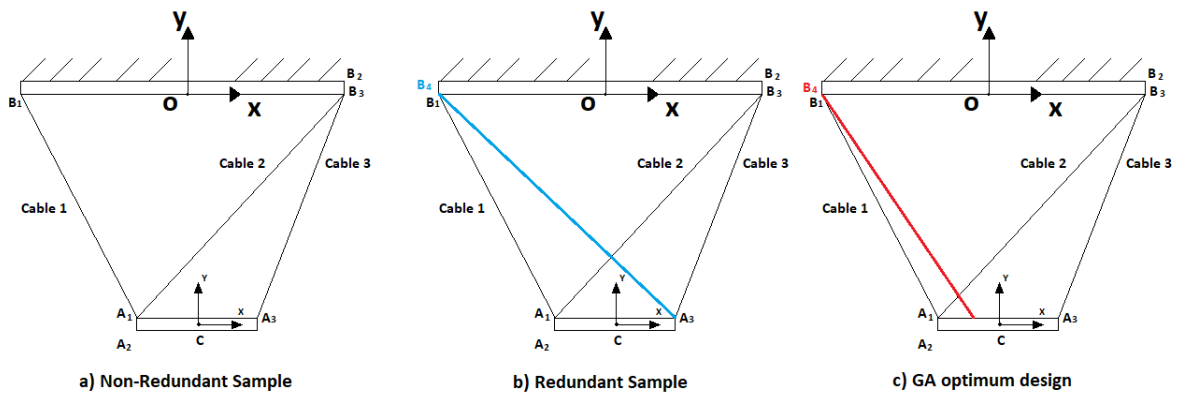


Figure 27. Configurations of planar CDDR [45]

Note that in all the cases, the target is the attachment points at the end-effector and not at the base-frame. The optimized configuration was obtained using two techniques combined together. A Genetic Algorithm, and a Pontryagin minimum principal techniques. Given the path and the cables' tensions and velocities, the results showed that the main advantage the optimized model offered is to reduce the time required to reach the final pose without violating the maximum limit of the velocity. However, the tensions in the cables were not analyzed.

A Dykstra-alternating-algorithm based research [46] was conducted on a CDDR to minimize the forces of individual cables. The minimum -2-norm solution of the actuators' forces is obtained as a projection of convex set being some of the variables in the system. Another interesting case is the mobile platform incorporated with a CDDR [33] where the motion of the end-effector of the CDDR is synchronized with the mobile platform in order to move the end-effector through a certain trajectory. A direct transcription optimization approach was adopted in order to plan the trajectory of the end-effector. The main advantage is the deploy-ability of the robot for a fast pick-and-place mission as needed within a certain area being a factory or a warehouse. Considering the obstacles in such environment, the paths produced to reach the target pose are obtained using the optimization approach mentioned above. The error between the actual and desired moving platform in a 3-D environment was presented and it was 20 mm compared to the 8 meters span of the trajectory which is around 0.25%. An optimal balancing problem of an under-constrained CDDR with two cables is derived in [47].

A given performance index is minimized using the Hamiltonian function in order to obtain the optimality conditions as differentiated values of the system variables, such as position and cable lengths. In Figure 28, one of the pulleys torques is compared between three different models, unbalanced, static balanced and the optimally balanced model. Results show that the response and the value of the torque was minimized using the optimally balanced model. Furthermore, the velocity profiles were also analyzed, and the optimized model reached the final pose with a more stable response.

A redundantly actuated CDDR with 8 cables and 6 DOFs was investigated in [48]. The optimum configuration at the end-effector was targeted, in other words, what

are the optimum attachment points that will give the minimum force required to reach the final pose of the end-effector. Four different configuration schemes were simulated, and experimental setup was designed to verify the results. Compared to previous presented work, the results show a similar pattern. Having a crossed configuration lead to a more stable motion and controllability of the motion. A spiral trajectory was created under MATLAB within the WFW. The kinematic and the dynamic model of the CDDR was derived.

Based on the aforementioned studies, the optimization of the attachment points at the base-frame was not targeted. The attachment points at the end-effector side for this study were chosen to be crossed due to all the advantages presented before. The optimization however focused on the base-frame attachment points.
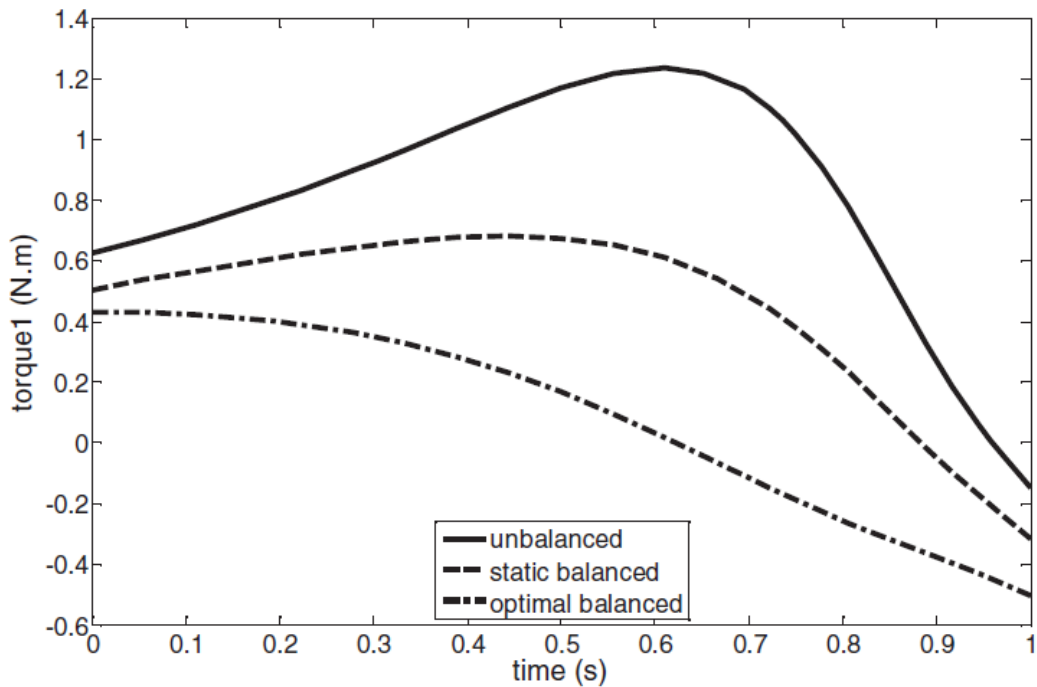


Figure 28. Torque of pulley 1 [47]

## 2.3. Optimization Toolbox under MATLAB

MATLAB provides a variety of ready-to-use optimization algorithms. In this study, the *fmincon* function will be used with the default algorithm.

The available optimization algorithms under MATLAB Optimization Toolbox [49] are:

1. *Fmincon* algorithms
2. *Fsolve* algorithms
3. *Fmincun* algorithms
4. *Lease Square* algorithms (*lsqnonlin, lsqlin,* etc…)
5. *Linear Programming* algorithms (*linprog* )
6. *Quadratic Programming* algorithms (*quadprog*)

There are other few algorithms but these are the most common ones.

**2.3.1. Fmincon algorithm.** It is a General smooth constraint type algorithm. The objective type could be linear, quadratic, least square and smooth linear. The available algorithms fmincon can utilize are as follows:

- 'interior-point'
- 'trust-region-reflective'
- 'sqp'
- 'sqp-legacy'
- 'active-set'

The default algorithm is 'interior-point'. This algorithm is recommended because it can handle sparse and wide range of problems as well as the small and dense variety. All the bounds are satisfied at all iterations and are recoverable from Nan or Inf results. All the other algorithms are designed for more complicated problems. The *fmincon* is used with a nonlinear constraint, or with a general nonlinear objective and at least one constraint and finds the minimum of a problem specified by:

$$
\min_x f(x) \; such \; that \begin{cases} c(x) \leq 0 \\ ceq(x) = 0 \\ A.x \leq b \\ Aeq.x = beq \\ lb \leq x \leq ub, \end{cases} \tag{1}
$$

A simple example of how *fmincon* is used where some constraints are integrated into the algorithm can be found in [50]. The Rosenbrock's function was used in this example. The problem is stated as follow: Find the minimum value of Rosenbrock's function when there is a linear inequality constraint. The objective function is based on the minimum objective value of 0 at the point (1,1). The function as stated in [50] is:

$$fun\ =\ @(x)100 \times (x(2) - x(1)^2)^2\ +\ \left(1 - x(1)\right)^2; \tag{2}$$

To find the minimum value starting from [-1,-2], constrained to have $x(1) + 2x(2) \leq 1$. Express this constraint in the form Ax <= b by taking A = [1,2] and b = 1. Notice that this constraint means that the solution will not be at the unconstrained solution (1,1), because at that point $x(1) + 2x(2) = 3 > 1$. The command to find the minimum is as following:

```
x0 = [-1,2];
A = [1,2];
b = 1;
x = fmincon(fun,x0,A,b)
```

This will calculate the local minimum that satisfies the above constraint of the function which is:

$x\ =\ 1 \times 2$

  0.5022  0.2489

**2.3.2.  Other algorithms.** The rest of the algorithms are used for a variety of problems, whether linear or non-linear, with or without bounds or constraints, depending on the problem and the objective function being used. A comparison between the results of 3 algorithms will be shown in Chapter 5.

# Chapter 3.  Methodology

Even though optimization of CDDRs has been targeted by few researches, none of them focused on the attachment point of the cables to the base-frame. In this thesis, this aspect will be the main objective where the forces are minimized for several trajectories, hence saving energy.

This chapter will demonstrate the problem of cable robots and solve its general model, followed by specific models investigated, then using a comprehensive Cable-Robot Analysis and Simulation Platform for the Research (CASPR) [51]  which is an open source platform, the simulation of the unoptimized models will be carried out as a preliminary results. Based on CASPR simulation and previous studies, the final model for optimization will be selected and implemented under MATLAB to be optimized.

## 3.1.    Problem Formulation

The problem can be divided into the following parts, design, modeling and simulation. In the design part, the number of cables, in order to produce the desired trajectories to be followed within the required workspace, is determined along with the dimensions and the geometry of the base-frame and the end effector where the attachment point of the cables to both sides is determined. After that, based on the desired degrees of freedom, the kinematic and the dynamic models of the system are solved. After acquiring the necessary formulations, the simulation of the system can be carried out in two steps. The first one uses CASPR for basic trajectories of an unoptimized cable model, and the second one derives and codes the equations and implement the optimization algorithms to achieve the best design. Note that several algorithms were used at first, then a comparison of the results between the algorithms was carried out in order to determine which algorithm is most efficient. After that, within the selected algorithms, the options including the sub-algorithm were selected based on the results where a comparison when changing them took place.

 First the general case [52] is shown in Figure 29, where there are $n$ cables attached to a fixed base-frame. Typically, all the cables are actuated.
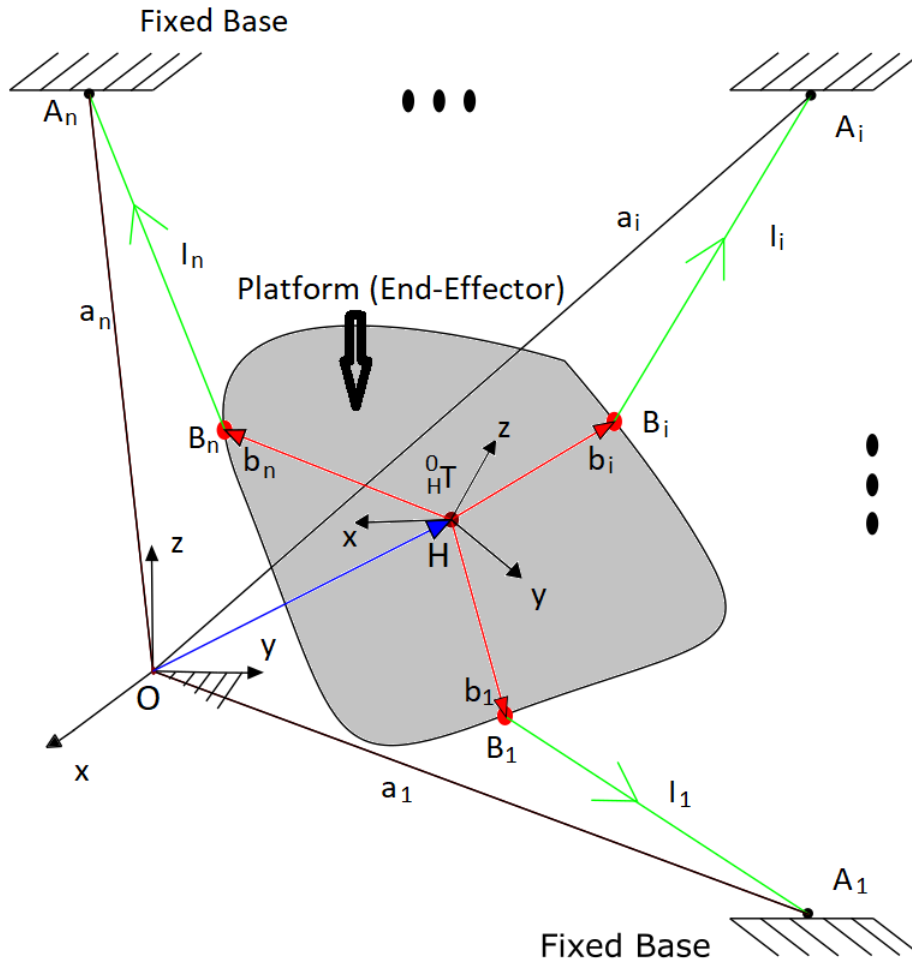
Figure 29. Kinematic schematic diagram of a general CDDR

## 3.2.   CDDR Configurations

In this study, selected models have been analyzed and simulated. The first two models are planar CDDRs, one using 3 cables with 2 DOFs shown in Figure 30 and the other uses 4 uncrossed cables as shown in Figure 31 . Then the optimized model will have the same number of cables as in Figure 32 but the cable configuration is crossed. Figure 30 shows the configuration of the first CDDR.

Since the cables can only exert tension, the number of cables needed to control an $n$ DOF CDDR is $n + 1$ creating a one degree of actuation redundancy. Thus, for the case where 3 cables are used, two DOFs can be achieved given as $X = \{x\ y\}^T$. The origin of the base-frame (global origin) {O} for all the cases is centered in the middle of the platform. The coordinates of the end-effector are represented with respect to the

global origin in all the models. The attachment point of the cables to the base-frame are fixed to the corners of the platform and called $A_i = \{A_{ix}\ A_{iy}\}^T$.
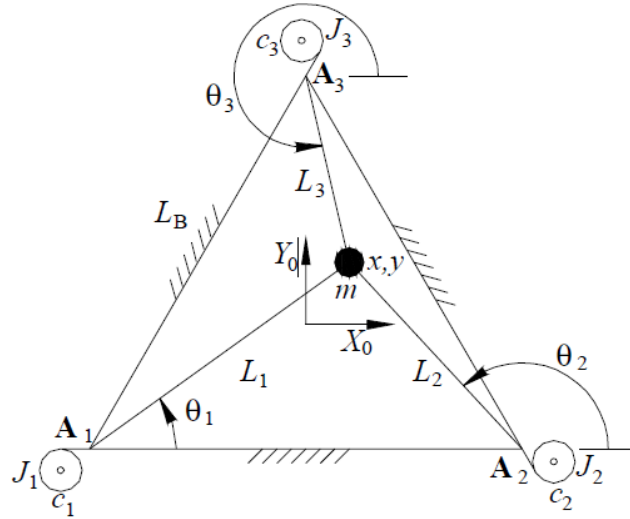


Figure 30. Planar 2 DOF CDDR with 3 cables [53]

$L_i$ is the $i^{th}$ cable length where the corresponding angle of each cable is $\theta_i$. The rotational inertias for each motor is $J_i$ $(i = 1, ..., n)$ and the mass of the end effector is $m$. Ideally, the end-effector can reach any point within the workspace. However, the limitations due to the size of the end effector, the pulley locations and the cable interferences, limit the size of the workspace. However, for the case in Figure 30, there is no cable interference and the reduction can happen based on the size of the end-effector. Since a point-mass is being considered, the maximum workspace can be achieved representing the area between the attachment points to the base-frame creating a triangle. This applies for all the models investigated in this study. Figure 31 shows the configuration of the second model to be simulated in CASPR.

The final model is the main target of this study. Figure 32 shows the crossed-cables configuration to be investigated. This model will be simulated using MATLAB with the optimization toolbox and not CASPR. In this case, the attachment points at $A_i = \{A_{ix}\ A_{iy}\}^T$ are not fixed. In this particular case, $i = 1,2,3,4$ and $n = 1,2,3,4$. The region in which they are being optimized will be shown later. The third DOF is the rotation of the end-effector $\Phi$ around the vertical z-axis with respect to the horizontal axis.

42
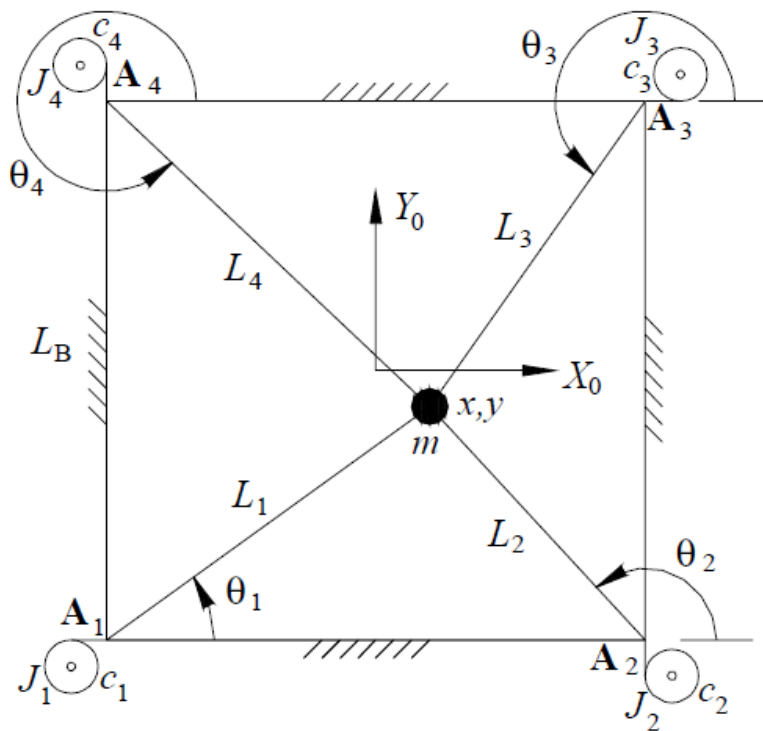
Figure 31. Planar 2 DOF CDDR with 4 cables (uncrossed) [53]
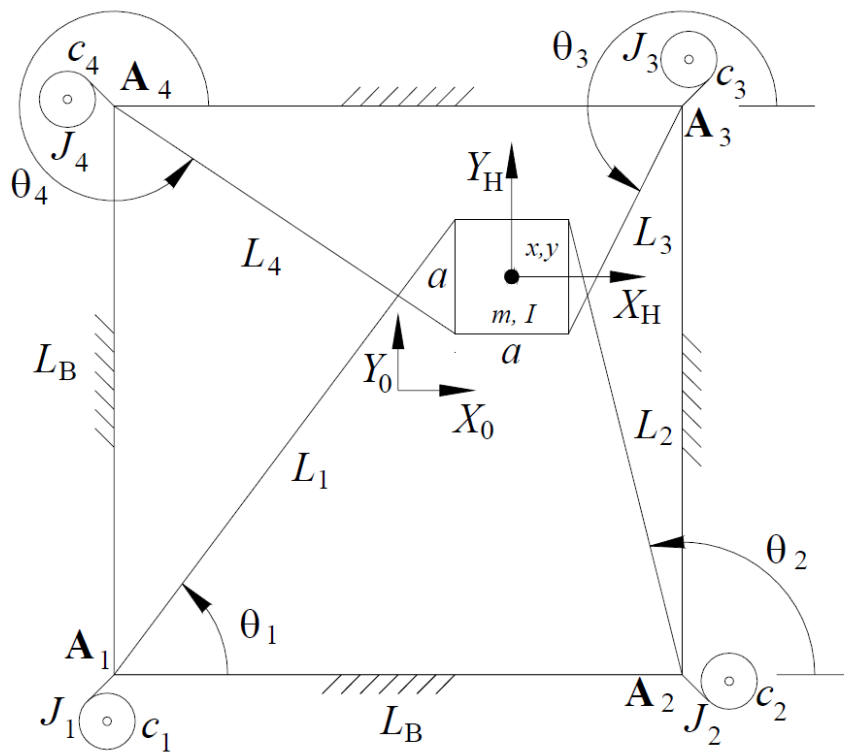


Figure 32. Crossed configuration of the 3 DOF CDDR with 4 cables [23]

Based on [54], the symmetry of the end-effector geometry can cause uncertainty in the forward pose kinematics, and thus the dimensions will be chosen such that it is a rectangle. As mentioned before, since cables can only exert tension, 4 cables are needed to fully control the three DOFs of this configuration. The local reference (origin) at the end-effector frame is {H}. The moment of the system is I and it will be calculated based on the geometry and the mass of the end-effector. The workspace of this configuration can reach any point within the base-frame in an ideal case; however, few constraints reduce the workspace. First, the end-effector horizontal and vertical sides will reduce the workspace by $\frac{L_e}{2}$ $and$ $\frac{W_e}{2}$ where $L_e$ and $W_e$ are the length and the width of the end-effector. Furthermore, the rotation of the end-effector around the Z-axis will also reduce the workspace by a small margin which will be considered in the simulation.

In this case, cable interference will always be present. For experimental purposes, it is advised to select the cable material with low friction which will allow the cables to slide freely against each other. The rotation of the end-effector is also limited due to cables interference with the end-effector body. For this study, the maximum rotation was chosen to be $\frac{\pi}{12}$ degrees to eliminate this interference.

## 3.3.    Modeling of CDDR

Kinematics modeling takes into consideration the pose of the end-effector, Jacobian matrices and the static model of the system. It also accounts for the fact that all cables must always stay in tension with a minimum value to be determined based on the mass and the motors to be used. In this study, the minimum tension is chosen arbitrarily on an educated guess based on the literature review to be *0.3* Newtons [2], [47], [55].

**3.3.1.  Pose Kinematics.** The inverse kinematic problem is stated: given the Cartesian position $X = \{x\ y\}^T$ calculate the cable lengths $L_i$. The solution is to calculate the Euclidean norm[54] between the moving point $X = \{x\ y\}^T$ and attachment point at the base frame $A_i$.

$$L_i = \sqrt{(x - A_{ix})^2 + (y - A_{iy})^2};\ \ where\ i = 1, ..., N \tag{3}$$

Note that this equation can only be used when the end effector is a point-mass. For case 2 and 3 with crossed and uncrossed configurations, Eq. 3 becomes:

$$L_i = \sqrt{(x - A_{ix} + h_{ix}\,c\phi - h_{iy}\,s\phi)^2 + (y - A_{iy} + h_{ix}\,s\phi + h_{iy}\,c\phi)^2} \qquad (4)$$

Note that c and s refer to cos and sin respectively. $h_{ix}$ and $h_{iy}$ are the distances from the center of the end-effector to its horizontal and vertical sides in the x-axis and y-axis respectively.

The cables' angles are necessary to be used in velocity kinematics and statics and they can be found as follows:

$$\theta_i = tan^{-1}\left(\frac{y - A_{iy} + h_{ix}\,s\phi + h_{iy}\,c\phi}{x - A_{ix} + h_{ix}\,c\phi - h_{iy}\,s\phi}\right) \qquad (5)$$

The forward kinematics solution is not as simple as that of the inverse kinematics. In this case, the solution of over constrained coupled nonlinear equations is required.

Let $^0_H T$ be the pose of the end-effector with respect to the global origin. $^0_H T$ contains the position and the orientation $^0_H R$. The Euler convention using $Z$-$Y$-$X$ $\alpha, \beta, \gamma$ is:

$$^0_H T = \begin{bmatrix} [^0_H R] & \{^0 x_H\} \\ 0 \quad 0 & 0 \quad 1 \end{bmatrix}$$

where $^0_H R$ is the 3×3 rotation matrix shown in Eq. 6 when $^0_H T$ becomes:

$$^0_H T = \begin{bmatrix} c\alpha c\beta & -s\alpha c\gamma + c\alpha s\beta s\gamma & s\alpha s\gamma + c\alpha s\beta c\gamma & x \\ s\alpha c\beta & c\alpha c\gamma + s\alpha s\beta s\gamma & -c\alpha s\gamma + s\alpha s\beta c\gamma & y \\ -s\beta & c\beta s\gamma & c\beta c\gamma & z \\ 0 & 0 & 0 & 1 \end{bmatrix} \qquad (6)$$

Based on the configuration, the vector loop-closure equation relates the cables with the end-effector pose as follows:

$$^0 A_i + {}^0 L_i = {}^0 L_i + {}^0_H R_i\,{}^H h_i = {}^0 H_i \qquad \text{where } i = 1,2 \dots, n \qquad (7)$$

Eq. 7 calculates the pose of the end-effector given the cable lengths and it is not straightforward. To solve this equation, the solution of coupled non-linear equations

that result in multiple solutions in most cases is required. The authors of [56] applied a least square method to calculate the approximate pose of the end-effector of a spatial CDDR. A closed loop chain equation for another spatial CDDR investigated by [57] was used to solve this complex equation.

In this study, we are not concerned with forward kinematics since our goal is to move the end-effector in a certain given trajectory. It can be used in path planning related studies when there is feedback from sensors that will give you cable lengths, and hence the pose can be approximated in forward kinematics. Hence, the focus is shifted to inverse kinematics for a pure simulation approach of a given trajectory.

**3.3.2. Statics modeling.** Solving Eq. 3 and 4, the cables' lengths and angles can be obtained. In this section, only the crossed-configuration CDDR with 4 cables will be solved since each model has its own equations. Since the first two models will be simulated using CASPR platform in which the static and dynamic models can be solved by the platform itself and there is no need to code them manually. To save such tedious work, only the optimized model equations will be solved.

The static equations of the 4 crossed-cables CDDR system are as follows:

$$\sum_{i=1}^{4} t_i = -\sum_{i=1}^{4} t_i \widehat{L_1} = F_R \tag{8}$$

$$\sum_{i=1}^{4} m_i = -\sum_{i=1}^{4} ({}_{H}^{0}R h_i) \times t_i = M_R \tag{9}$$

where $t_i$ is the cable tension applied to the $i^{th}$ cable. $\widehat{L_i}$ is the negative cable length unit direction. $h_i$ is the pose vector from the local origin of {H} to the $i^{th}$ cable connection. In order to find the instantaneous cables' tensions, the forces have first to be calculated. $F_R$ and $M_R$ are the resultant vector force and moment that amount to the wrench vector when added together $W_R$, where $W_R = \{F_R \ M_R\}^T = \{F_{Rx} \ F_{Ry} \ M_{Rz}\}^T$.

Adding Eq. 8 and 9 and substituting the above, $W_R$ and S (the static Jacobian matrix) which can be expressed with respect to the global origin as follow:

$$ST = W_R \tag{10}$$

where $T = \{t_1 \; t_2 \; t_3 \; t_4\}^T$.

$$S = \begin{bmatrix} -c\theta_1 & -c\theta_2 & -c\theta_3 & -c\theta_4 \\ -s\theta_1 & -s\theta_2 & -s\theta_3 & -s\theta_4 \\ c\theta_1 h_{1y}\gamma - s\theta_1 h_{1x} & c\theta_2 h_{2y}\gamma - s\theta_2 h_{2x} & c\theta_3 h_{3y}\gamma - s\theta_3 h_{3x} & c\theta_4 h_{4y}\gamma - s\theta_4 h_{4x} \end{bmatrix} \tag{11}$$

where $h_i = \{h_{ix} \; h_{iy}\}^T$. In Eq. 11, the orientation of the end-effector is assumed to be 0. To account for that, each element of the last row should be substituted by $c\theta_i(h_{ix}s\phi + h_{iy}c\phi) - s\theta_i(h_{ix}c\phi - h_{iy}s\phi)$ accordingly.

The forces $F_R$ are calculated by differentiating the position of the end effector twice to obtain the acceleration, then multiplying it by the mass of the end effector as follows:

$$F_R = \{F_x \; F_y\}^T = \left\{ m \times \frac{d}{dt}\left(\frac{dx}{dt}\right) \quad m \times \frac{d}{dt}\left(\frac{dy}{dt}\right) \right\}^T \tag{12}$$

This differentiation is done numerically at each step to collect all the instantaneous forces exerted on the end-effector throughout the specified trajectory. Similarly, differentiation the angle $\phi$ twice at each step and multiplying it by the mass $m$ will produce the instantaneous moment required for further calculations.

$$M_R = I \times \frac{d}{dt}\left(\frac{d\phi}{dt}\right) \tag{13}$$

Both Eq. 12 and 13 are done numerically based on initial guesses of values equal to 0. Concatenating both forces and moment will produce the wrench vector $W_R$.

**3.3.3. Maintaining positive cable tension.** In order to make sure that all cables stay in tension, the homogeneous solution will not suffice. A particular solution has to be added with a constant coefficient corresponding to each case where the minimum limit of the tension is added. This is due to the over-constrained case where there are infinite solutions of Eq. 9. The general solution becomes:

$$T = S^+ W_R + (I_n - S^+ S)z \qquad (14)$$

where $I_n$ is the n×n identity matrix. $S^+$ is the under-constrained pseudo inverse of S and z being an arbitrary vector. The first term is the particular solution and the second term is the homogeneous solution. Replacing both terms of Eq. 11 we get:

$$T = \begin{Bmatrix} t_{p1} \\ t_{p2} \\ t_{p3} \\ t_{p4} \end{Bmatrix} + \alpha \begin{Bmatrix} n_1 \\ n_2 \\ n_3 \\ n_4 \end{Bmatrix} \qquad (15)$$

Based on [58], the method to determine whether a point is within the static workspace depends on the Kernel vector components. In Eq. 15 the kernel vector N of S is the vector present in the homogenous solution and it consists of $\{n_1 \ n_2 \ n_3 \ n_4\}^T$ multiplied by an arbitrary scalar $\alpha$. To ensure that all the cables have positive tension values greater than the specified minimum, all the components of the Kernel vector must have the same sign ($n_i > 0 \ or \ n_i < 0$). When this condition is satisfied, a scalar $\alpha$ present in Eq. 15 can be found to attain a positive tension of all cables. If the calculated values of all the components in the particular solution are greater than the minimum tension, $\alpha$ will be a negative scalar in order to minimize the minimum value in the particular solution and vice versa. This method is effective and simple and can be applied to any planar or spatial CDDR with one actuation redundancy. It also reduces the computational complexity of the code and will take less time to compute the solution unlike other methods such as the optimization toolbox to find the minimum set of tensions. Since the workspace has already been discussed and will be hardcoded to be less than the maximum theoretical workspace as previously discussed, the solutions of the Kernel vector for any trajectory will not have a 0 value for $n_i$.

The creation of this workspace will eliminate all singularities resulted from the interference between the end-effector and the base-frame. However, there is a function in MATLAB that calculates the kernel vector considering the rotation of the end-effector into account, and that is *null*. It calculates the singular value decomposition of the matrix, *[U,S,V] = svd(A,0).* The Kernel vector can be symbolically expressed when $\phi = 0$ on null space basis as follows:

$$N = \begin{Bmatrix} n_1 \\ n_2 \\ n_3 \\ n_4 \end{Bmatrix} = \begin{pmatrix} c(\theta_2 - \theta_3 + \theta_4) - c(\theta_2 - \theta_3 - \theta_4) + s(\theta_2 - \theta_3 + \theta_4) - s(\theta_2 + \theta_3 - \theta_4) \\ c(\theta_1 - \theta_3 - \theta_4) - c(\theta_1 + \theta_3 - \theta_4) + s(\theta_1 + \theta_3 - \theta_4) - s(\theta_1 - \theta_3 + \theta_4) \\ c(\theta_1 + \theta_2 - \theta_4) - c(\theta_1 - \theta_2 - \theta_4) + s(\theta_1 - \theta_2 - \theta_4) + s(\theta_1 - \theta_2 + \theta_4) \\ c(\theta_1 - \theta_2 + \theta_3) - c(\theta_1 + \theta_2 - \theta_3) - s(\theta_1 - \theta_2 + \theta_3) - s(\theta_1 - \theta_2 - \theta_3) \end{pmatrix} \quad (16)$$

The columns of V that do not correspond to nonzero singular values form a set of orthonormal basis vectors for the null space. The "rational" basis for the null space *null(A,'r')* is obtained from the reduced row echelon form of A, as calculated by *rref*. Furthermore, each cable has a maximum angle $\theta_i$ that can be reached. These ranges are $0° < \theta_1 < 90°$ , $90° < \theta_2 < 180°$, $180° < \theta_3 < 270°$ , and $270° < \theta_4 < 360°$. By analyzing all the combinations of these angles for each $n_i$.

Table 1. Kernel vector components' analysis

| $n_1$ | cos | sin |
|---|---|---|
| $180° < \theta_2 - \theta_3 + \theta_4 < 270°$ | (-Ve) | (-Ve) |
| $0 < \theta_2 + \theta_3 - \theta_4 < 90°$ | +Ve | (+Ve) |
| $-360° < \theta_2 - \theta_3 - \theta_4 < -450°$ | (+Ve) | -Ve |
| | | |
| $n_2$ | cos | sin |
| $90° < \theta_1 - \theta_3 + \theta_4 < 180°$ | (-Ve) | (+Ve) |
| $-450° < \theta_1 - \theta_3 - \theta_4 < -540°$ | (-Ve) | -Ve |
| $-90° < \theta_1 + \theta_3 - \theta_4 < 0$ | (+Ve) | -Ve |
| | | |
| $n_3$ | cos | sin |
| $-360° < \theta_1 - \theta_2 - \theta_4 < -450°$ | (+Ve) | (-Ve) |
| $180° < \theta_1 - \theta_2 + \theta_4 < 270°$ | -Ve | (-Ve) |
| $-180° < \theta_1 + \theta_2 - \theta_4 < -90°$ | (-Ve) | -Ve |
| | | |
| $n_4$ | cos | sin |
| $90° < \theta_1 - \theta_2 + \theta_3 < 180°$ | (-Ve) | (+Ve) |
| $-270° < \theta_1 - \theta_2 - \theta_3 < -360°$ | +Ve | (+Ve) |
| $-90° < \theta_1 + \theta_2 - \theta_3 < 0$ | (+Ve) | -Ve |

In Table 1, the values of the Kernel vector components can be analyzed as follows: When using the analysis in Table 1 and substituting in Eq. 16, all the values of $n$ are either positive or negative for any set of points within the determined workspace.

## 3.4.    Simulation using CASPR

A preliminary simulation has been done to show basic results of cable lengths, forces, and position of the end-effector through a given trajectory. CASPR toolbox [51] has been utilized and the detailed formation of the first two configurations of the proposed CDDRs are shown below.

### 3.4.1.  CASPR: A Comprehensive Cable-Robot Analysis and Simulation platform for the Research of Cable-Driven Parallel Robots. In this part, CASPR [51] (A Comprehensive Cable-Robot Analysis and Simulation platform for the Research of Cable-Driven Parallel Robots) will be introduced. CASPR is a MATLAB based platform which allows the study of arbitrary types and structures of CDPRs, such as single and multi-link CDPRs for a wide range of analyses, including dynamics, kinematics, control, and workspace analysis. Moreover, CDPRs can be defined using Extensible Markup Language (XML) with out-of-the-box availability of an extensive range of robots and analysis tools. The open-source platform aims to provide both a communal environment for the researchers to use and add models and algorithms to. The example case studies demonstrate the potential to perform analysis on CDPRs, directly compare algorithms and conveniently add new models and analyses. There is a specific process that has to be followed step by step to install and integrate this platform with MATLAB [59]. After that, initializing the platform is basically running a file inside the main directory of the platform. Then, learning how to use the platform becomes easier.

Two simple models were created for simulation, note that these models are used to show preliminary results and will be improved upon in the optimized model. After successfully installing the platform, a file called *initialise_CASPR* must be run to initialize the setup, then the two main commands to use the platform are:

1.  *CASPR_Model_Manager*;     which opens the window shown in Figure 33.

This window allows either the removal or the addition of a new model. After naming the new robot and pressing add model, the corresponding file to the type of the robot (planar, spatial, etc…) has to be chosen.

After that, an xml file has to be created to enter the data related to the model, such as, mass of the end-effector, moment of inertia, display range, and the initial location of the end-effector with respect to the base frame.
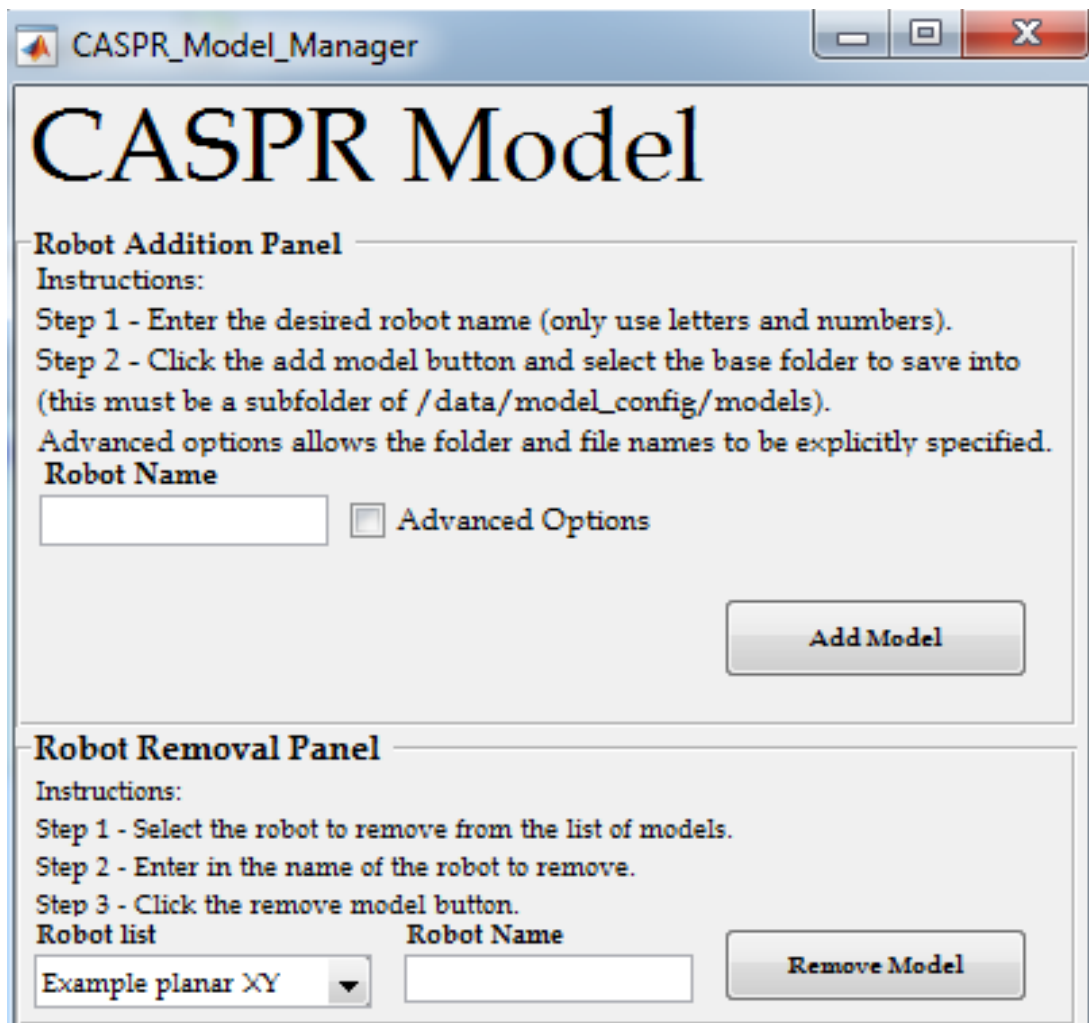


Figure 33. CASPR Model Manager

Once the model is successfully created, it can be viewed in CASPR Graphical User Interfaces (GUI) using the command *CASPR_GUI,* this command opens the GUI interface which mainly allows the loading of models and running simulation as shown in Figure 34. The home window of the GUI contains the following elements:

I. Model setup options to allow users to select different CDPR models and cable sets.

II. Simulators selection to allow users to choose which simulator to open.

III. Model view to visually display the CDPR in different poses or cable sets.

IV. Model pose to allow users to change the pose to display in the model view.

2. *CASPR_GUI*; which opens the window shown in Figure 34.
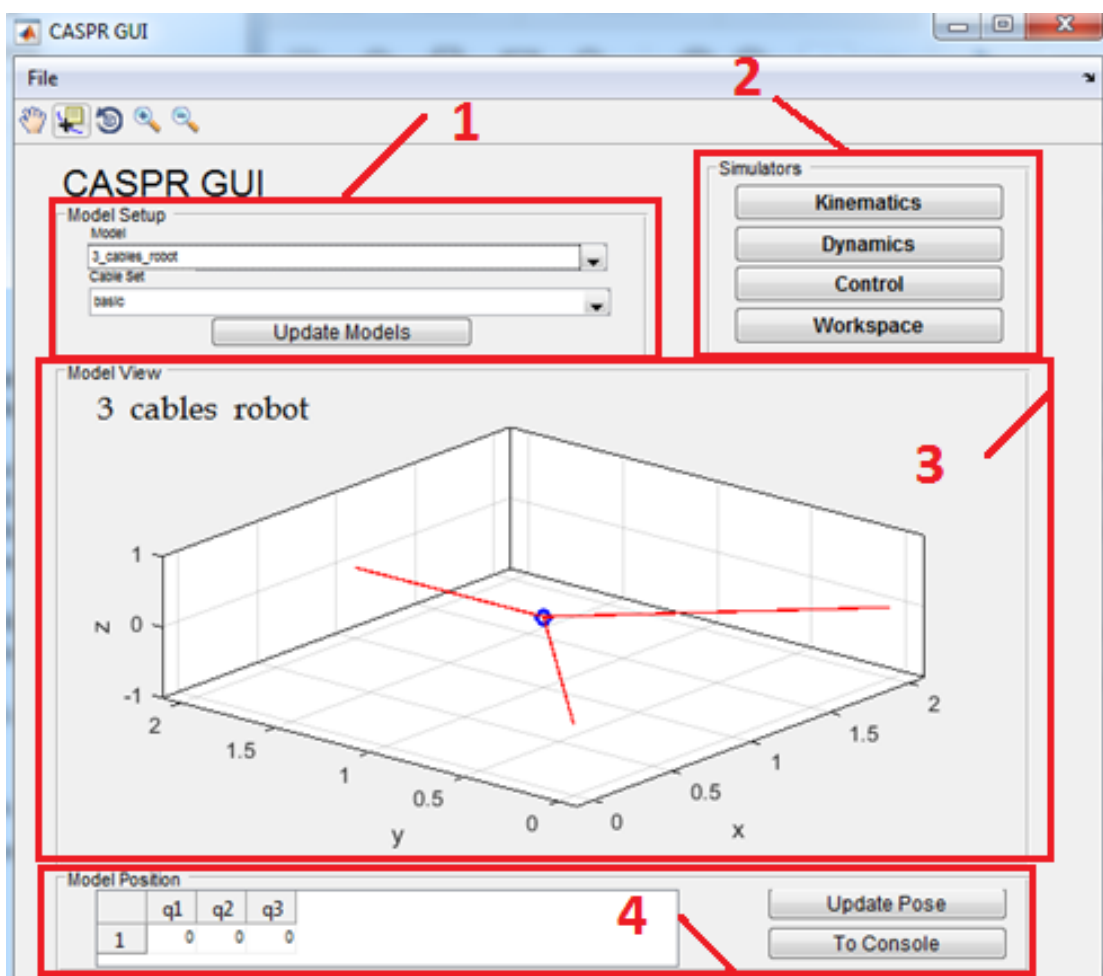


Figure 34. CASPR GUI sections

The next step is to create a new xml file which describes the number of the cables and their corresponding attachment point on the base frame and the end-effector. Finally, a trajectory xml file containing the set of trajectories desired.

Note that a list of trajectories can be created by coding it into the trajectories XML file inside the specific folder of the model. The GUI is capable of calculating the kinematics and dynamics equation of the selected model when the trajectory is created correctly. Also, the pose of the end effector can be updated without solving the model for visual purposes.

**3.4.2. Models created using CASPR.** As previously mentioned, two models were created using CASPR platform. The first model is a 2 DOF CDDR with three cables attached to a point-mass at the center of the platform shown in Figure 35. These models do not reprtesent the final design which will be used to run the optimization. The results of these models when the end-effector is following a simple trajectory will be shown later. The second model is the planar 2 DOF CDDR with 4 cables where the 4 cables are also attached to a point mass.
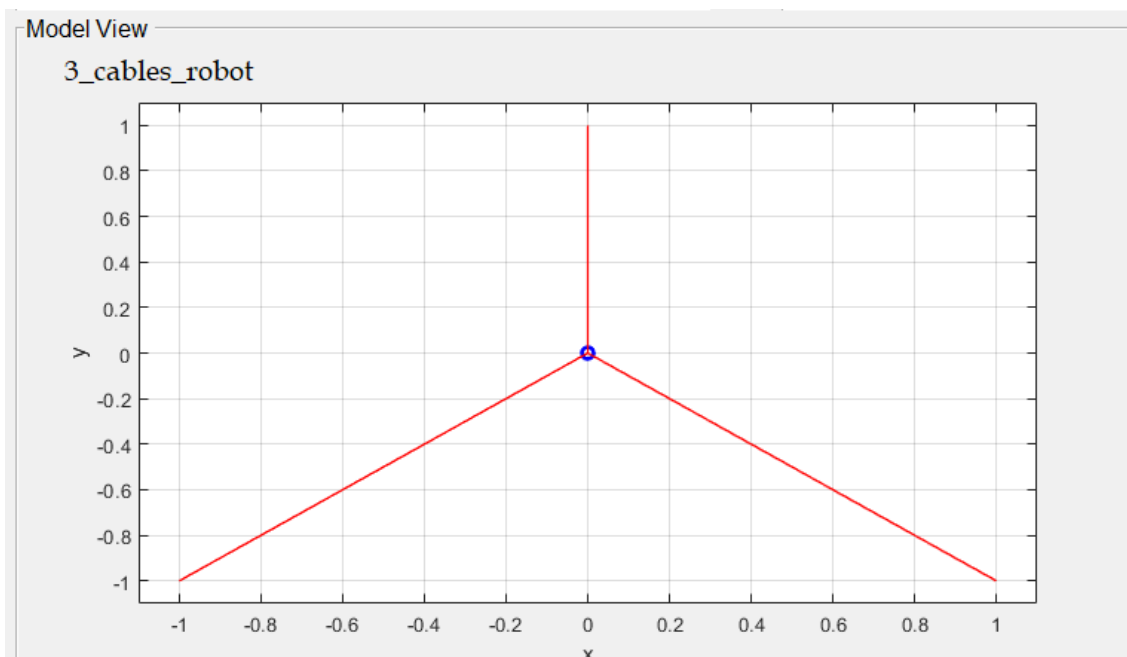


Figure 35. Planar CDDR with 3 cables

Figure 36 shows the configuration of a basic model. Note that this model only has two DOFs. No optimization has been performed on either configuration since the CASPR platform was utilized for simulation. Each model has its own parameters depending on the number of cables and the end-effector geometry. The base-frame dimensions were fixed for all 3 models.

53

The main difference between the three models is the variable attachment point at the base-frame which is only applicable to the third model that has to be optimized. In this case, an initial assumption of the attachment points being the corners of the base-frame as the other models is first considered, then the optimization algorithm changes these anchor points based on the objective function. Table 2 shows the model parameters of the planar CDDR with 3 cables.

Table 2. Model parameters for 3 cables CDDR

| Model parameters | Abbreviation | value | Unit |
|---|---|---|---|
| Number of Cables | $L_i \; where \; i = 1,2,3$ | 3 | NA |
| Platform side length | LB | 2 | m |
| Origin | $O$ | 0,0 | m |
| Cable 1 base | $A_1$ | $-1,-1$ | m |
| Cable 2 base | $A_2$ | $1,-1$ | m |
| Cable 3 base | $A_3$ | 0,1 | m |
| Minimum cable Tension | $T_{min}$ | 0.5 | N |
| Attachment points coordinates at the end effector | $A$ | NA (Point mass) | m |

Table 3 shows the parameters of the CDDR with 4 cables where all these cables are attached to a point mass at the end-effector side. Figure 36 shows the model of the planar CDDR with 4 cables and 2 DOFs where the cables are attached to a point mass at the end-effector corresponding to Table 3. Note that these parameters change from one model to another, some of them are fixed for the first two models such as, the attachment point at the end-effector, the attachment points at the base-frame, the minimum tension in each cable which is the same for all the cases and can be changed based on the data sheet of the actuators used, the number of cables as per model since model 1 has 3 cables and model 2 and model 3 have 4 cables, and the mass of the end-effector which is null for the first two cases (point mass) and 0.2 kg for case 3 since the end-effector is a rectangular platform. The behavior of the models depends on all these parameters.
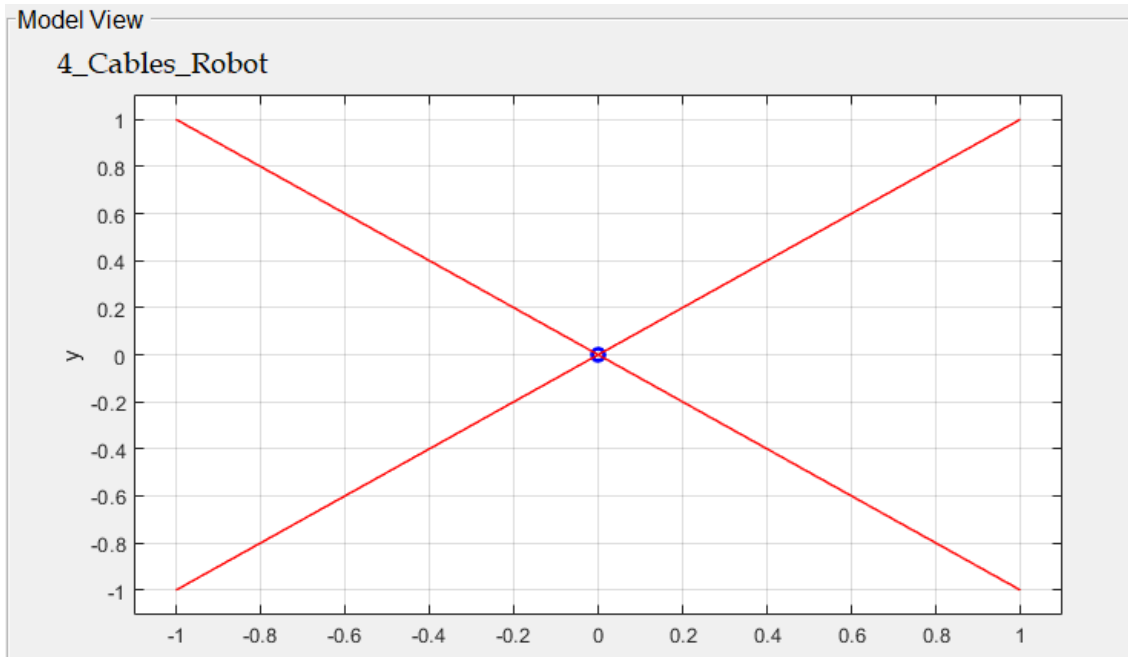
Figure 36. Planar CDDR with 4 cables

Table 3. Model parameter for 4 cables CDDR

| Model parameters | Abbreviation | value | Unit |
|---|---|---|---|
| Number of Cables | $L_i \; where \; i = 1,2,3,4$ | 4 | NA |
| Platform side length | LB | 2 | m |
| Origin | $O$ | 0,0 | m |
| Cable 1 base | $A_1$ | $-1,-1$ | m |
| Cable 2 base | $A_2$ | $1,-1$ | m |
| Cable 3 base | $A_3$ | 1,1 | m |
| Cable 4 base | $A_4$ | $-1,1$ | m |
| Minimum cable Tension | $T_{min}$ | 0.5 | N |
| Attachment points coordinates at the end effector | $A$ | NA (Point mass) | m |

## 3.5. Optimized Model

This section presents the optimized model under MATLAB. First, the basic model has been created with the same dimensions shown in Figure 36. The optimized model

differs from the previous model in two ways. First, the attachment points of the cables at the end-effector side are on a rectangular platform with a specified length and width. Furthermore, the attachment points at the base-frame are not fixed. Optimization will be carried out for different trajectory, then a comprehensive comparison between the optimized configurations will determine which set of pulley locations are most suitable for a general application given by set of trajectories. This optimum configuration might work for some trajectories better than others since it is used for general applications. For a case-specific trajectory, the corresponding optimum configuration is best fit for that application. For instance, if the application of the CDDR under study is to perform in a factory for a pick-and-place mission, it will only move from point A to point B, in this case, the optimization can be performed on that particular trajectory back and forth and the corresponding optimum configuration should be used where the minimum exerted cables' tensions is generated. Figure 37 shows the model with 4 cables to be optimized along with its parameters in Table 4.
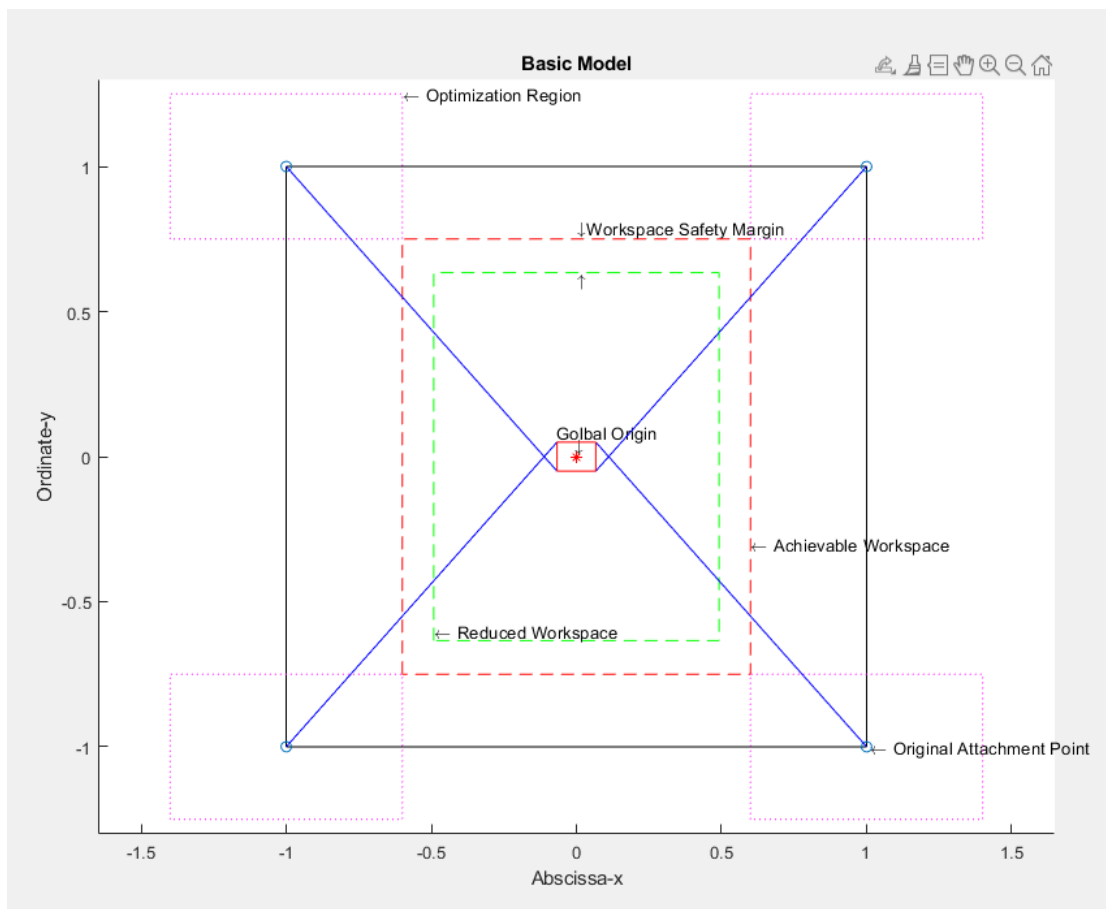


Figure 37. CDDR to be optimized

Table 4. Model parameters of the optimized CDDR

| Model parameters | Abbreviation | value | Unit |
|---|---|---|---|
| Platform side length | LB | 2 | m |
| End-effector length | $l_{endefff}$ | $\dfrac{LB}{16}$ | m |
| End-effector width | $w_{endefff}$ | $\dfrac{LB}{20}$ | m |
| Optimization region length | $a_x$ | $a_x = \dfrac{LB}{5}$ | m |
| Optimization region width | $a_y$ | $a_y = \dfrac{LB}{8}$ | m |
| Attachment points coordinates (anticlockwise) | $A_{ix}, \qquad A_{iy}$ $where\ i = 1,2,3,4$ | NA | m |

## 3.6. Optimization Algorithm

In this section, the flowchart of the code is illustrated. Note that there is a general flowchart and more detailed ones for each part of the optimization algorithm.

The flowchart in Figure 38 shows the general steps the code is following in order to obtain the optimized cable attachment points at the base. The global parameters, such as the end-effector dimensions, the minimum and maximum tensions, the workspace and the Wrench Feasible Workspace (WFW) are all selected before running the code.

After setting the global parameters, the first step is to calculate the wrench feasible workspace to avoid any singularities. After that, 8 different sets of trajectories are created. The forces and torques of the end-effector corresponding to the given trajectories are calculated based on the speed profile of the end effector which will be shown later. After that, the cables' tensions are calculated for the default pulley configuration. When all the above data is available, the inverse kinematic equations are solved, that is Eq. 4 to get cables' lengths, Eq. 5 to obtain cables' angles, local coordinates of the vertices of the end-effector based on the rotation angle $\phi$ and the statics Jacobian matrix $S$ for each trajectory. The optimization algorithm uses all the

sets of data calculated and uses *fmincon* default algorithm to optimize the attachment points.



Figure 38. Generalized flowchart of the optimization process

Figure 38 shows the generalized flowchart of the optimization process. Table 5 shows the global parameters of the optimized model.

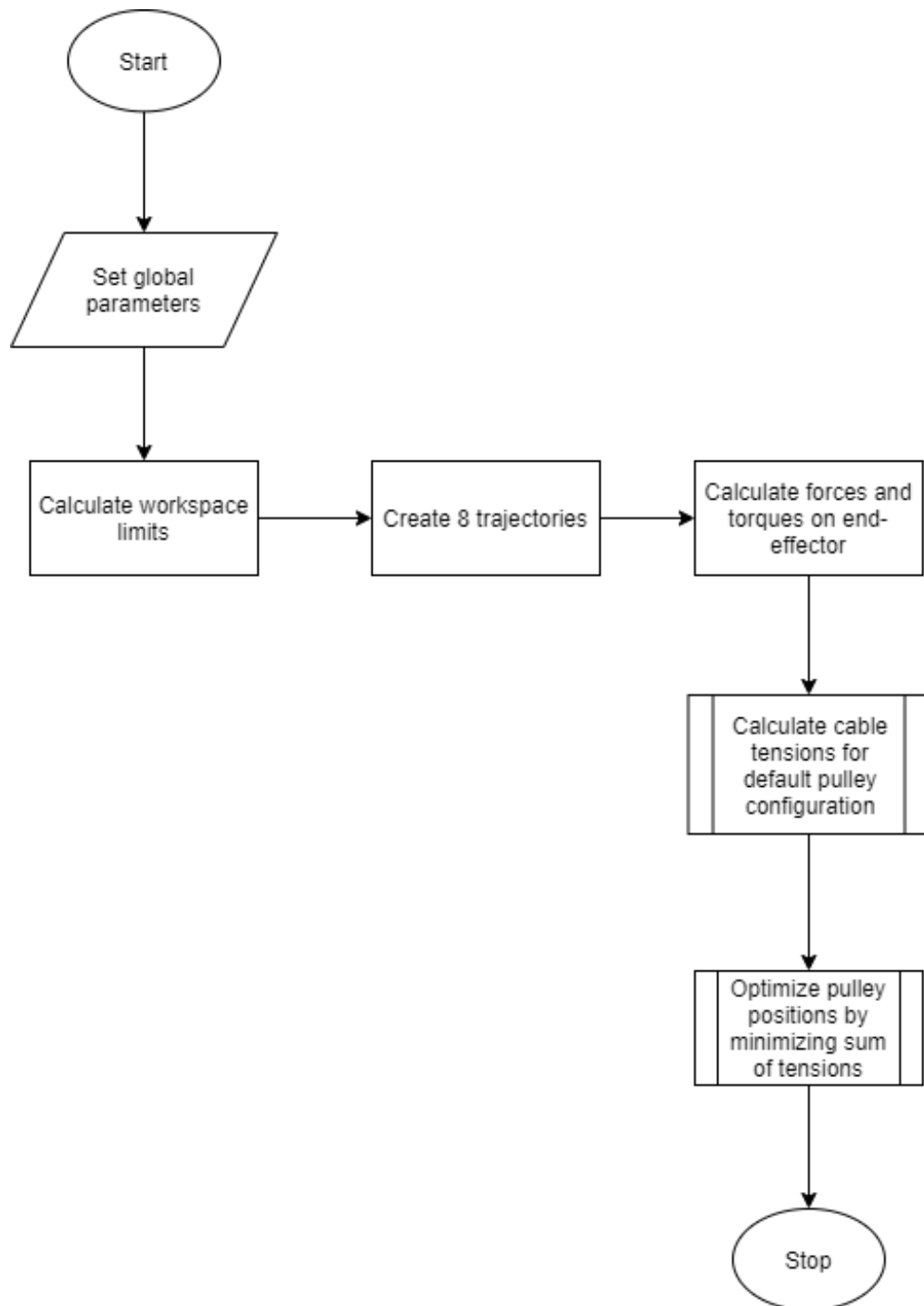Table 5. Global parameters

| Global parameters | Abbreviation | value | Unit |
|---|---|---|---|
| End-effector mass | M | 0.2 | Kg |
| Number of cables | $N$ | 4 | NA |
| Minimum tension | $T_{min}$ | 0.5 | N |
| Maximum tension | $T_{max}$ | 200 | N |
| Workspace safety margin | $safety margin$ | 5 | NA |
| Maximum velocity | $V_{max}$ | 0.3 | $\dfrac{m}{s}$ |
| Rotation angle | $\phi$ | $\dfrac{\pi}{12}$ | ° |

## 3.7. Proposed Solution

Instead of choosing the four corners of the platform as the location of the pulley, this study focuses on changing the attachment points such that the total tension exerted by the cables when following most trajectories within the WFW is reduced. There are two ways to benefit from this optimization. First, if the cable robot is set to repeat the same trajectory for a specific mission whether it is printing one object or pick-and-place, the optimization can only be performed for that trajectory and it will guarantee less cables' tensions compared to any other configuration within the WFW as will the results show later. The second way of benefiting from the configuration is to investigate different optimum configurations with different trajectories and compare them with each other. This comprehensive analysis will run all 8 trajectories across all 8 configurations. The total tension for each trajectory will be presented as a percentage with respect to the default configuration and the results will be compared for individual trajectories and across configurations.

For each single trajectory, the optimization function will vary the pulley location and calculate the summation of the tension exerted when that specific configuration is set. Then, the pulleys' locations will change at each iteration and the total tension will be recalculated again. When the optimization is done, the results will

give the optimum pulleys' location where the total tension is minimum for a particular trajectory. 8 different sets of trajectories are created and will be shown in the results.

The CDDR parameters and cable tensions are updated at each iteration. The objective function is the summation of all tensions in the cables to be minimized and can be presented by letting $T_{ij}$ be the cable tension magnitude of the $j$-th cable when the end-effector centre-of-mass is at the $i$-th point of the trajectory. Then the objective function becomes:

$$z = \sum_i \sum_j T_{ij} \tag{27}$$

where $z$ is the objective function representing the grand total cables' tensions for a single predefined trajectory. The optimization algorithm will select the optimum configuration such that $z$ is minimized compared to other several iterations. Once it achieves the desired accuracy, which is set by tolerance values included in the global parameters, it will stop.

The MATLAB command that performs the optimization for a particular CDDR model with fixed anchor points is:

**vOpt = fmincon(@objFun,v0,[], [],[],[],lb,ub,@constrFun,options);**

Figure 39 shows the optimization algorithm flowchart for the third model. The "*objFun*" is the objective function previously explained. $v_0$ is the initial estimation of the optimization vector and all the values of this vector are set to 0 at the start. *lb and ub* are the lower and upper bounds of the attachment points' abscissa and ordinate, and that of the cables' tensions respectively. The "**@constrFun**" depends on Eq. 10. We can form a column vector $\boldsymbol{T}$ with the 4 cable tension magnitudes. This vector of cable tension magnitudes can be written as the sum of a particular solution and a homogeneous solution. The particular solution is $\boldsymbol{S^+W}$, where $\boldsymbol{S^+}$ is the Moore-Penrose pseudoinverse of $\boldsymbol{S}$ and $\boldsymbol{W} = \left[F_{Rx}, F_{Ry}, M_R\right]^T$, $F_{Rx}$ and $F_{Ry}$ are the x- and y-components of the force on the end-effector and $M_R$ is the torque on the end-effector. The homogeneous solution is $\alpha\boldsymbol{N}$, where $\boldsymbol{N}$ is the kernel vector of $\boldsymbol{S}$ and $\alpha$ is an arbitrary scalar. $\alpha$ is chosen so that all the cable tensions are greater than or equal to a minimum tension magnitude.
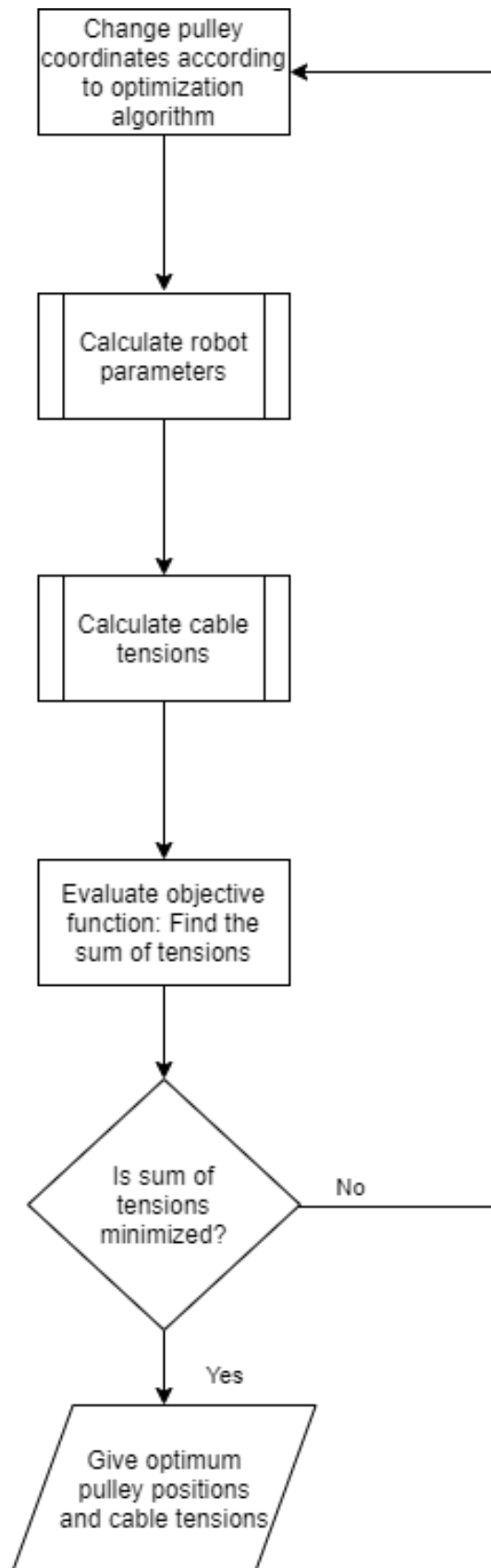
Figure 39. Optimization algorithm flowchart

Then we compute $T = S^+W + \alpha N$ and find the tensions. *options* in the optimization command refers to the following:

1.  The maximum number of function evaluations
    (options.MaxFunctionEvaluations = 200000;)

2.  The maximum number of iterations
    (options.MaxIterations = 10000;)

3.  The optimality tolerance (options.OptimalityTolerance = 1e-4;)

4.  And the step tolerance (options.StepTolerance = 1e-6;)

5.  The above values for their corresponding options are not default, they have been changed based on the optimization for best results.

# Chapter 4.  Experimental Setup

Due to the unfortunate recent pandemic outbreak, a full experimental implementation of the system was not possible. However, a basic experimental setup was used to perform basic tasks and move the end-effector to follow simple trajectories as will be shown in this section.

## 4.1.    Hardware

The hardware components will be introduced in this part.

**4.1.1.   DYNAMIXEL MX64AT servo motors.** DYNAMIXEL is a DC servo motor with several capabilities and characteristics such as, reduction gearhead, controller, network, and a driver [60].   It is classified as a robot-exclusive-smart actuator. The MX series is a new concept of said DC motor with more advanced functions including PID control and high-speed communication.



Figure 40. DYNNAMIXEL MX-A series [60]

Figure 40 shows the MX-64AR model of the MX-A series. This series is described by its heat distribution. When the motor is being used for a long time, it will eventually heat up, however, this series allows an even distribution and dissipation of

the heat due to the aluminum case covering the motor which protects it against any harmful buildup of heat. Four of the MX-64AT motors will be used to complete the configuration of the CDDR.

**4.1.2. Setup.** In this section, the setup will be introduced along with the dimensions and the component.
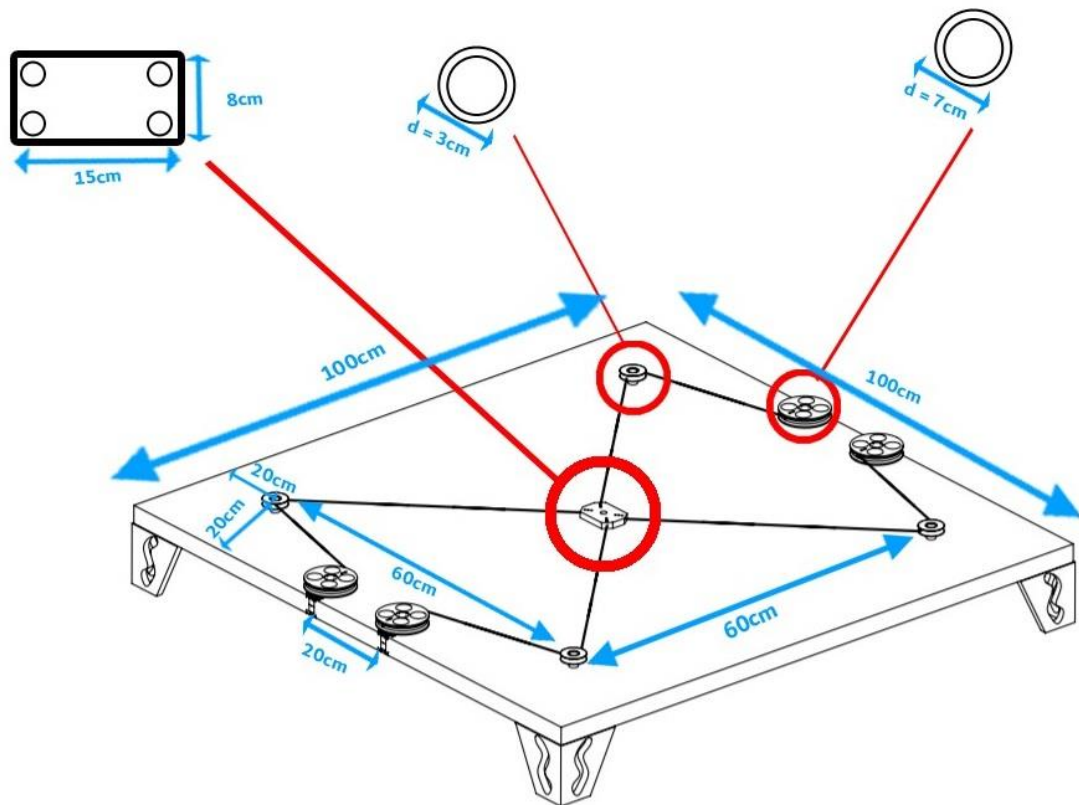


Figure 41. Experimental setup model and dimensions[61]

Figure 41 is the modified setup used for experimentation. The platform is a 100cm×100cm and the end-effector is 15cm×8cm. the pulley locations are symmetrical and equidistant from the center of the platform and separated by 60cm creating a square base for the maximum possible workspace. Note that the anchor point at the end-effector are in an uncrossed configuration. This could have been improved to a crossed configuration but due to the limited time spent on the setup, the experimental implementation only took place on this particular configuration. Originally, a metal cables were used and rolled on the pully. Due to the high stiffness of these cables, they got deformed over time and thus higher minimum tension was required to keep them

unbent. Hence, they were replaced with fishing lines which are characterized by lower stiffness and more flexibility making them easy to roll on the pulleys and connect to the end-effector. The end-effector is a transparent brick made from plastic with a very low mass (approximately 0.1 kg). As can be seen in Figure 42, the cable has already deformed after performing few experiments.
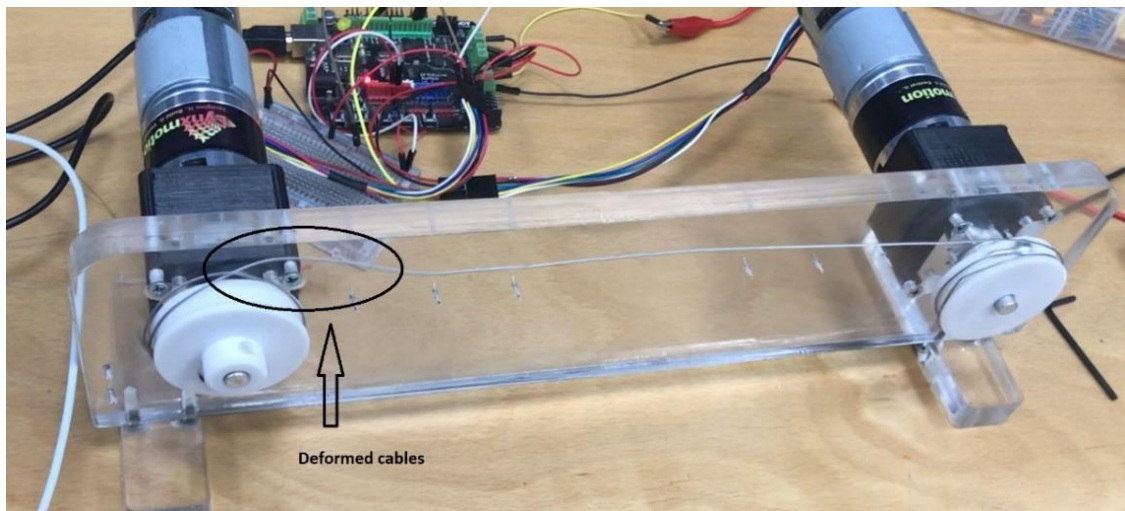


Figure 42. Deformed metal cables

## 4.2. Software implementation

In order to control the 4 DYNAMIXEL motors, an Arduino Mega board was used with a 12V power supply to give enough power to supply to the motors. All the motors were connected to one pin as shown in Figure 43. The command was sent serially sending power from one motor to the next. The trajectories were created using CASPR platform from which the input data was extracted as the rotation of the pulleys in degrees and then converted to radians to be used as an input. Two simple trajectories were created and tested, a straight line and a square.

The setup was run simultaneously using MATLAB and Arduino software. After obtaining the data from the CASPR platform, it was saved and then used in the MATLAB code which runs with the Arduino code simultaneously. The data obtained was in degree, it had to be converted to radians. After that, the serial communication starts with the motors and the data is sent through Arduino. After defining and calibrating the motors, the data which was sent from MATLAB is read using Arduino

and converted to match the resolution of the motors. Each set of data is read at a specific step chosen in order to control the speed at which the data is being sent.
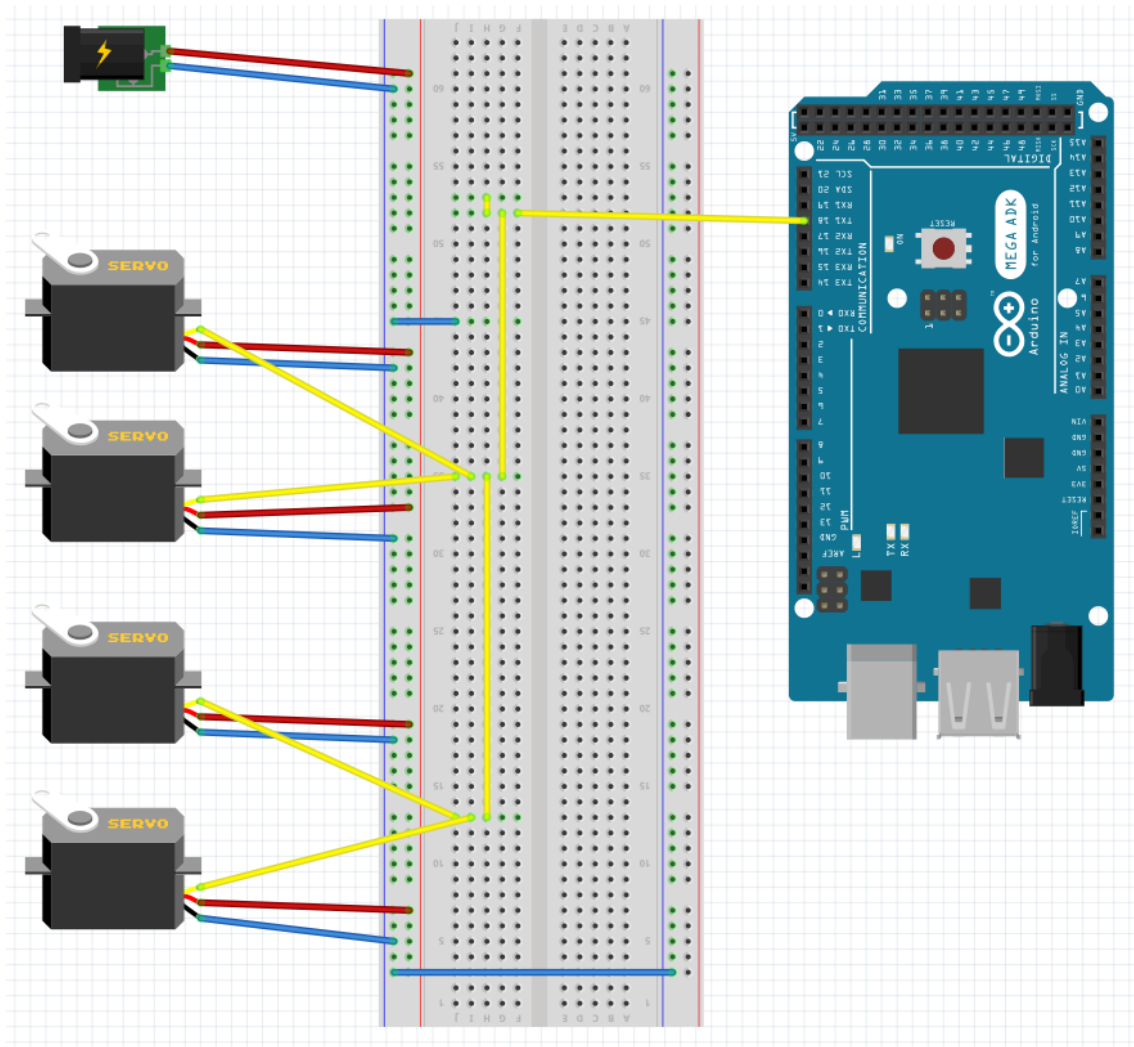


Figure 43. Motors' connection

Figure 44 and Figure 45 show how Arduino software is being used in conjunction with MATLAB to send data to the motors. This connection was created based on the basic experiment which was conducted. For more complicated application, the connection should be taken into consideration to ensure that the data being sent is executed by the code. Furthermore, the power supply should be limited based on the data sheet of the actuators to ensure that they do not get burnt.
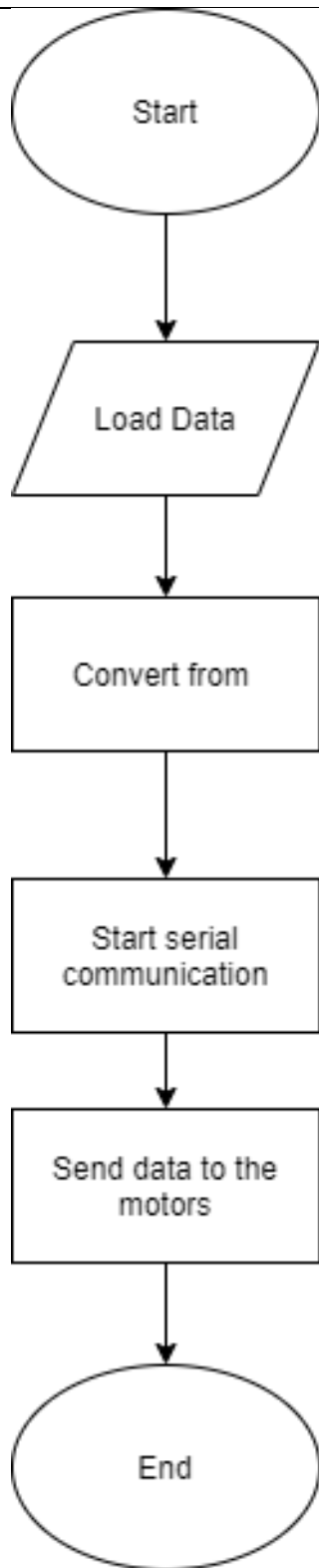
| Figure 44. MATLAB flowchart | Figure 45. Arduino Flowchart |
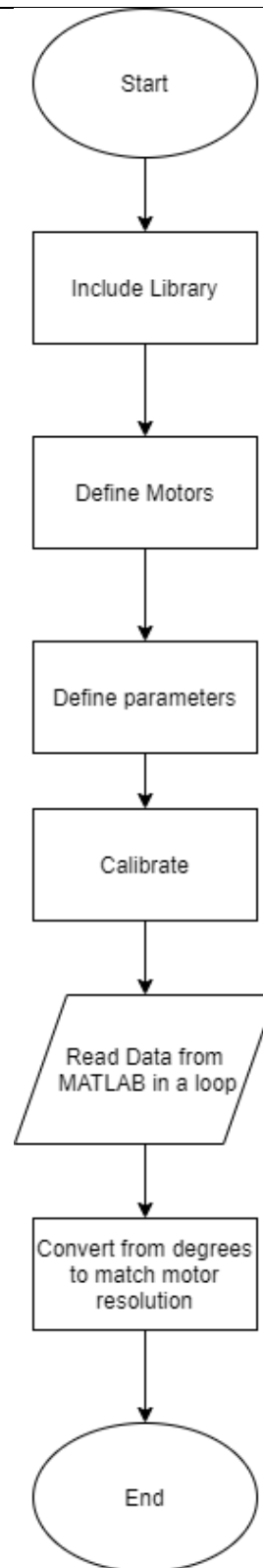
### 4.3. Experimental Results

Both MATLAB and Arduino were synchronized to send data to the motors. Both trajectories were run and the results for low speed showed that the end-effector is following the trajectory slowly with no jerks in the motion unlike the motion produced when the speed increased. The results of the experiment were recorded and can be found in [62]. Figure 46 shows the experimental setup while the end-effector is following a square trajectory.
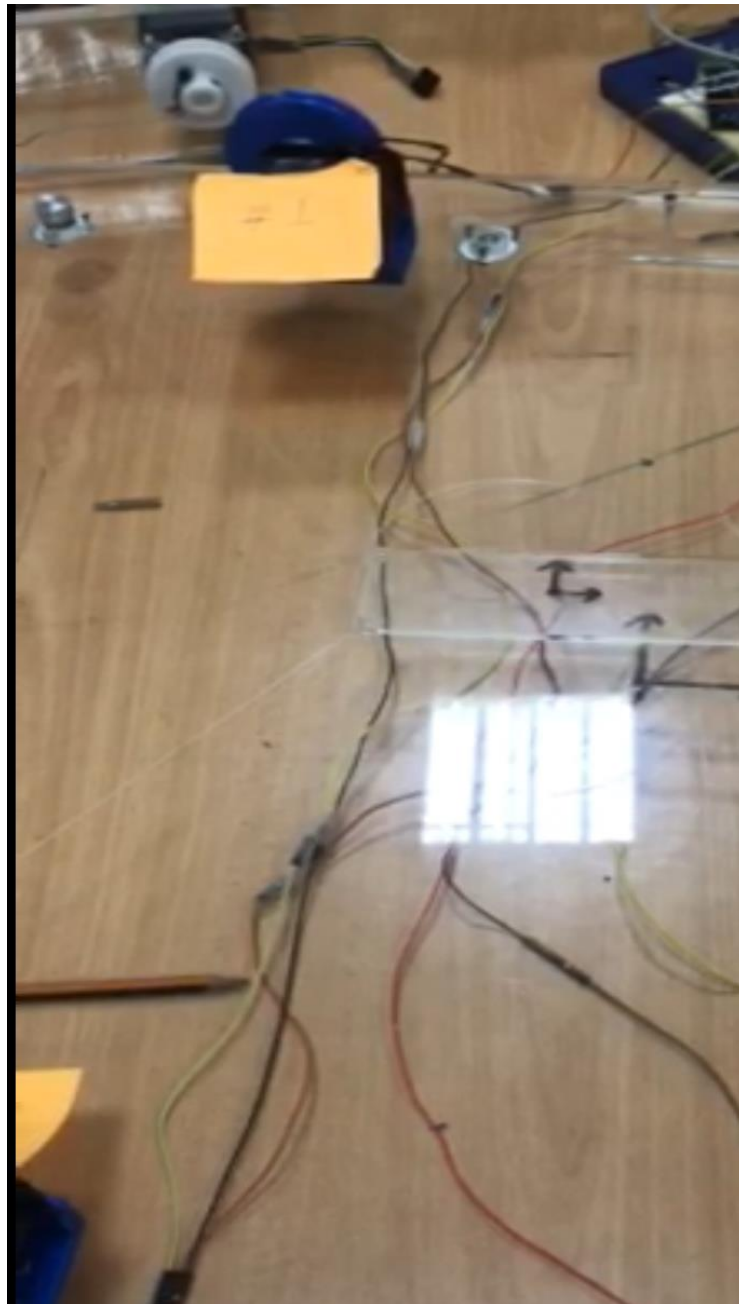


Figure 46. Experimental setup under testing for a square trajectory

# Chapter 5.  Simulation Results

In this chapter, the results of CASPR simulations and the optimized models will be represented and compared in order to create a comprehensive analysis and comparison between the simulated models. First, a comparison between CASPR models' performance will be presented for two different trajectories. Then, the optimization will run on 8 different trajectories to obtain the optimum design. After that, each configuration for a specific trajectory will run all the 8 trajectories creating a total of 64 simulations. All the results of these simulations will be compared based on the objective function of the optimization algorithm.

## 5.1.    CASPR Models' Results

Two models were created under CASPR platform. Each model configuration will be simulated with the same trajectories where the first one is a straight line and the second is a square.

### 5.1.1.   Planar CDDR with 3 cables and two DOF. Figure 35 shows the model being investigated in this section. The coordinate of the straight-line's trajectory start-point is *(-0.5, -0.5)* and that of the endpoint is *(0.2,0.2)*. The straight-line trajectory is shown in Figure 47.
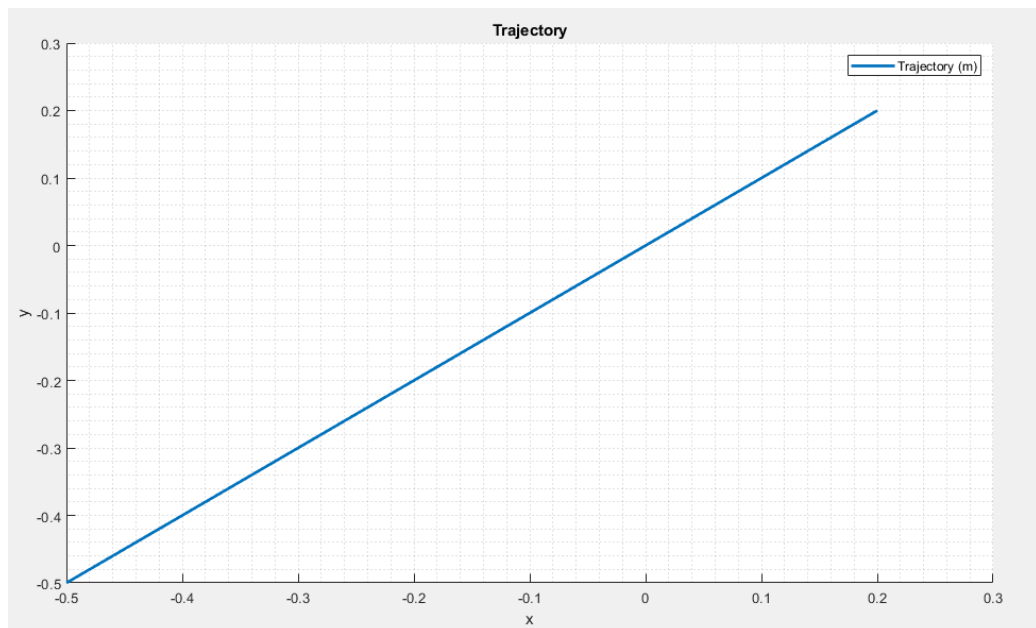


Figure 47. Straight-line trajectory
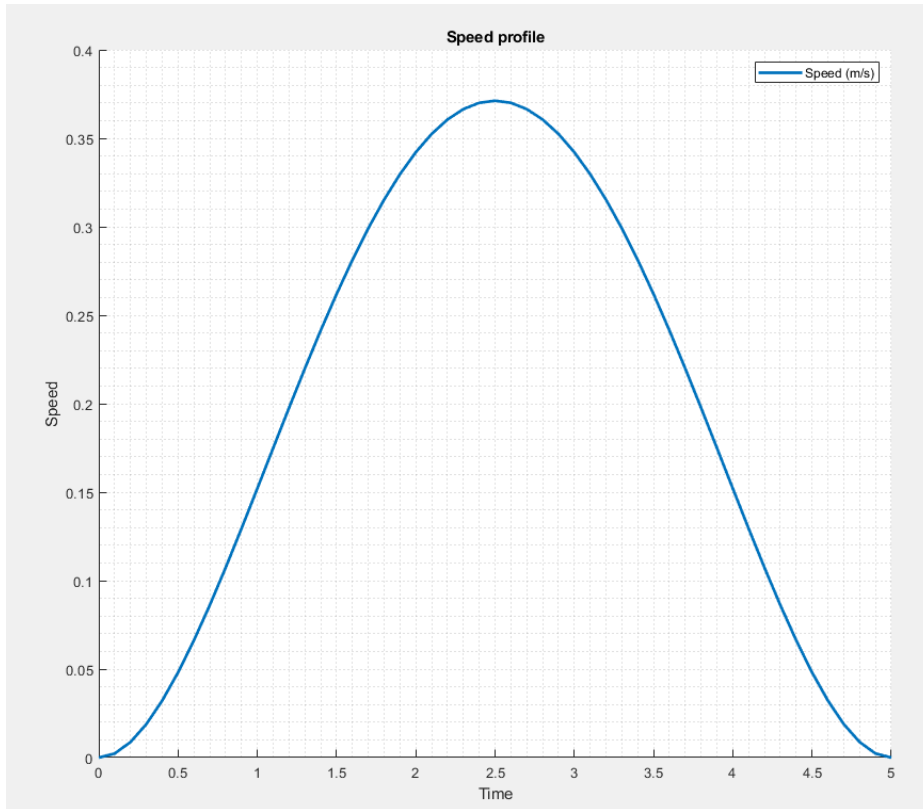
Figure 48. Speed profile of a straight-line trajectory
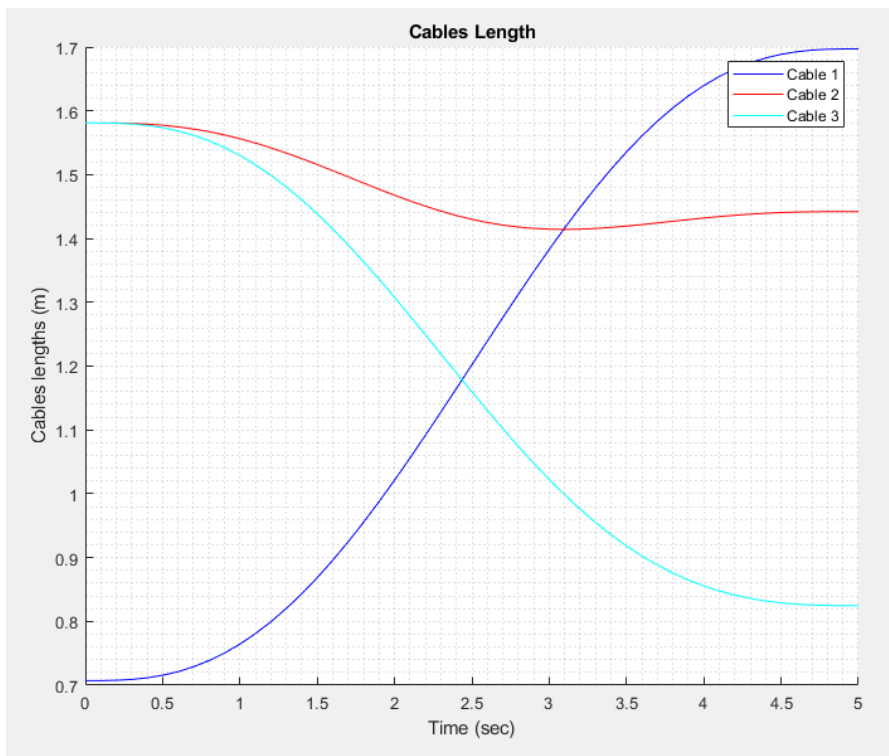


Figure 49. Cables' lengths for a straight-line trajectory

The speed profile of the of the end effector following a straight line is shown in Figure 48. Figure 49 shows individual cable's lengths for a straight-line trajectory. As can be seen in Figure 50, the square trajectory created has sharp edges. The total exerted tension by all the cables is *121.706 N*. Figure 49 shows the cables' lengths for the straight line trajectory simulated using the 3 cables model. The square trajectory is centered around *(0,0)* and has a side of *0.4 m*. Its speed profile is shown in Figure 51.
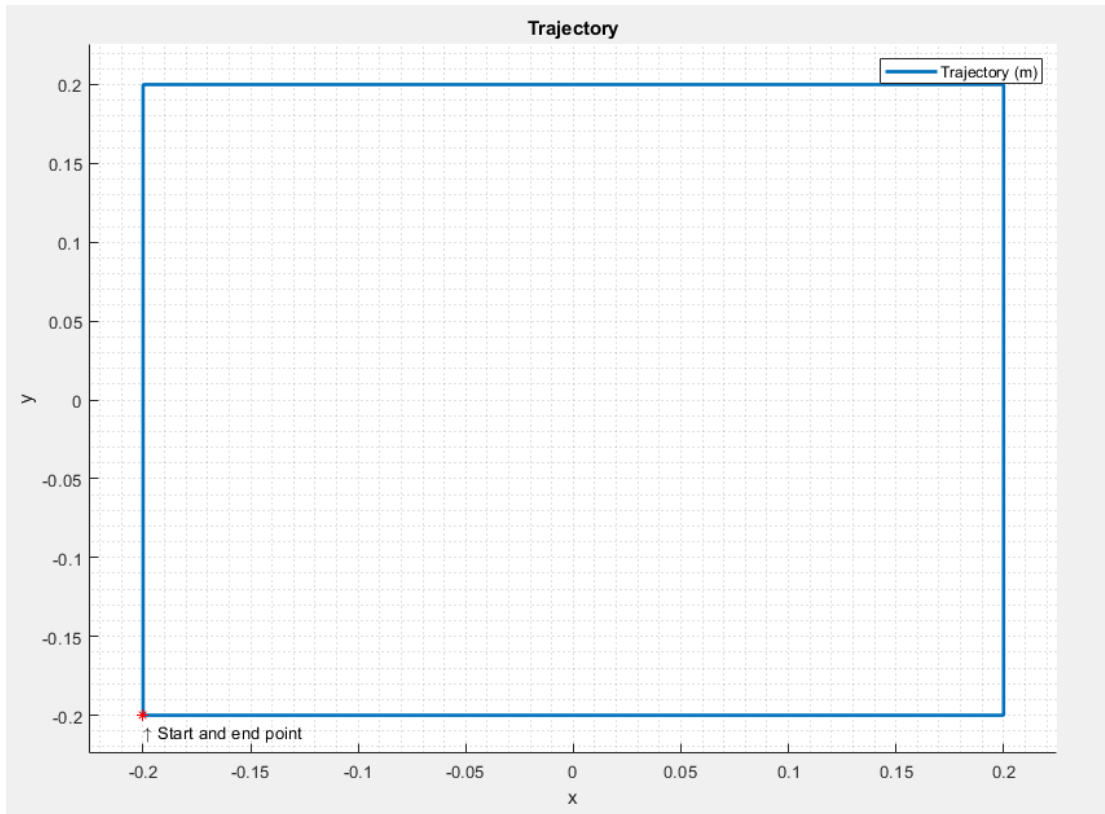


Figure 50. Square trajectory

Note that both speed trajectories are created based on the quantic spline approach adopted by the CASPR platform. It ensures a smooth motion and eliminates all jerks at sharp turns and at the beginning and the end of the motion. As can be seen in Figure 51, the speed resembles that of a sine wave profile where its value is $0\frac{m}{s}$ at $t = 0\ s$, then it reaches a maximum about the middle of the first side, then it gradually decreases to reach $0\frac{m}{s}$ at the first vertex of the square, then this motion is repeated for every vertex and side in the trajectory. Figure 52 shows the cables' lengths for a straight-line trajectory.
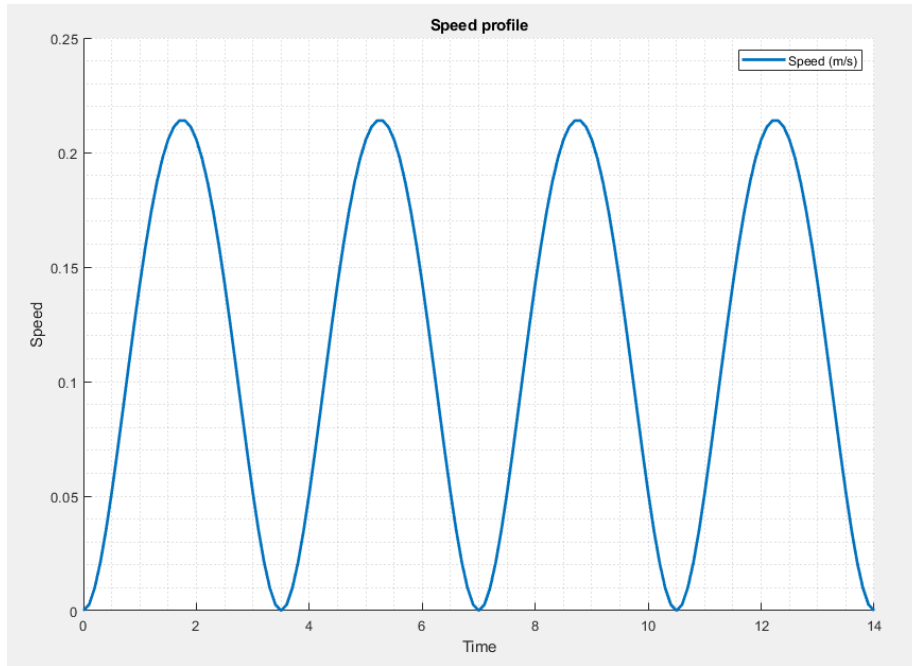
Figure 51. Speed profile of a square trajectory

**5.1.2.   Comparison between planar CDDRs using CASPR platform.** As shown in Figure 36, this model has an extra cable. The over-constrained CDDR will have a larger workspace than the previous model as previously explained. The exact same trajectories shown in Figure 47 and Figure 50 will be repeated**.**
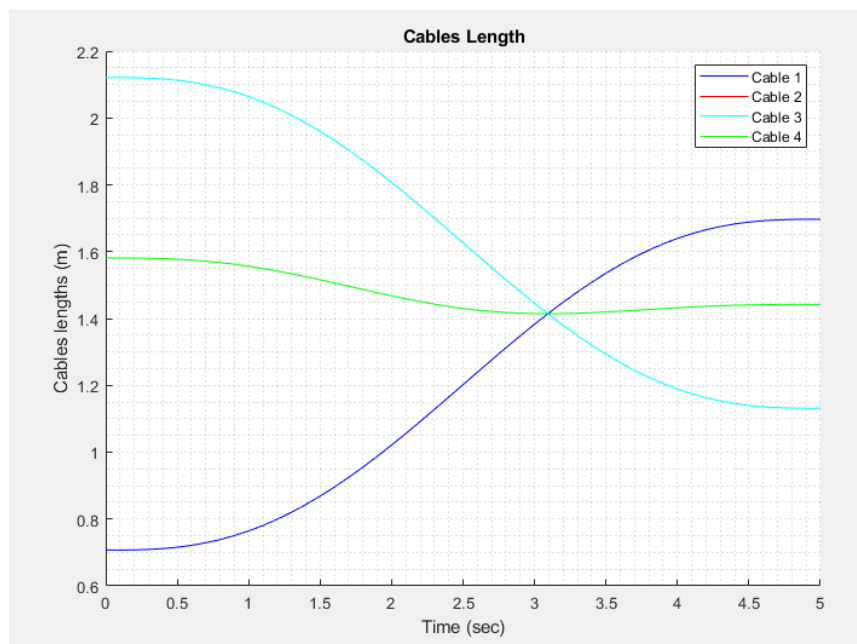


Figure 52. Cables' lengths for a straight-line Trajectory

72
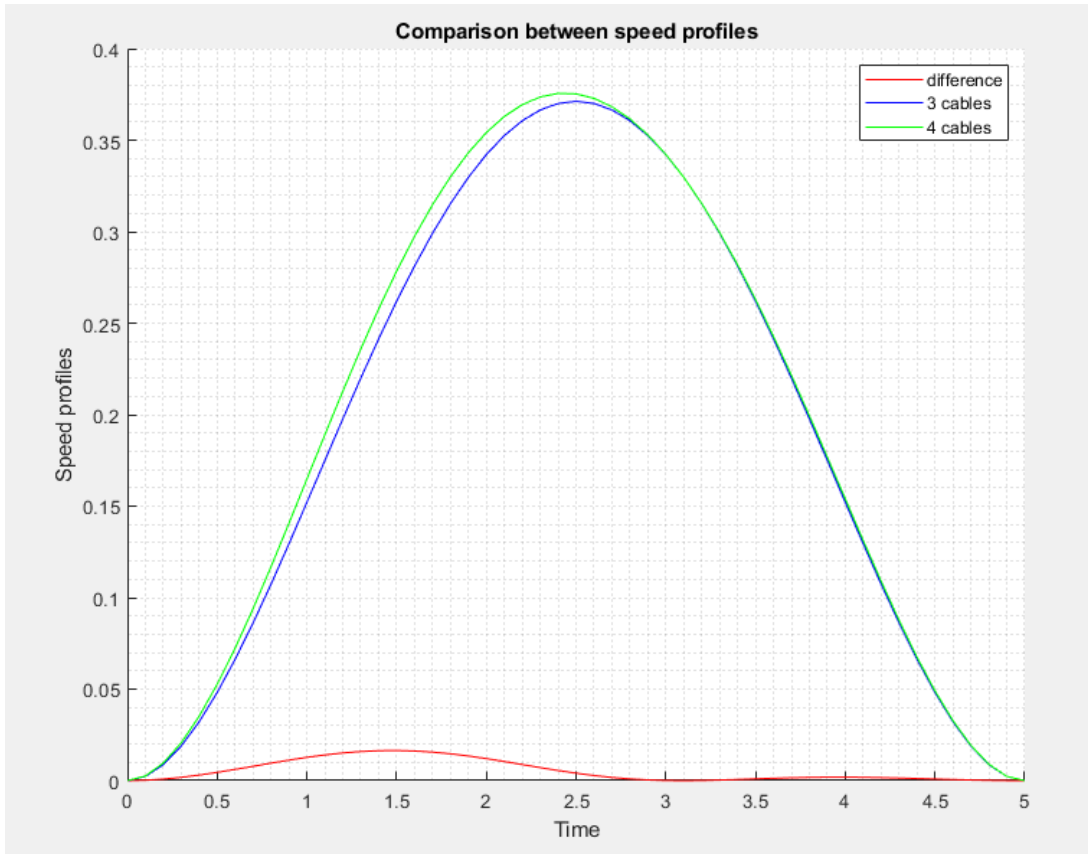
Figure 53. Speed profiles comparison for a straight-line trajectory
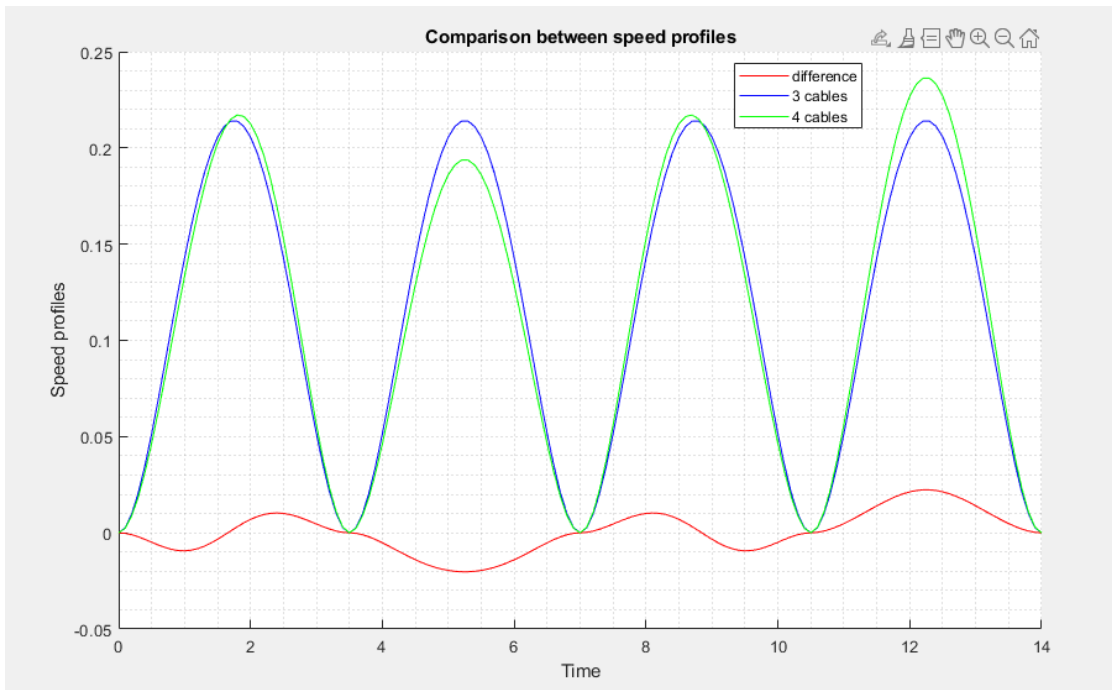


Figure 54. Speed profile comparison for a square trajectory

In Figure 53, the speed profiles of both models when following a straight-line trajectory are shown in blue for the 3-cables model and in green for the 4-cables model. The difference between them is shown in red. As can be seen, both profiles are almost identical, however, it can be noticed that the 4 cables' model responds quicker than the 3 cables due to the extra tension and the over-constrained nature of the model. In other words, the maximum specified speed can be reached faster when more cables are being used.

For a more complex trajectories, the location of the cables determines the speed of the end-effector. The speed profiles in Figure 54 are divided into 4 sections where each section corresponds to one side of the square. The second and last sides can be analyzed based on the number of cables and their attachment points. When the end-effector is moving through the second side, the number of cables that are exerting tension in the same direction as the motion are 2 for both designs. However, the number of cables exerting a tension in the opposite direction of the motion are 2 for the 4-cables design unlike the other model where only one cable is decreasing the speed of the end-effector. Thus, 3-cables configuration will have a better response. The opposite response can be noticed for the last side since the motion is reversed. The importance of this comparison lies in the behavior of the end effector as well as the total tension exerted throughout the motion.

The total tension exerted by 3-cables model being 121.76 N and 339.71 N is greater than that of 4-cables model being 113.12 N and 312.1 N for a straight-line and a square trajectory, respectively. It can be concluded that the 4-cables model exerts less tension for most trajectories with a better control over the DOFs of the system.

## 5.2. Optimized Model results

In this section, the results of the optimized model along with all the optimum configurations for 8 trajectories will be presented and compared. The performance is based on the grand total of tensions exerted by the cables when the same trajectories run on each model. Figure 37 shows the basic configuration of the 4-cables CDDR with crossed configuration that will be assumed as the initial design to be optimized for each trajectory.

74

**5.2.1. Optimum configurations.** In this section, all the optimum configurations will be shown from Figure 55 to Figure 62. Note that $x$ and $y$ are in meters (m).
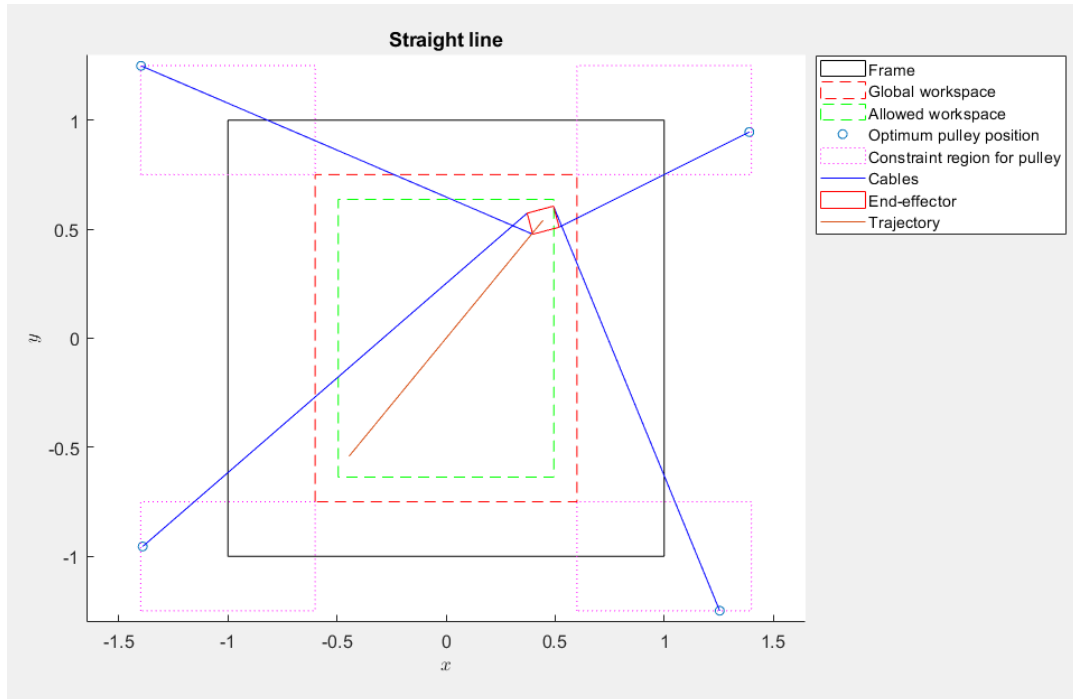


Figure 55. Optimum configuration for a straight-line trajectory
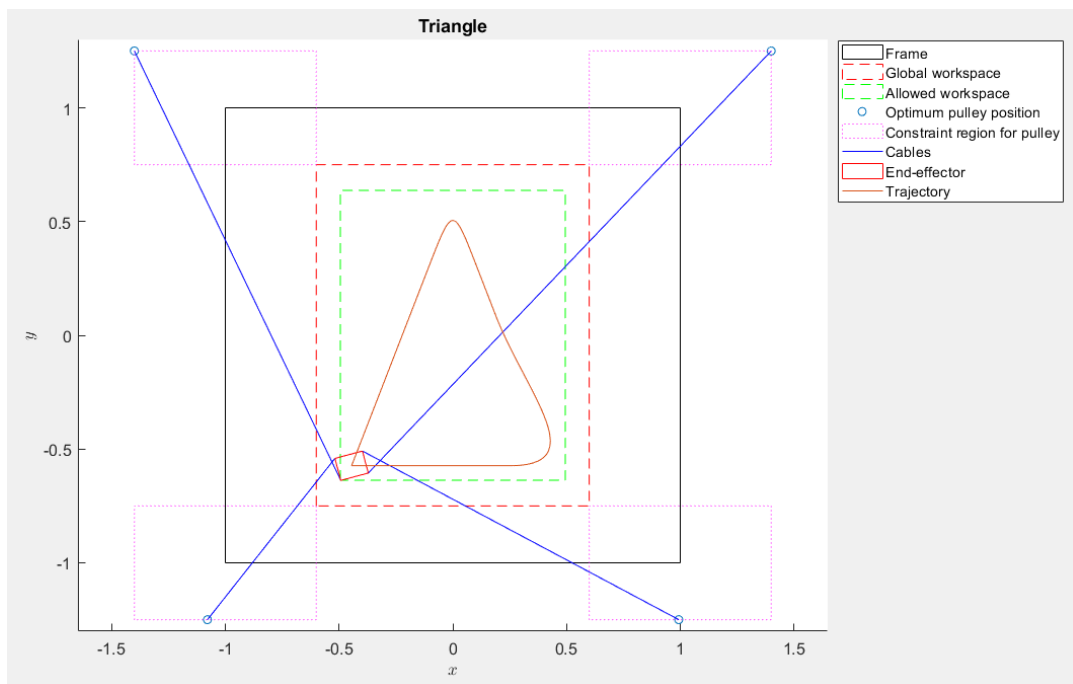


Figure 56. Optimum configuration for a triangular trajectory
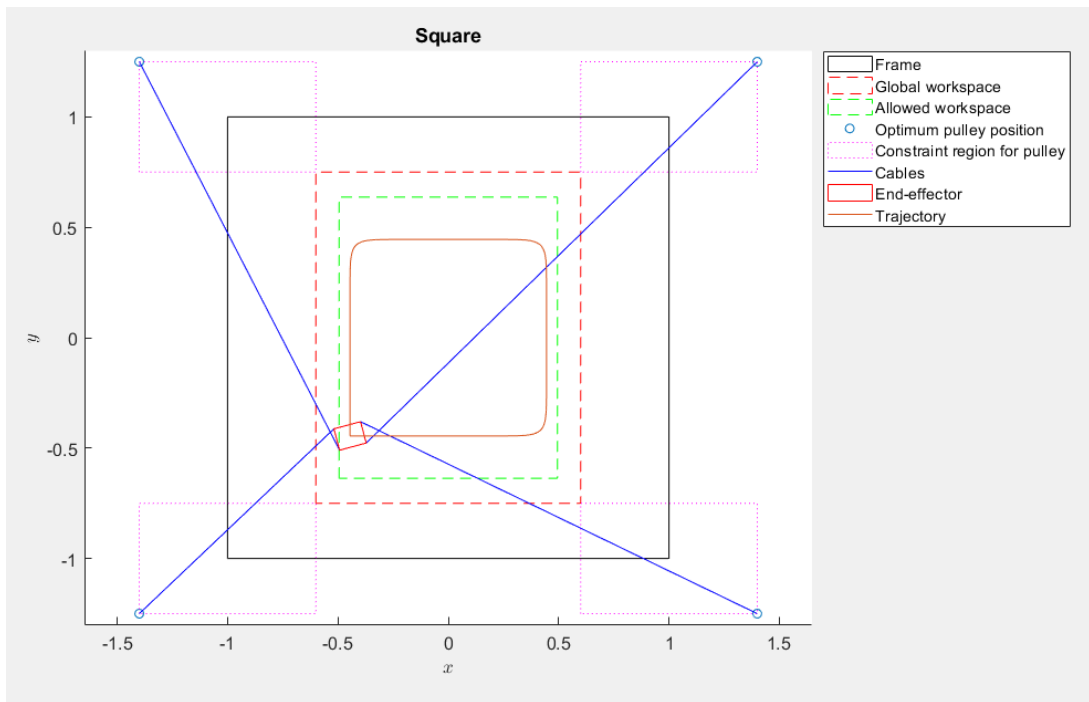
Figure 57. Optimum configuration for a Square trajectory
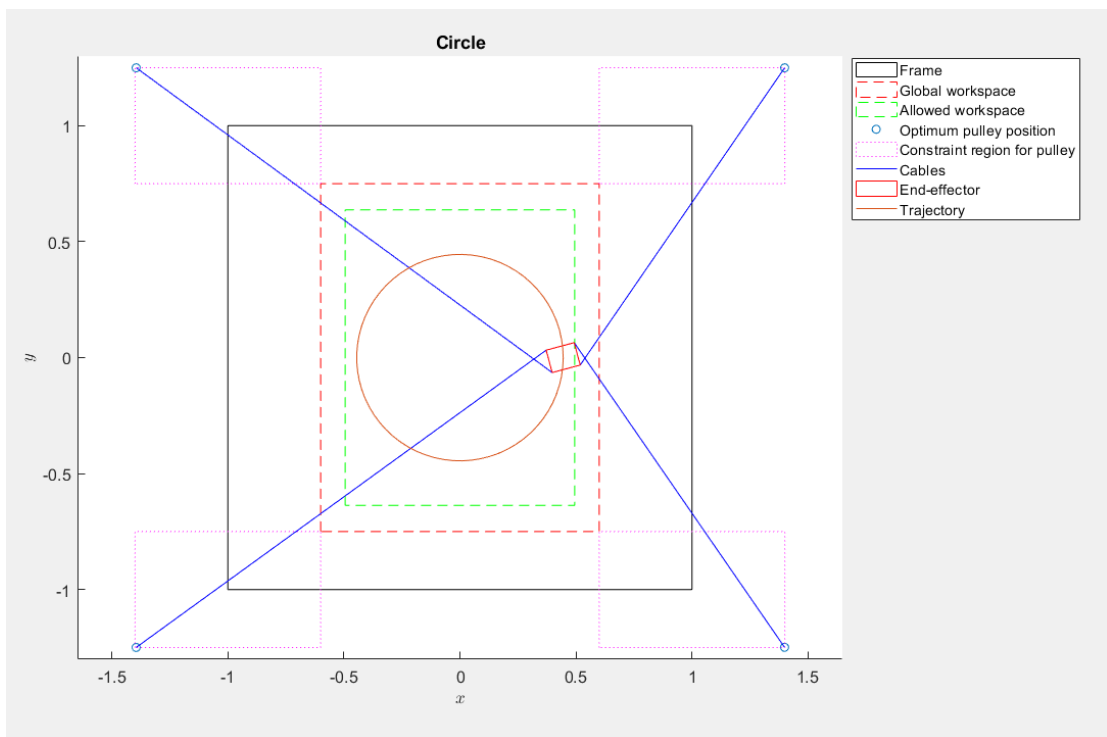


Figure 58. Optimum configuration for a circular trajectory

For the custom trajectory shown in Figure 62, the error in the output and the calculated torque are shown in Figure 67.
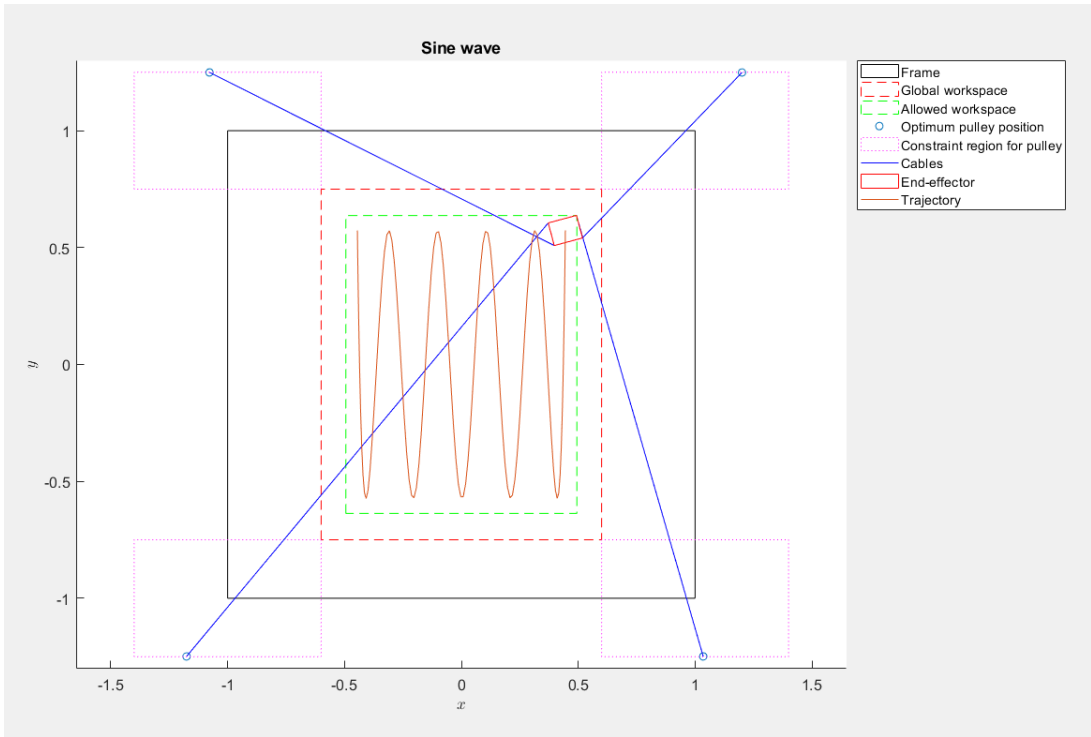
Figure 59. Optimum configuration for a sine-wave trajectory
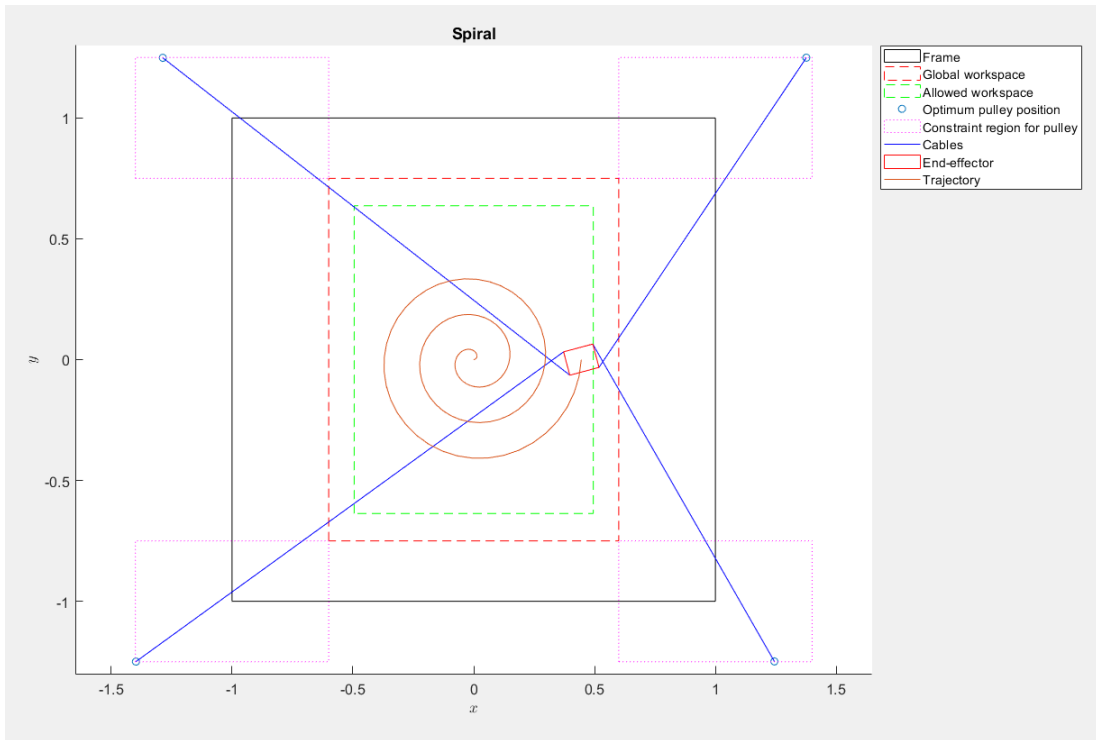


Figure 60. Optimum configuration for a spiral trajectory

Note that trajectories were created while taking the number of points $N$ into consideration.
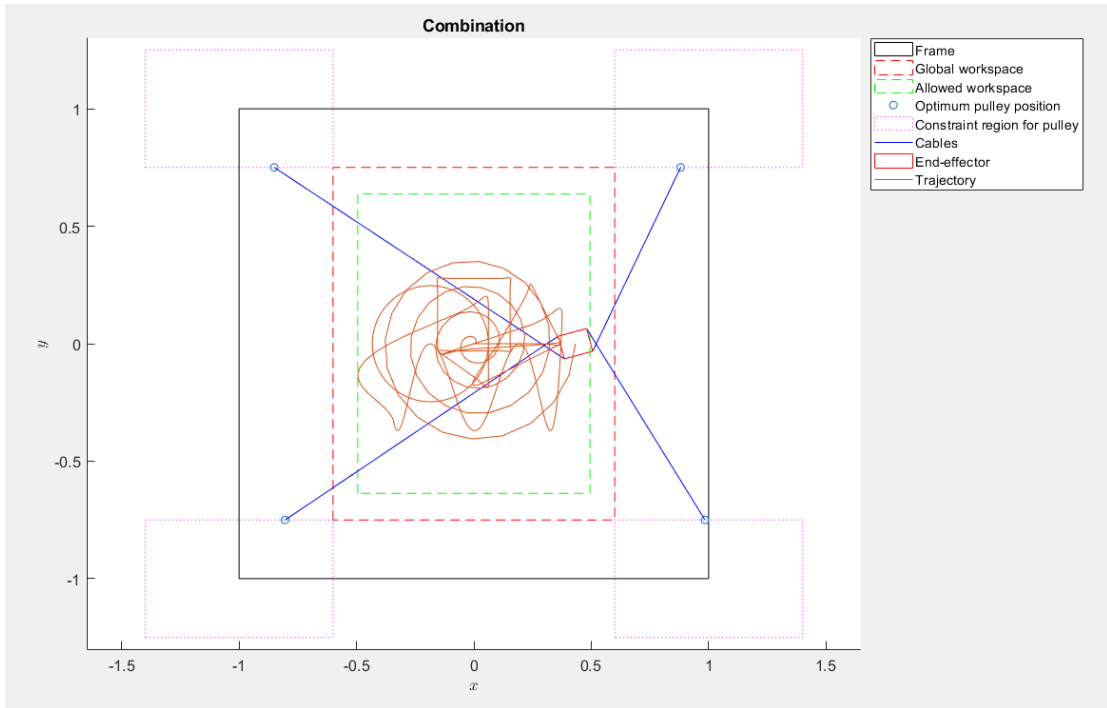
Figure 61. Optimum configuration for a combined trajectory
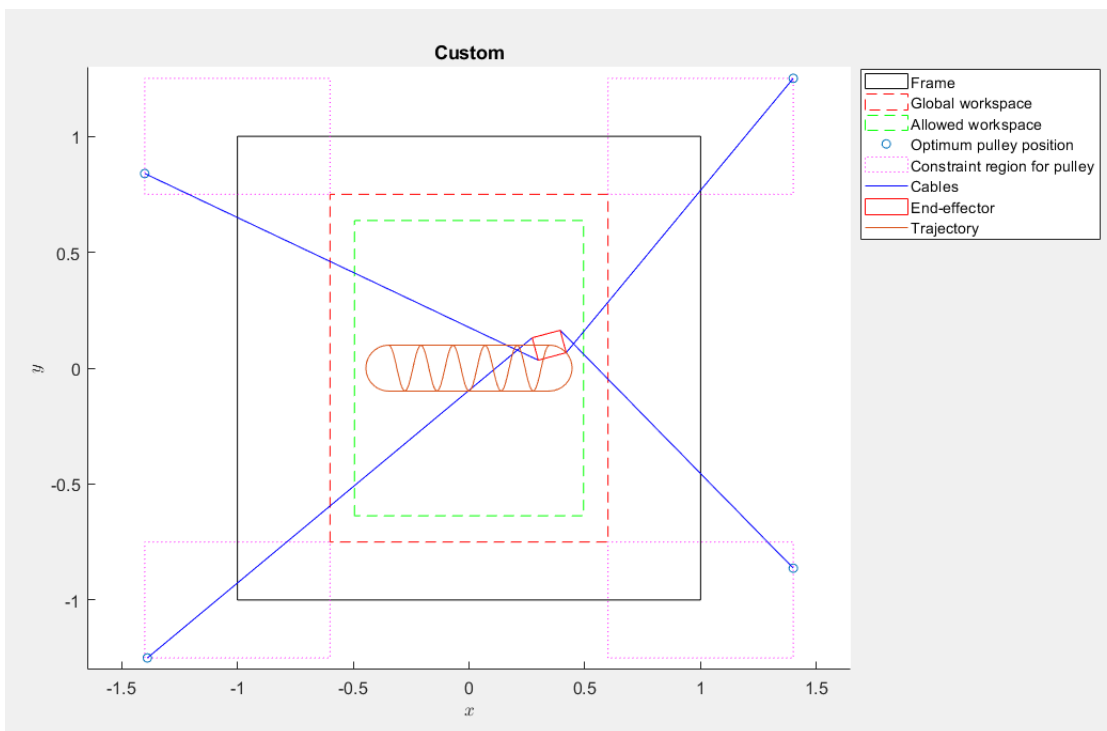


Figure 62. Optimum configuration for a custom trajectory

Note that all the attachment points of the cables at the base-frame are at the edges of the optimization region where in fact it can be anywhere inside that region.
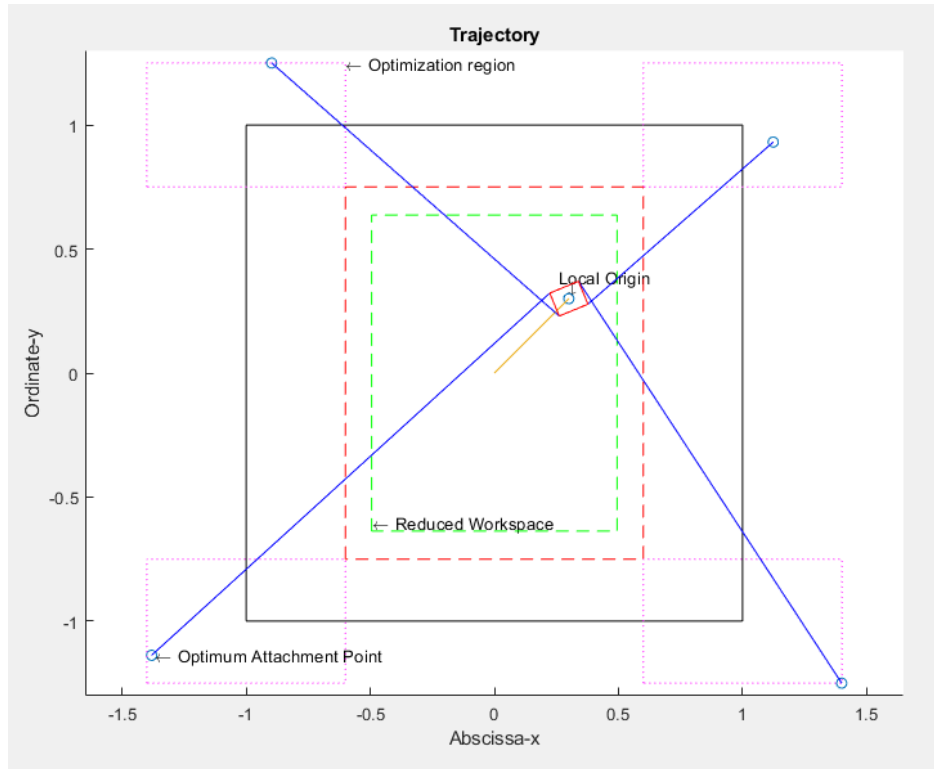
Figure 63. Optimum attachment point inside the optimization region

As can be seen in Figure 63, the attachment point of cable 3 is inside the region and not at the edges.

**5.2.2. Validation of forces and torques**. In this section, the results of the forces and the torques from the simulation are validated. Note that not all the trajectories will be shown since there are 64 simulations and hence 64 graphs. Only few graphs will be shown where $F_R$ is in N.

Figure 64 shows the given force and the calculated forces for a straight-line trajectory. As can be seen, the forces are identical.

Using Eq. 12 and 13, the given forces and moments are calculated using the instantaneous acceleration and angular acceleration. After calculating the tensions using Eq. 15 for the optimum configuration of the respective trajectory, the resulting tension vector is substituted in Eq. 10 to obtain the calculated forces shown in Figure 64.

Figure 65 corresponds to the comparison between the forces of the combined path where all the 7 basic trajectories are combined in one. Both values are identical throughout the simulation.
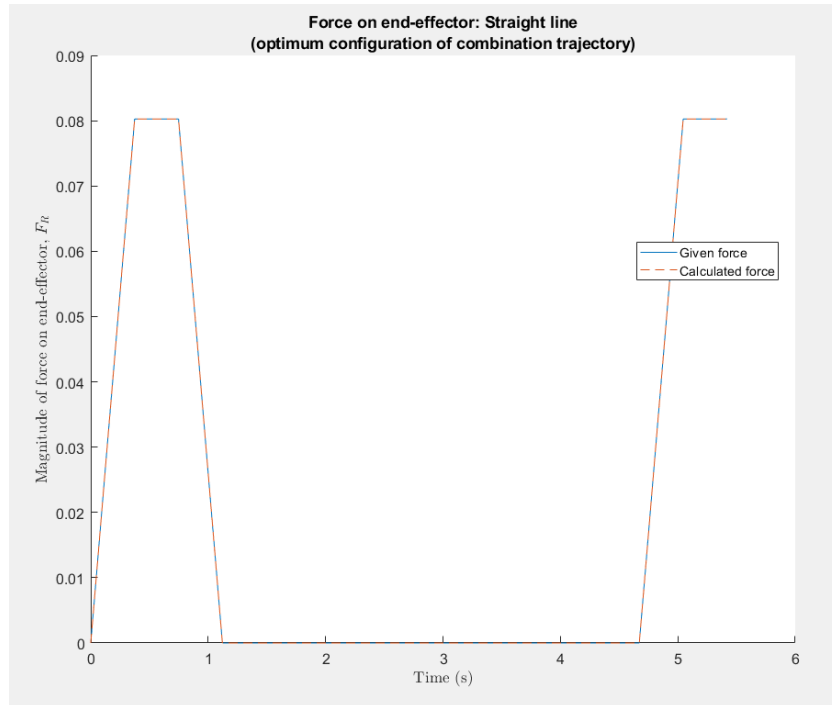


Figure 64. Given and calculated force for a straight-line trajectory
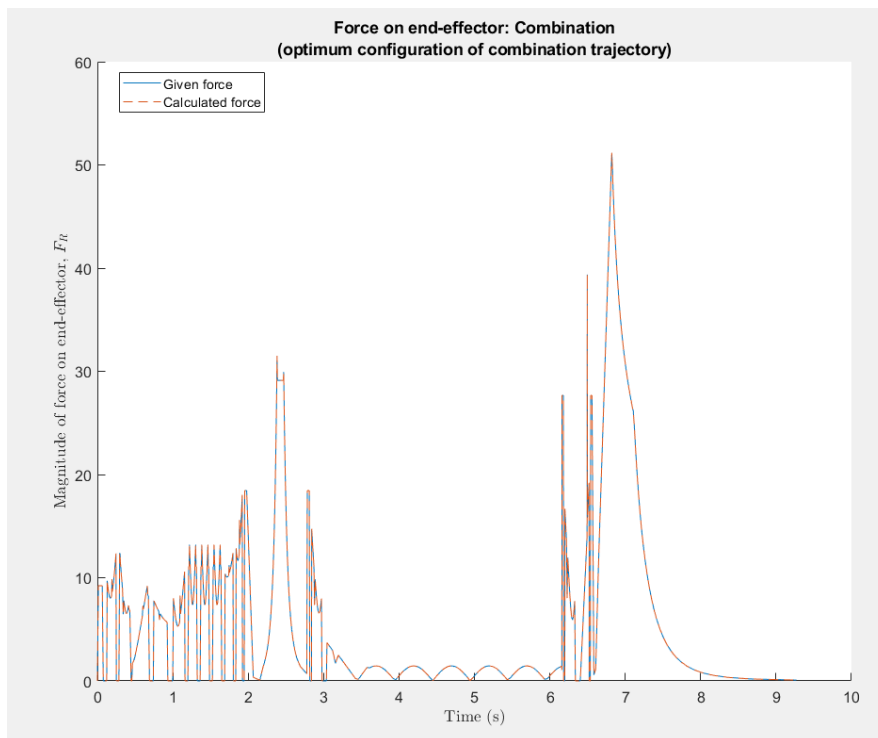


Figure 65. Forces comparison for a combined trajectory
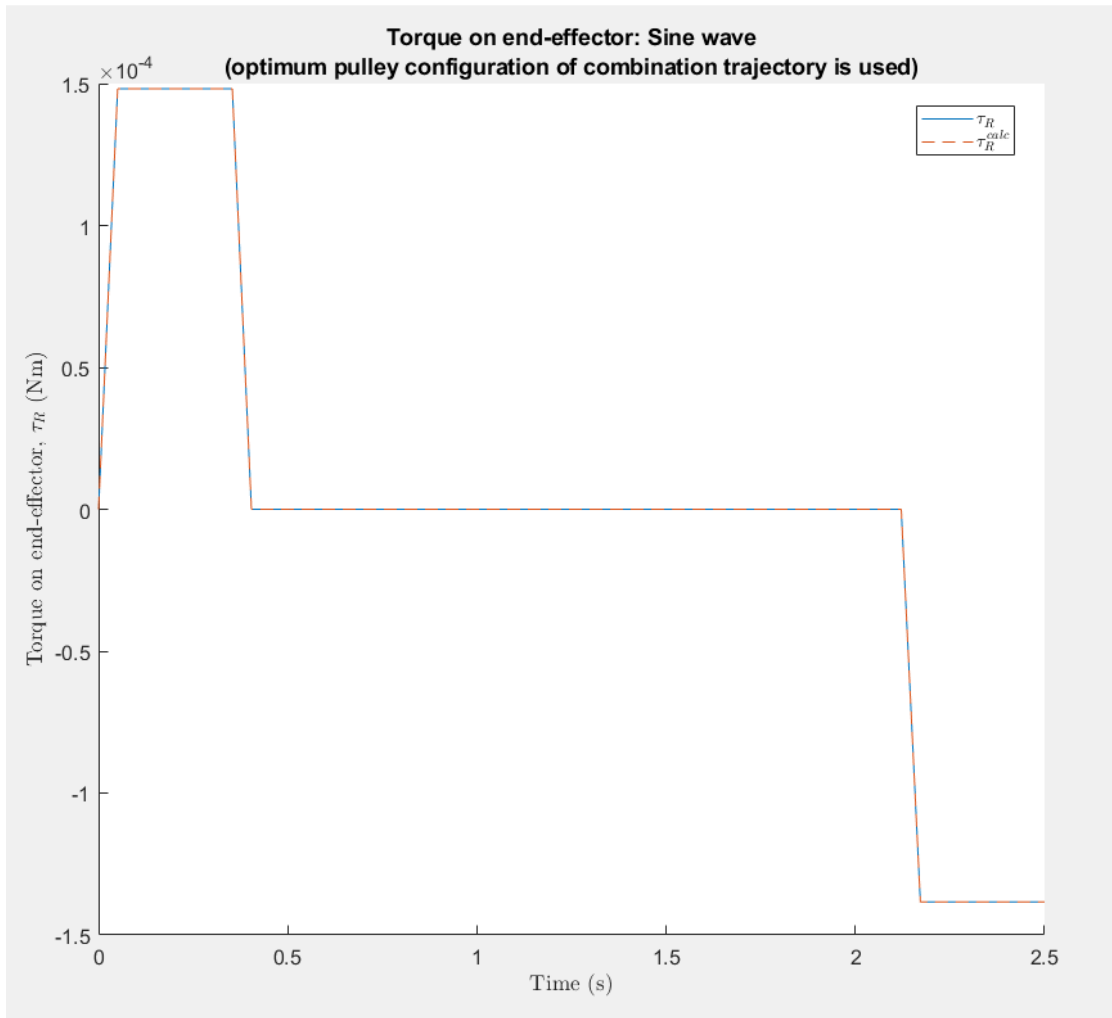
Figure 66. Sine wave torques

Table 6. Forces and torques maximum error

| Optimum configuration | Maximum Error in Forces (N) | Maximum Error in torques (N.M) |
|---|---|---|
| Straight Line | $5.4879e^{-16}$ | $6.9389e^{-17}$ |
| Triangle | $7.3552e^{-16}$ | $7.5442e^{-17}$ |
| Square | $6.6613e^{-16}$ | $6.3886e^{-17}$ |
| Circle | $7.2164e^{-16}$ | $6.4252e^{-17}$ |
| Sine wave | $1.4211e^{-14}$ | $6.9882e^{-16}$ |
| Spiral | $7.5027e^{-16}$ | $6.3250e^{-17}$ |
| Combination | $2.1316e^{-14}$ | $1.8146e^{-15}$ |
| Custom | $4.9960e^{-16}$ | $6.9297e^{-17}$ |

Table 6 shows the maximum error of forces and torques for validation. As can be seen in Figure 66, the maximum error between the given and the calculated torque is almost null. Figure 67 shows all the maximum errors between the given and the calculated forces and torques for all optimum configurations when their corresponding trajectory is run.
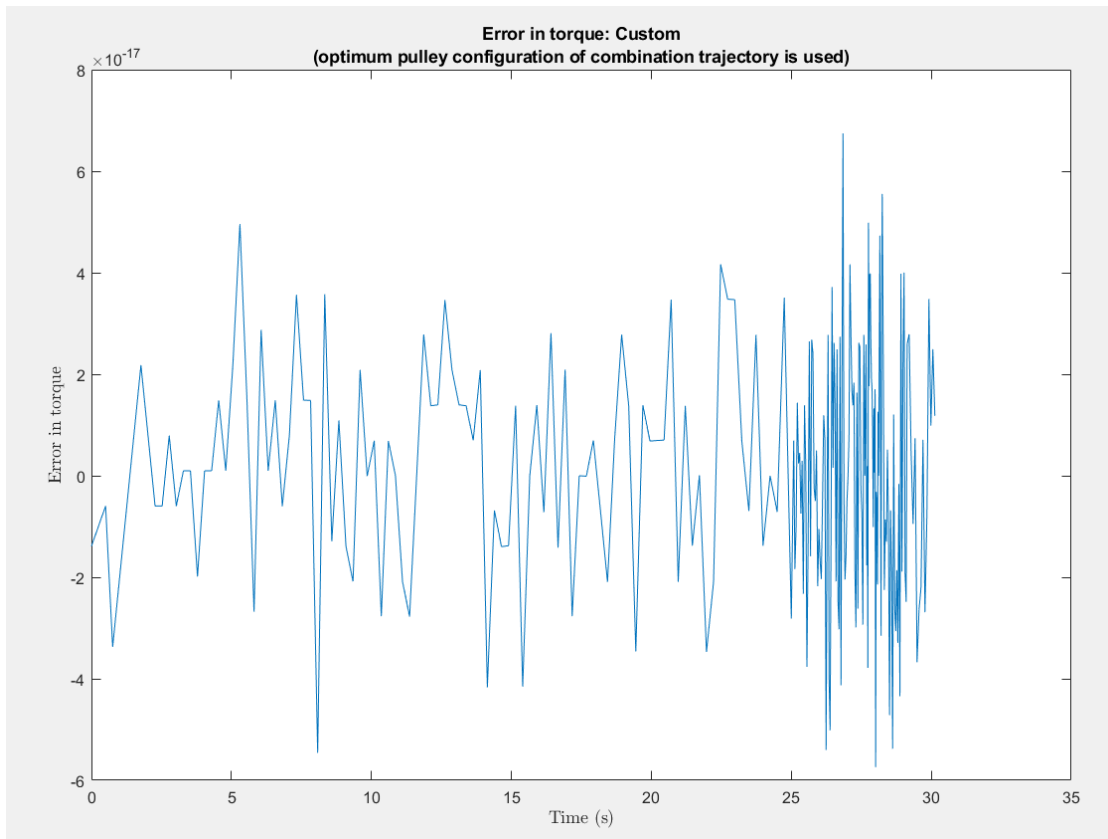


Figure 67. Error between output and calculated torques

Figure 67 shows the instantaneous error between the torques throughout the trajectory that was custom made to resemble the pattern used when printing a simple 3D object.

**5.2.3. Cable Tensions and behavior**. Figure 68 shows the difference between the instantaneous tensions when using the optimum cables' attachment point against the default basic model where the cables are attached to the corners of the platform. All the cables showed less tensions when using the optimum configuration than the default one. Solid lines correspond to the optimum configuration and dashed lines to the default one. To properly read the plot, cable 1 (solid line) should be compared to cable 1

(dashed line) and so on. Note that none of the cables tensions in both configurations dropped below 0.5 N which is necessary to maintain control over the end-effector. This validates the Kernel vector approach adopted in Eq. 15. Similarly, when using the optimum configurations for a specific trajectory, the cables' tensions when compared to the default configuration showed less tensions in most cases. However, the total tensions were always less than that of the default configurations. Due to the high number of simulations, all the other plots of cables' tensions comparisons will not be shown. Instead, an instantaneous cumulative sum concatenated after each step is shown for some cases as in Figure 69 which corresponds to the sum of the 4 cables' tensions. Figure 68 shows the individual cable's tensions for a straight-line trajectory.
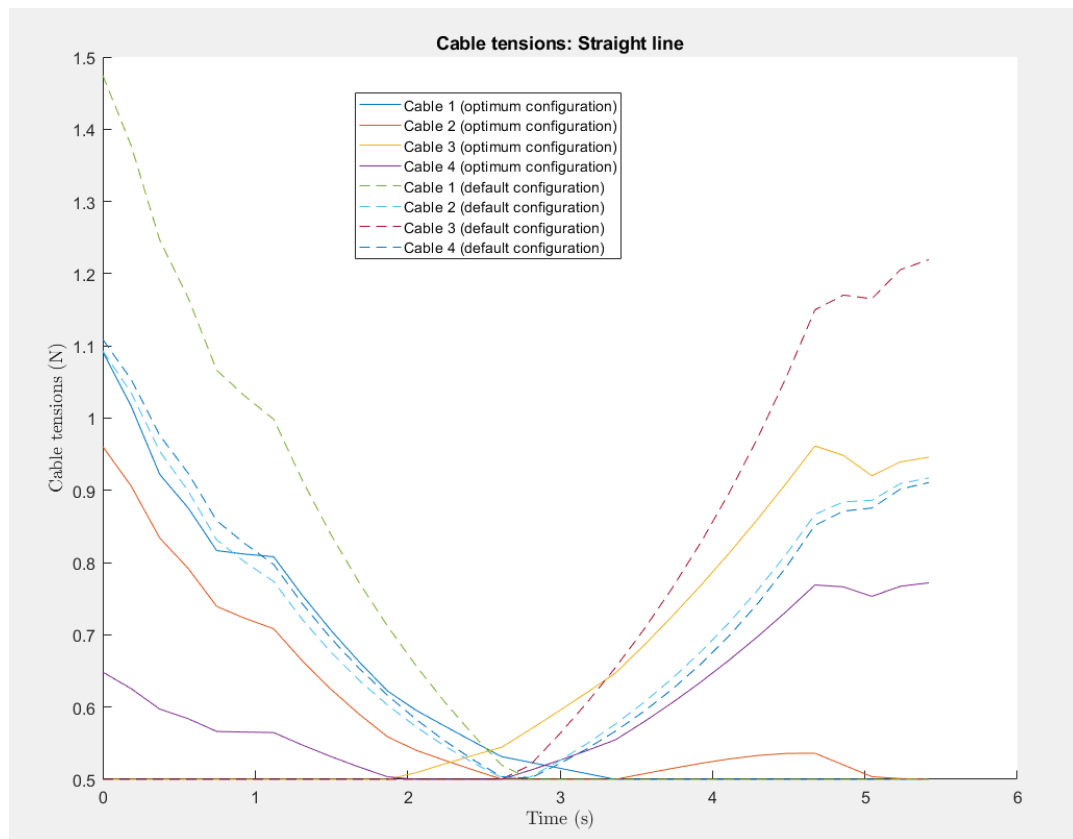


Figure 68. Optimum vs default cables' tensions

As can be seen in Figure 69, the cumulative sum (solid line) is never above the dashed line, which means that the summation of the tensions is less in the optimum configuration than that of the default one. This plot is easier to read than the previous one since only one value is being shown. The velocity profile in Figure 70 was created

to eliminate the jerk that happens when the velocity jumps from minimum to maximum instantaneously.
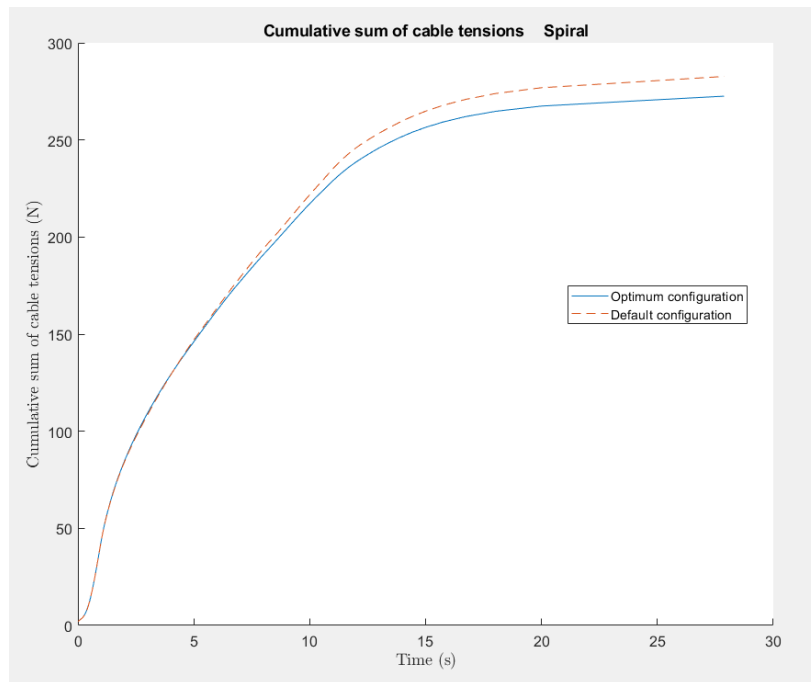


Figure 69. Cumulative sum of concatenated cables' tensions for a spiral trajectory
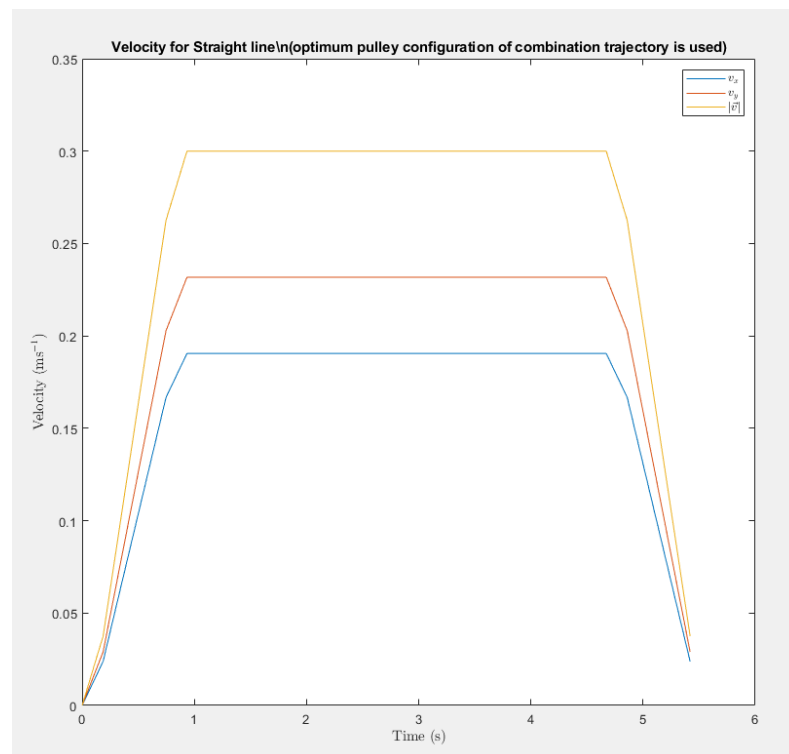


Figure 70. Velocity profile for a straight-line trajectory

A semi-trapezoidal geometry was created using the parametric equations of a straight line for $v_x$ and $v_y$, thus forming the velocities shown in Figure 70. Furthermore, the maximum velocity was limited to $0.3 \frac{m}{s}$ arbitrarily. This value however can be changed based on the datasheet of the actuators being used.
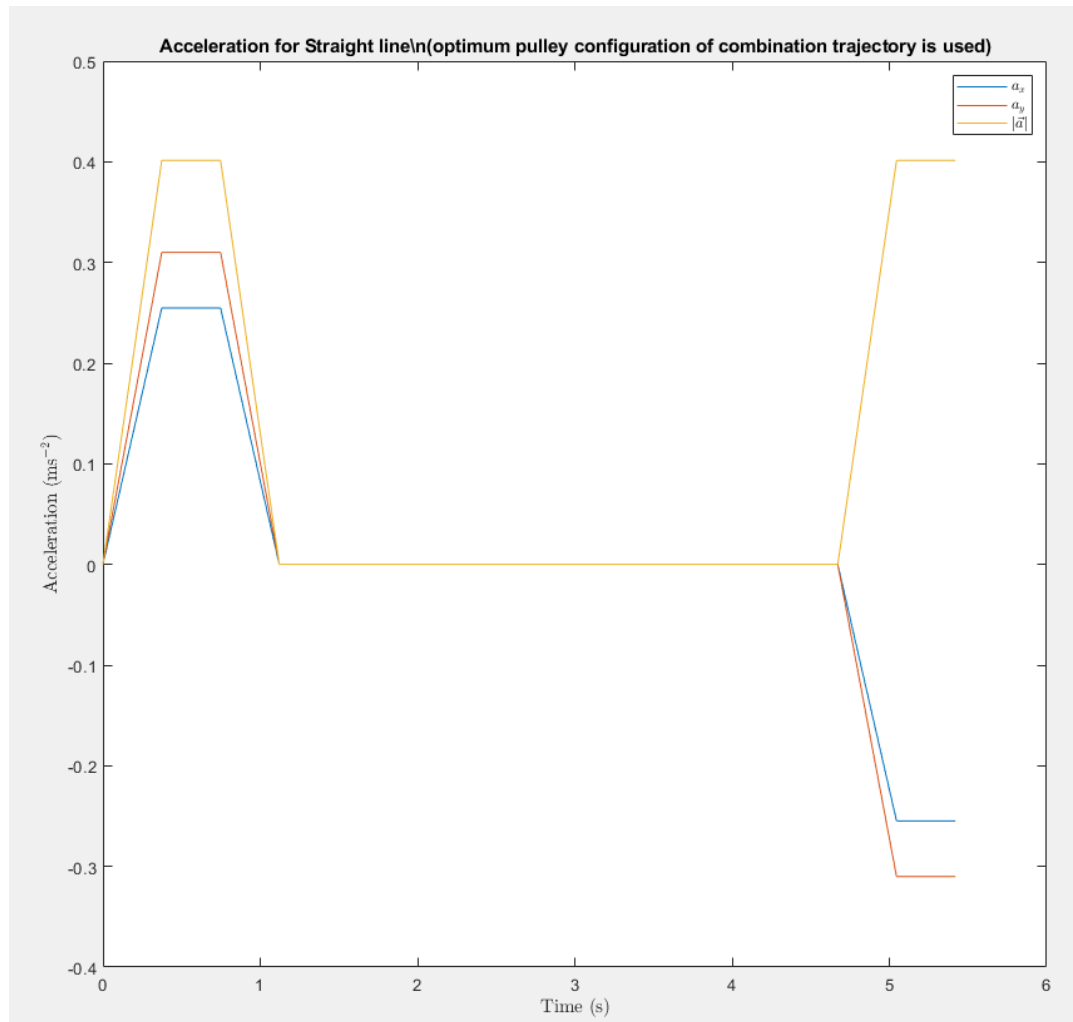


Figure 71. Acceleration of the end effector

Similarly, the acceleration guarantees that the end-effector reaches maximum velocity smoothly. Figure 71 shows the acceleration profile for a straight-line trajectory. When the maximum velocity is achieved at approximately *t=1.1s*, the acceleration remains constant until it reaches the region where the end-effector slows down to come to a complete stop at the destination. These two profiles have been created for every trajectory simulated. A total of 7 simulations for each optimum model configuration were carried out in addition to the default model making it 72 simulations.

Given the angular rotation of the end-effector shown in Figure 72, the pose becomes $X = [x\ y\ \phi]$ at any given point in the trajectory. The final value of $\phi$ is 15 ° for every trajectory created in order to show the results when the value of the third DOF is not 0.
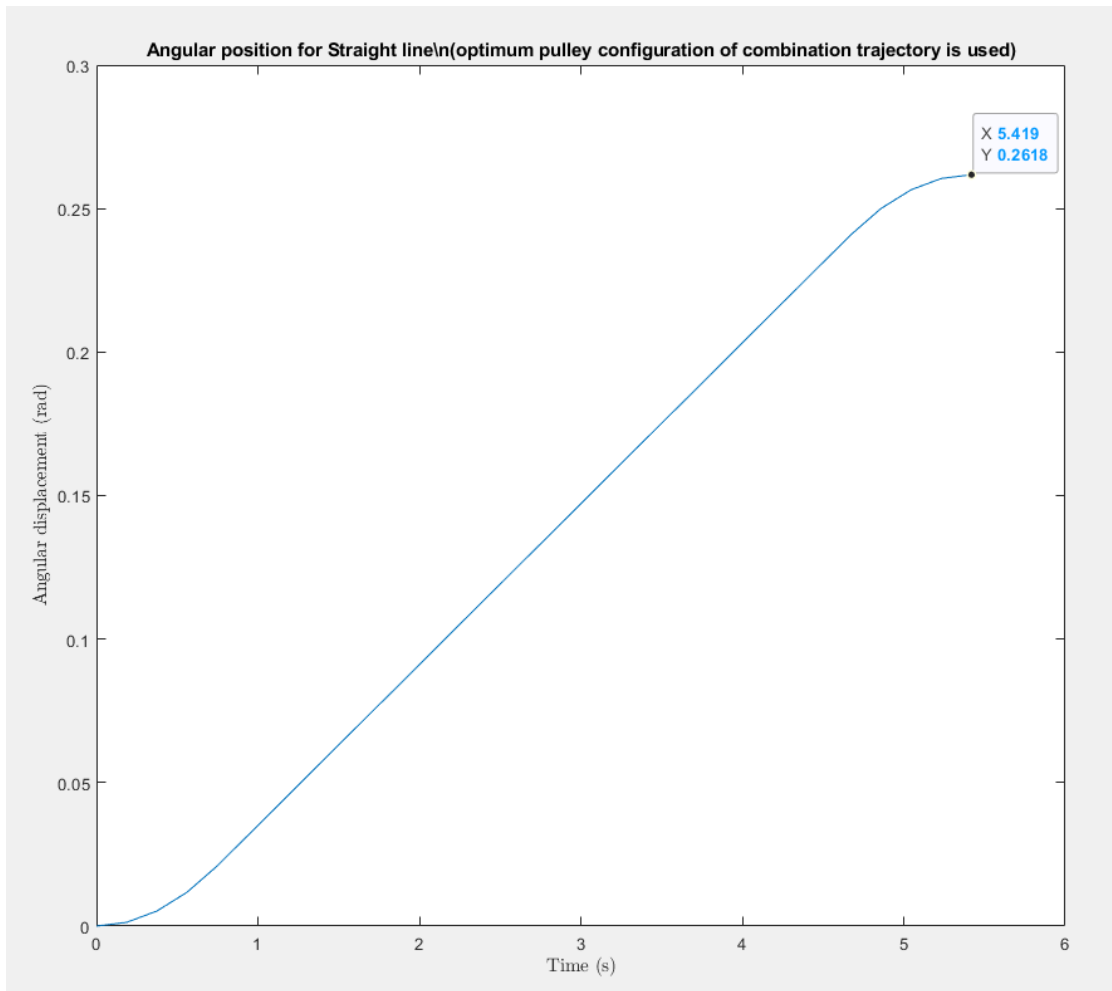


Figure 72. End-effector angular rotation $\phi$

As shown in Figure 56 and Figure 57, the sharp edges of the triangle and the square were smoothened using the MATLAB built in function *round*. The number of points is determined by the *smoothLengthPercent,* which is one of the input parameters of the system. The speed profiles for both trajectories are shown in  Figure 73.

The angular position of the end-effector depends on the angular velocity profile. Similarly, the angular velocity is created in a semi-trapezoidal shape throughout the whole trajectory to avoid the spike behavior the end-effector motion exhibits when the

86

speed plummet instantaneously. This profile is common for most simple trajectories, such as, straight line, circle, etc.
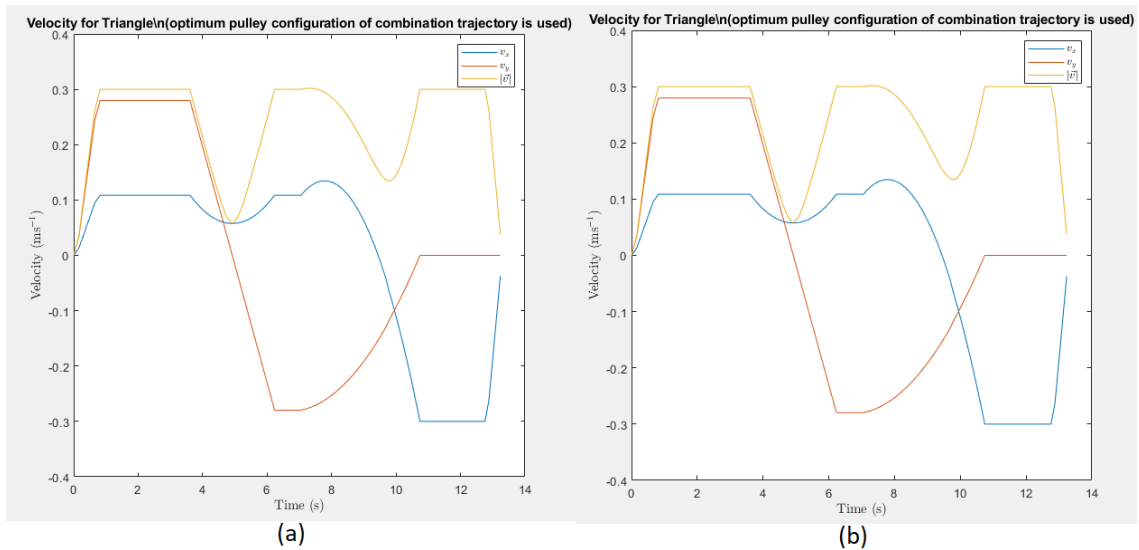


Figure 73. Speed profiles of a triangular and square trajectories

After all the data has been collected from the simulations, a comprehensive analysis and comparison was carried out. As will be shown in the next section, the results have been analyzed from multiple angles to show the effectiveness and the efficiency of this study.

## 5.3.    Comprehensive Analysis and Comparison

To validate the efficiency of the optimum pulley configurations obtained, a comprehensive analysis of the obtained results was carried out in two stages. First, the total tensions in all the cable when the CDDR is following all the trajectories are presented. Note that each optimum configuration was run with all the trajectories. The number of trajectories simulated are 8, creating one optimum configuration for each trajectory. The total number of simulations is the number of the optimum models in addition to the default basic configuration (a total of 9) creating a total of 72 simulations. As discussed before, it is not possible to show all the results because each trajectory has a number of plots corresponding to its speed profile, acceleration profile, instantaneous torques, etc., that is why few chosen samples have been presented and analyzed.

Table 7. Total cables' tensions in N for each trajectory simulation

| Config/Traj | Straight line | Triangle | Square | Circle | Sine wave | Spiral | Combination | Custom |
|---|---|---|---|---|---|---|---|---|
| Default | 87 | 277 | 381 | 199 | 1729 | 283 | 12399 | 564 |
| Straight line | 74 | 273 | 347 | 188 | 1784 | 282 | 12584 | 542 |
| Triangle | 80 | 237 | 346 | 188 | 1719 | 283 | 12629 | 578 |
| Square | 76 | 245 | 327 | 178 | 1745 | 273 | 12441 | 535 |
| Circle | 76 | 245 | 327 | 178 | 1744 | 273 | 12439 | 535 |
| Sine wave | 81 | 246 | 348 | 186 | 1706 | 275 | 12577 | 555 |
| Spiral | 77 | 244 | 330 | 179 | 1729 | 273 | 12450 | 538 |
| Combination | 98 | 383 | 460 | 229 | 1750 | 301 | 12241 | 581 |
| Custom | 83 | 266 | 343 | 186 | 1806 | 276 | 12600 | 534 |

Since the straight-line trajectory is the shortest and the one that has the least number of points, it is evident that the summation of the tensions in column two will be less than all the other tensions unlike that of the Combination column which combines all the trajectories in one and has the highest sum. Reading Table 7 is a bit tedious since all the numbers are mixed and have no easy reference to see. However, the most important values are the ones corresponding to their own optimum configuration which will be the smallest value in that column. For example, the smallest sum in the straight-line trajectory column (column 2) is the one corresponding to the straight-line optimum configuration which was 74 N. Following the same logic, the minimum values can be obtained as such.

To easily read the data, the values in Table 7 have been compared to the sum of cables' tensions in the default configuration taken as 'reference' for this case and the percentage difference was shown. When the percentage is less than 0%, then the sum of tension of that configuration is less than that of the default configuration also referred to as reference.

As can be seen in Table 8, the lowest percentage change in each column is corresponding to the optimum configuration of that trajectory. This means that the optimization algorithm has reduced the total tensions based on the objective function as stated in the methodology section.

The best results can be seen when applying simple geometrical trajectories, such as a straight line, a triangle, a circle and a square, which ranges between -10.5% up to -14%. For instance, the optimum configuration obtained when the model is optimized

for a square trajectory is shows best results when it is applied for that particular trajectory. The values are collected in Table 10.

Table 8. Percentage change compared to the default configuration

| | Straight line | Triangle | Square | Circle | Sine wave | Spiral | Combination | Custom |
|---|---|---|---|---|---|---|---|---|
| **Default** | | | | | | | | |
| **Straight line** | **-13.97** | -1.57 | -8.98 | -5.48 | 3.17 | -0.11 | 1.50 | -3.96 |
| **Triangle** | -7.92 | **-14.60** | -9.33 | -5.75 | -0.58 | -0.02 | 1.86 | 2.34 |
| **Square** | -12.66 | -11.59 | **-14.27** | -10.57 | 0.90 | -3.54 | 0.34 | -5.25 |
| **Circle** | -12.61 | -11.58 | -14.24 | **-10.57** | 0.87 | -3.53 | 0.33 | -5.24 |
| **Sine wave** | -6.15 | -11.20 | -8.79 | -6.68 | **-1.35** | -2.58 | 1.44 | -1.62 |
| **Spiral** | -11.27 | -11.80 | -13.41 | -9.99 | -0.04 | **-3.60** | 0.41 | -4.60 |
| **Combination** | 13.62 | 38.15 | 20.70 | 15.18 | 1.18 | 6.45 | **-1.27** | 2.97 |
| **Custom** | -4.61 | -4.02 | -9.99 | -6.58 | 4.42 | -2.37 | 1.62 | **-5.42** |

Table 9. Optimum trajectory vs default configuration tensions

| Trajectory | Sum of tensions (optimum configuration) | Sum of tensions (default configuration) | % change |
|---|---|---|---|
| Straight line | 74.4 | 86.5 | -14.0 |
| Triangle | 236.7 | 277.1 | -14.6 |
| Square | 327.0 | 381.4 | -14.3 |
| Circle | 178.2 | 199.2 | -10.6 |
| Sine wave | 1706.0 | 1729.4 | -1.4 |
| Spiral | 272.5 | 282.7 | -3.6 |
| Combination | 12240.8 | 12398.5 | -1.3 |
| Custom | 533.7 | 564.3 | -5.4 |

Similarly, for all other trajectories, each corresponding optimum configuration will result in the least total cables' tensions compared to other configurations as shown in Table 9.

This percentage is represented in Eq. 16.

$$\% \, change = \frac{Optimized - Reference}{Reference} \times 100 \qquad (18)$$

Based on Eq. 18, the 'Reference' is the total sum of cables' tensions of the output the 'Optimized' is being compared to. Several references have been chosen to make a general comparison between models.

Table 10 shows the percentage change of the grand total for all 7 trajectories when simulated using all optimum configurations separately. The 'combined trajectory' has been eliminated from the grand total since it is a combination of all the other trajectories. Compared to the default configuration of the CDDR shown in Figure 37, all the other configurations showed better results. The grand total of all 7 trajectories across all 7 optimum configurations are less than that of the default configuration ranging from -0.8% down to -4.3%. This proves that the optimized configurations perform better than the default configuration for most general trajectories.

The grand total of tensions was also compared to that when using the straight-line optimum configuration. Unlike Table 10, the results showed some positive values since the configuration we are comparing to is already using an optimized model.

Table 10. General comparison with default model

| Configuration | Grand total of tensions | Grand total of tensions (default configuration) | % change |
|---|---|---|---|
| Straight line | 3491.2 | 3520.6 | -0.8 |
| Triangle | 3429.3 | 3520.6 | -2.6 |
| Square | 3378.0 | 3520.6 | -4.1 |
| Circle | 3377.8 | 3520.6 | -4.1 |
| Sine wave | 3397.6 | 3520.6 | -3.5 |
| Spiral | 3370.2 | 3520.6 | -4.3 |
| Custom | 3493.3 | 3520.6 | -0.8 |

However, these positive percentages are less than 1%. The results are shown in

Table 11. The values obtained in Table 12 are all greater than or equal 0% except for a spiral optimum configuration. Based on Eq. 15, 0 % means equal performance, a positive percentage means that more tension was exerted by the cables and vice versa.

In conclusion, for each individual optimum configuration, the best performance (lowest sum of tensions) was for the corresponding trajectory of optimization. When an

overall comparison was carried out, all trajectories were ran on all optimum configurations and a comprehensive analysis showed that the most efficient design (configuration) was for optimum configuration corresponding to a square, a circle and a spiral. Based on the location of the attachment points, the corners of the outer edges of the optimization region are most suitable for the attachment points for all common trajectories.

Table 11. General comparison with Straight-line optimized model

| Configuration | Grand total of tensions | Grand total of tensions (straight line optimum configuration) | % change |
|---|---|---|---|
| Default configuration | 3520.62 | 3491.16 | 0.84 |
| Straight line | 3491.16 | 3491.16 | 0.00 |
| Triangle | 3429.35 | 3491.16 | -1.77 |
| Square | 3378.02 | 3491.16 | -3.24 |
| Circle | 3377.79 | 3491.16 | -3.25 |
| Sine wave | 3397.59 | 3491.16 | -2.68 |
| Spiral | 3370.21 | 3491.16 | -3.46 |
| Custom | 3493.35 | 3491.16 | 0.06 |

Table 12. General comparison with a square optimized model

| Configuration | Grand total of tensions | Grand total of tensions (square optimum configuration) | % change |
|---|---|---|---|
| Default configuration | 3520.6 | 3378.0 | 4.2 |
| Straight line | 3491.2 | 3378.0 | 3.3 |
| Triangle | 3429.3 | 3378.0 | 1.5 |
| Square | 3378.0 | 3378.0 | 0.0 |
| Circle | 3377.8 | 3378.0 | 0.0 |
| Sine wave | 3397.6 | 3378.0 | 0.6 |
| Spiral | 3370.2 | 3378.0 | -0.2 |
| Custom | 3493.3 | 3378.0 | 3.4 |

## 5.4. Fmincon Algorithms

[49] introduces the optimization algorithms that Fmincon utilizes. In this section, three different algorithms will be compared based on the results the Fmincon

produces. The three algorithms are Interior point, Sequential Quadratic Programming (SQP) and Active Set.
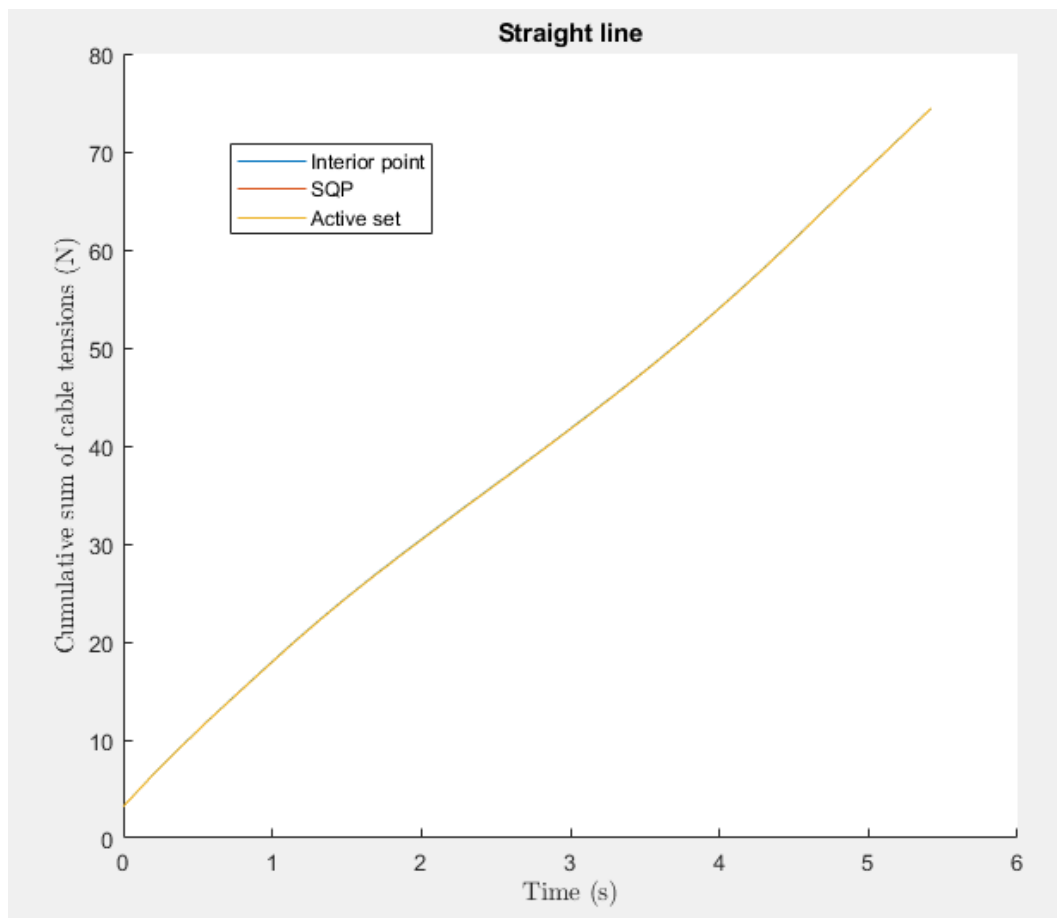


Figure 74. Fmincon algorithms for a straight-line trajectory

Figure 74 and Figure 75 show the cumulative sum of tensions when the configuration of the CDDR is being optimized to follow a straight-line and square trajectories respectively. It is obvious that there is no noticeable difference between the tensions for all the algorithms used.

Similarly for a square trajectory, the optimization algorithms performs the same creating the same cumulative optimum cables' tensions when the end effector is following a square trajectory.

Hence, the default option was selected to be used for the optimization run for all other trajectories due to its flexibility to handle a wide range of problems making it a large-scale algorithm.
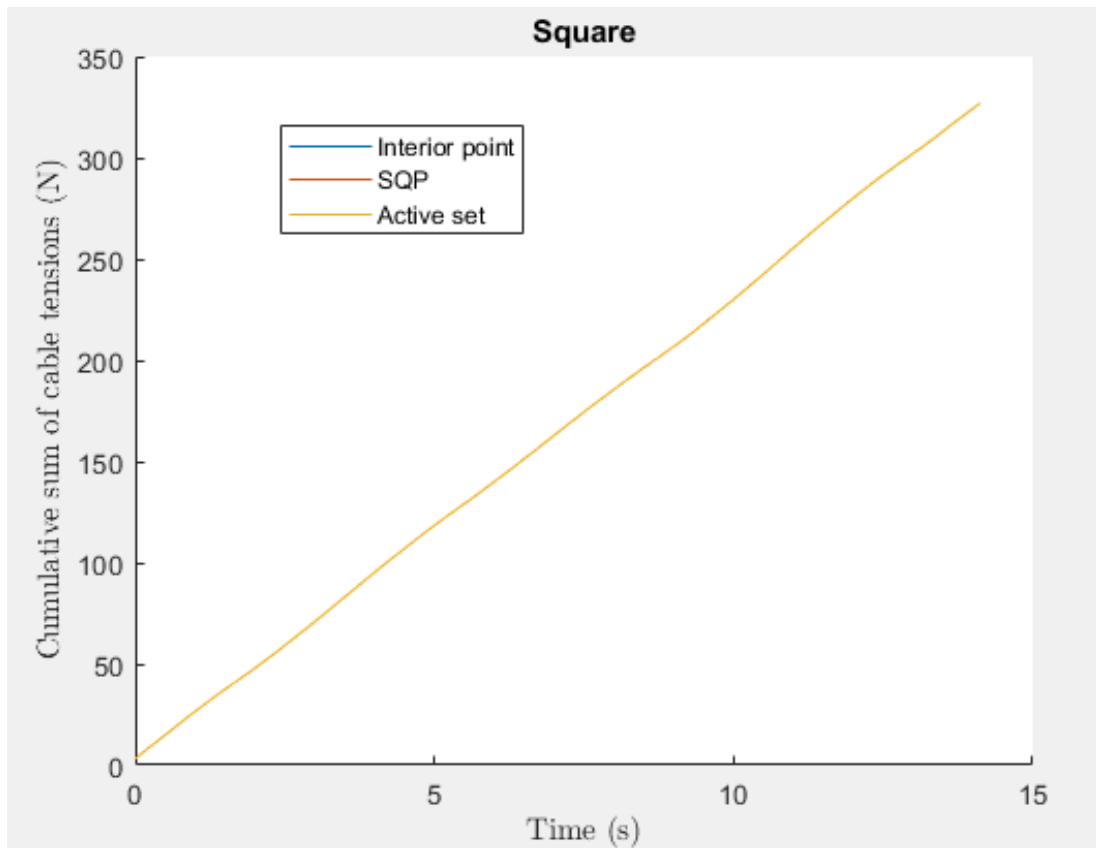
Figure 75. Fmincon algorithms for a square trajectory

## 5.5. Other Algorithms

There are several algorithms that can be used for optimization. Some are case-specific where the problem is either constrained, non-constrained, linear or non-linear. These algorithms are explained in [63]. Three were selected that fit the characteristics of our problem and can give us results. In this thesis, three algorithms' performance will be compared. These algorithms are Fmincon, Least Square Algorithm (LSQ), and Genetic Algorithm (GA). For the LSQ, the non-linear option was selected based on our problem, which is non-linear, making the algorithm option *lsqnonlin*.

As can be seen in Figure 76, all the algorithms give almost the same results with Fmincon being slightly more efficient since the cumulative sum of tensions for a straight-line trajectory using the Fmincon algorithm is better with a very small difference compared to the other algorithms.

93

To verify the performance of these algorithms for individual cables, each cable's tension when the algorithms are run separately is shown in Figure 77. The solid lines represent the cable's tension when the Fmincon algorithm is being used.

Similarly, a spiral trajectory shows that all the algorithms are performing the same as shown in Figure 80. If we look at each individual cable's tension for this trajectory, it is noticed that in some regions, LSQ is performing than the other algorithms and in other regions of the trajectory, Fmincon would be performing better. This means that for more complicated trajectories, LSQ will perform better than Fmincon in some region and vice versa. Figure 81 shows individual cable's tensions to confirm the above.
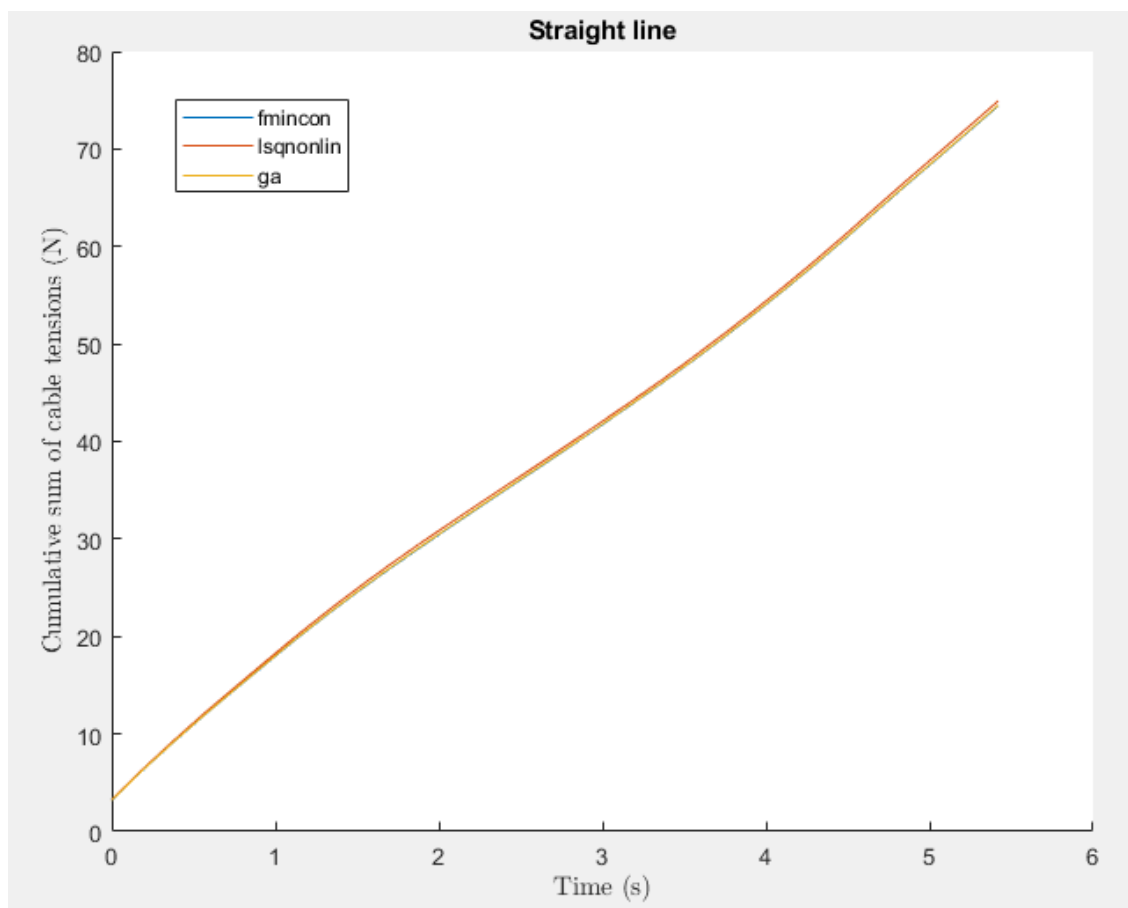


Figure 76. Cumulative tension for a straight-line trajectory with three algorithms

Figure 76 and Figure 77 refer to the cumulative cables' tensions and individual cable's tensions for a straight-line trajectory.
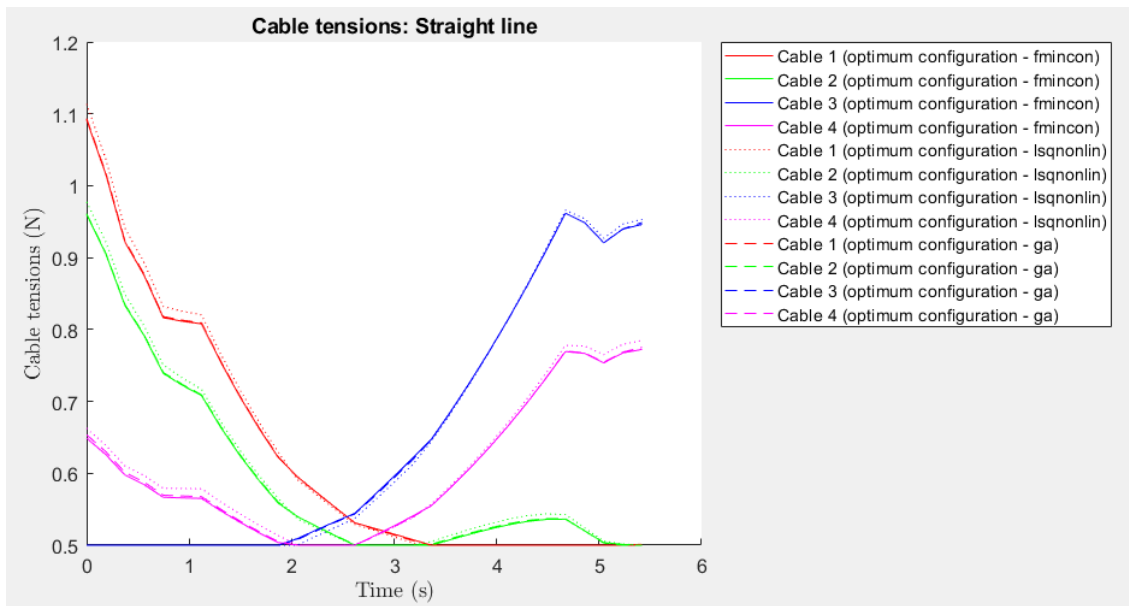
Figure 77. Cables' tensions for a straight-line trajectory
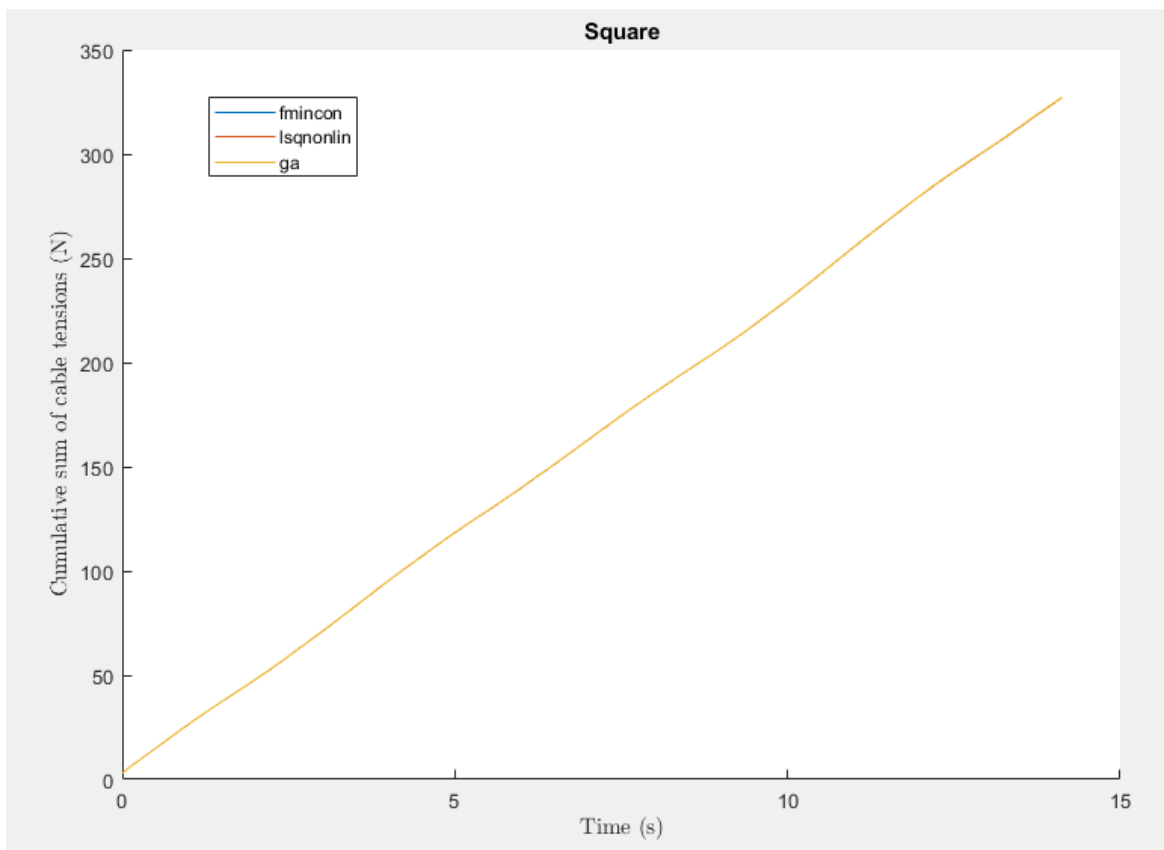


Figure 78. Cumulative tension for a square trajectory with three algorithms

Figure 78 and Figure 79 refer to the cumulative cables' tensions and individual cable's tensions for a square trajectory.
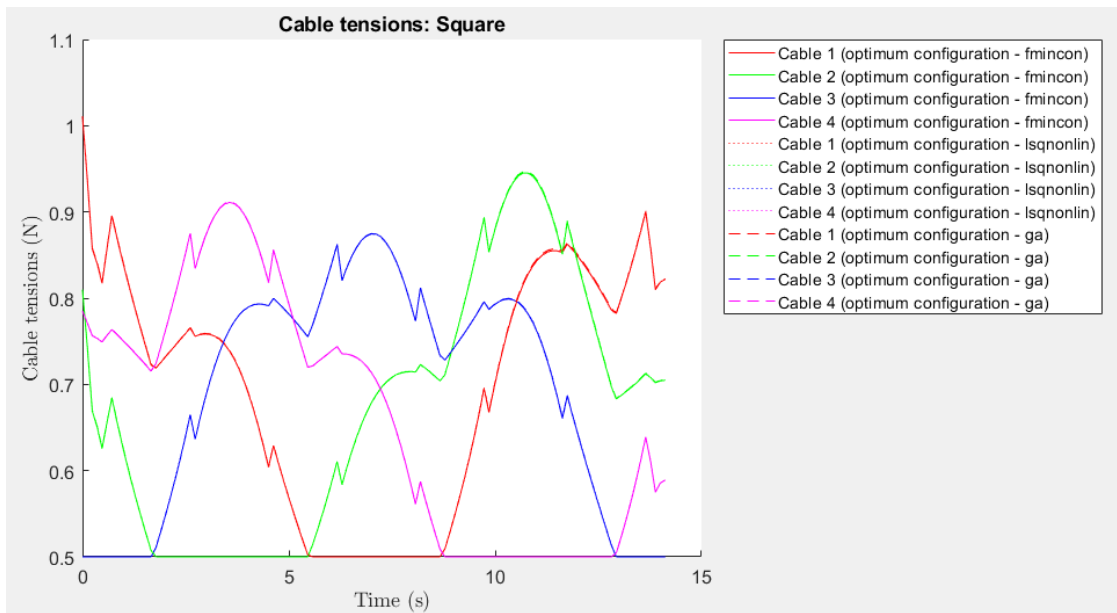
Figure 79. Cables' tensions for a square trajectory
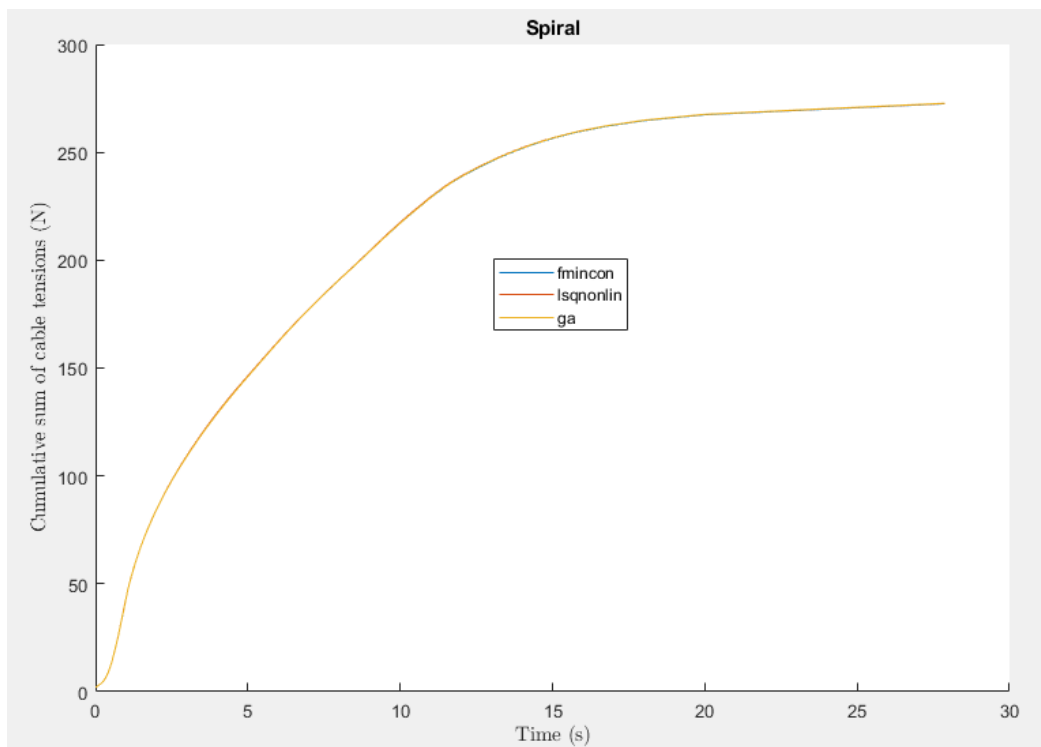


Figure 80. Cumulative tension for a spiral trajectory with three algorithms

Figure 80 and Figure 81 show almost identical cumulative and cables' tensions for all the algorithms respectively. This is to ensure that the Fmioncon algorithm which will be used with all the trajectories is performing as good as the other algorithms in the least if not better.

96
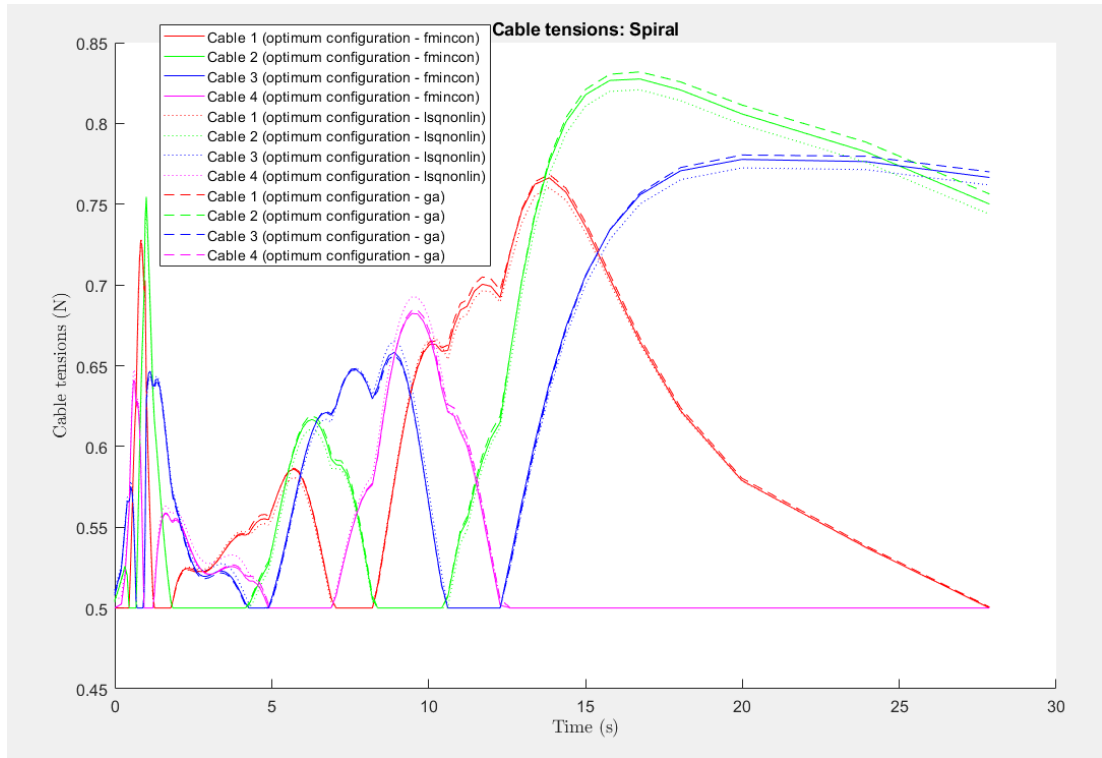
Figure 81. Cables' tensions for a spiral trajectory

Based on all the results in this section, Fmincon algorithm proves to be the most efficient algorithm to be used with all the other trajectories.

Table 13. Algorithms comparison

| | Trajectory | Algorithm | | | Sum of tensions (default configuration) | Average % change |
|---|---|---|---|---|---|---|
| | | Fmincon | Laqnonlin | GA | | |
| | Straight line | 74.48 | 74.92 | 74.48 | 87 | -15 |
| | Square | 327 | 327 | 327.1 | 381 | -14 |
| | Spiral | 272.5 | 272.6 | 272.7 | 283 | -3.6 |
| Total | | 673.98 | 674.52 | 674.28 | 751 | |
| Average % change per algorithm | | -10.26 | -10.18 | -10.21 | | |

As shown in Table 13, the algorithms are performing almost the same for the total tensions in the cables for the 3 trajectories which are square, straight line, and spiral.

# Chapter 6. Conclusion and Future Work

## 6.1.    Conclusion

Several researchers have studied different aspects of the cable-direct-driven robot to improve its performance, response, and control. This study focused on a slightly different aspect which targeted the design, especially the attachment points of the cables.

The simulation of the basic models was carried out using CASPR platform under MATLAB, where two 2-DOF CDDRs with a point-mass end-effector; one with 3 cables and the second with 4 cables; were created and simulated for a straight-line and a square trajectory. The results were investigated and compared to prove that each model has its advantages and disadvantages based on the trajectory. The 4-cables model allows a larger workspace, but its modeling and control proves more tedious.

MATLAB was used to create a 3 DOF CDDR with 4 cables where the end-effector is a rectangular platform. Based on previous studies, the attachment points of the cables at the end-effector side were chosen to be crossed for three main reasons. First, it allows more control over the 3$^{rd}$ DOF, which is a rotation around the z-axis, and second, it eliminates uncertainties from the model and creates less computationally exhaustive calculations. Finally, it allows a larger wrench feasible workspace (WFW).

Several trajectories were created with smooth edges when there is a sharp turn. A speed profile for each trajectory was created such that the motion is not abrupt, and the end-effector speeds up and slows down at the beginning and end of each motion.

The attachment points at the base-frame were optimized using an optimization algorithm under MATLAB for each trajectory, separately. The objective function of the optimization algorithm is the summation of all cables' tension exerted by the cables to be minimized when the end-effector is following a certain trajectory. After that, all the trajectories, including the custom and the combined trajectories, were run across all 7 optimum configurations for further comparison.

The results showed that for each trajectory, its corresponding optimum configuration produced the least sums of tensions for that specific motion. For instance, an optimum configuration based on a straight-line trajectory will exert the least cables'

tensions when the trajectory is a straight line when compared to all other case-specific optimum configurations. Since the exact model and configuration of the cable robot model is a result of the optimization algorithm, it is possible to compare the results with studies that has targeted this particular aspect of the problem, but none were found focusing on the anchor points at the base-frame.

On the other hand, a comprehensive comparison when a random trajectory is being followed on any optimum configuration showed different results. All the optimum configurations are more efficient than the default configuration for almost any random trajectory, however, each optimum configuration cannot be used as a general case except for 3 cases, the spiral optimum configuration, the square and the circle. Due to their symmetry, the resulting optimum configurations were almost identical and when other random trajectories are used, it still needed lower overall tensions.

## 6.2. Future Work

Different aspects of CDDR can be focused on in further studies. In our case, the most relevant future work to this thesis is presented in this section. The improvements can be made on the following parts.

1. Trajectory creation. Creating trajectories was extremely time consuming. An interactive GUI could be introduced in further studies which allows the user to either draw or select from a set of existing trajectories. The created or chosen trajectory can then be added as a vector with a velocity and acceleration profile to create a smooth motion.
2. The velocity profiles could be created using a more efficient method, such as a quantic spline polynomial approach.
3. The optimization could be applied to more than one design and different models. CDDR with 6 or 8 cables can be targeted, which will allow the control of more degrees of freedom.
4. Dynamic modeling can be incorporated taking into consideration the friction in the system. This will help control the system when an experimental setup is developed.
5. Other objective functions can be added to the optimization algorithm and more constraints as well in order to create a more accurate representation of CDDRs when all constraints are accounted for.

# References

[1] J. Albus, R. Bostelman, and N. Dagalakis, "NIST SPIDER, A Robot Crane," *J. Res. Natl. Inst. Stand. Technol.*, vol. 97, no. 3, pp. 373–385, 1992.

[2] W. Xiaoguang and L. Qi, "Numerical investigation on a cable-driven flight simulator with high-G acceleration capability," in *IEEE International Conference Robotics Biomimetics, ROBIO*, 2017, pp. 2212–2217.

[3] S. Gharatappeh, H. J. Asl, and J. Yoon, "Design of a novel Assist-As-Needed controller for gait rehabilitation using a cable-driven robot," in *International Conference Ubiquitous Robots Ambient Intelligence, URAI*, 2016, pp. 342–347.

[4] Q. Yang, J. Niu, and R. Song, "Admittance control of a 3-DOF cable-driven rehabilitation robot for upper-limb in three dimensional workspace," in *2nd International Conference Advanced Robotics Mechatronics, ICARM*, 2017, no. 2015, pp. 445–449.

[5] P. Rico, R. L. W. Ii, and D. Ph, "Five-Hundred Meter Aperture Spherical Radio Telescope (FAST) Cable-Suspended Robot Model and Comparison with the Arecibo Observatory," *Internet Publication*, 2015. https://www.ohio.edu/mechanical-faculty/williams/html/pdf/FAST.pdf (accessed Jul. 15, 2020).

[6] H. Li and G. Pan, "Simulation on High-Speed-Shaft-Rupture-Induced Shock Vibration of a Cable-Driven Parallel Robot of FAST," *Zhendong yu Chongji/Journal Vib. Shock*, vol. 36, pp. 75–82, 2017.

[7] J. Hao, F. Jing, G. Yang, Z. Liang, and L. Zhu, "Modeling, Control and Software Implementation of Astronomical Tracking of Focus Cabin Suspension of FAST," in *IEEE International Conference Robotics Biomimetics, ROBIO*, 2013, pp. 686–691.

[8] M. Filipovic and A. Djuric, "Mathematical Model of the Aerial Robotic Camera base on its Geometric Relationship," *FME Trans.*, vol. 42, no. 2, pp. 133–142, 2014.

[9] Max-Planck-Gesellschaft, "Seilroboter mit Passagier," 2015. https://www.mpg.de/9395107/seilroboter (accessed Jun. 26, 2020).

[10] E. Cabay, D. Culla, M. Rodriguez, and M. Barrado, "Large-Scale 3D Printing With Cable-Driven Parallel Robots," *Constr Robot*, vol. 1, no. 1–4, pp. 69–76, 2017.

[11] X. Wang and S. Bhattacharya, "A Topological Approach to Workspace and Motion Planning for a Cable-Controlled Robot in Cluttered Environments," *IEEE Robot. Autom. Lett.*, vol. 3, no. 3, pp. 2601–2607, 2018.

[12] P. Bosscher, A. T. Riechel, and I. Ebert-Uphoff, "Wrench-Feasible Workspace Generation for Cable-Driven Robots," *IEEE Trans. Robot.*, vol. 22, no. 5, pp. 890–902, 2006.

[13] M. Zamani, M. Karimi-Ghartemani, N. Sadati, and M. Parniani, "Design of a Fractional Order PID Controller for an AVR Using Particle Swarm

Optimization," *Control Eng. Pract.*, vol. 17, no. 12, pp. 1380–1387, 2009.

[14] N. Zhang, W. Shang, and S. Cong, "Design and Analysis of an Under-constrained Reconfigurable Cable-Driven Parallel Robot," in *IEEE International Conference Cybernetics Intelligent Systems, CIS, Robotics, Automation and Mechatronics, RAM*, 2017, pp. 13–18.

[15] Y. Mao and S. K. Agrawal, "Design of a Cable-Driven Arm Exoskeleton (CAREX) for Neural Rehabilitation," *IEEE Trans. Robot.*, vol. 28, no. 4, pp. 922–931, 2012.

[16] H. Li, J. Sun, G. Pan, and Q. Yang, "Preliminary Running and Performance Test of the Huge Cable Robot of FAST Telescope," in *Mechanisms Machine Science*, 2018, pp. 402–414.

[17] Z. Zake, F. Chaumette, N. Pedemonte, and S. Caro, "Vision-Based Control and Stability Analysis of a Cable-Driven Parallel Robot," *IEEE Robot. Autom. Lett.*, vol. 4, no. 2, pp. 1029–1036, 2019.

[18] J. Yoon, S. W. Hwang, J. H. Bak, and J. H. Park, "Adaptive Control for Cable Driven Parallel Robots," in *International Conference on Control, Automation and Systems, ICCAS*, 2017, pp. 416–419.

[19] A. Alikhani and M. Vali, "Modeling and Robust Control of a New Large Scale Suspended Cable-Driven Robot Under Input Constraint," in *URAI 8th International Conference of Ubiquitous Robots Ambient Intelligence*, 2011, pp. 238–243.

[20] M. Zarebidoki, A. Lotfavar, and H. R. Fahham, "Dynamic Modeling and Adaptive Control of a Cable-Suspended Robot," in *Proceedings World Congress on Engineering, WCE*, 2011, pp. 2469–2473.

[21] L. Scalera, A. Gasparetto, and D. Zanotto, "Design and Experimental Validation of a 3-DOF Underactuated Pendulum-Like Robot," vol. 25, no. 1, pp. 217–228, 2020.

[22] B. Zi, B. Y. Duan, J. L. Du, and H. Bao, "Dynamic Modeling and Active Control of a Cable-Suspended Parallel Robot," *Mechatronics*, vol. 18, no. 1, pp. 1–12, 2008.

[23] J. Piao, J. Jung, J. O. Park, S. Y. Ko, and S. Park, "Analysis of Configuration of Planar Cable-Driven Parallel Robot on Natural Frequency," in *IEEE International Conference on Robotics and Biomimetics, ROBIO*, 2016, pp. 1588–1593.

[24] Y. Shen, H. Osumi, and T. Arai, "Manipulability Indices in Multi-wire Driven Mechanisms," in *Distributed Autonomous Robotic Systems*, 1994, pp. 359–360.

[25] A. L. I. Ghasemi, M. Eghtesad, and M. Farid, "WORKSPACE ANALYSIS OF REDUNDANT CABLE ROBOTS," *World Autom. Congr.*, vol. 32, pp. 1–6, 2008.

[26] X. Jin, D. I. Jun, X. Jin, S. Park, J. O. Park, and S. Y. Ko, "Workspace analysis of upper limb for a planar cable-driven parallel robots toward upper limb rehabilitation," in *International Conference Control, Automation Systems*, 2014,

no. Iccas, pp. 352–356.

[27] S. J. Torres-Mendez, J. R. Mendoza-Vazquez, V. Ramirez-Palacios, and I. D. Rojas-Cuevas, "Analytical Workspace Delineation of a Translational Underconstrained Cable-based Robot," *International Conference Electronics, Communications Computers, CONIELECOMP*. IEEE, pp. 1–7, 2017.

[28] B. Wang, B. Zi, S. Qian, and D. Zhang, "Collision free force closure workspace determination of reconfigurable planar cable driven parallel robot," in *Proceedings Asia-Pacific Conference Intelligent Robot Systems, ACIRS*, 2016, pp. 26–30.

[29] D. Lau, J. Eden, S. K. Halgamuge, and D. Oetomo, "Cable function analysis for the musculoskeletal static workspace of a human shoulder," *Mech. Mach. Sci.*, vol. 32, no. 2, pp. 263–274, 2015.

[30] C. P. Robot, "Dynamic Point-to-Point Trajectory Planning of a Two-DOF Cable-Suspended Parallel Robot," *J. Tissue Viability*, vol. 8, no. 2, p. 24, 2014.

[31] P. H. Borgstrom, B. L. Jordan, G. S. Sukhatme, M. A. Batalin, and W. J. Kaiser, "Rapid computation of optimally safe tension distributions for parallel cable-driven robots," *IEEE Trans. Robot.*, vol. 25, no. 6, pp. 1271–1281, 2009.

[32] L. Tang, X. Tang, X. Jiang, and C. Gosselin, "Dynamic trajectory planning study of planar two-dof redundantly actuated cable-suspended parallel robots," in *IEEE/RSJ International Conference Intelligent Robots Systems*, 2015, vol. 30, no. Iros, pp. 187–197.

[33] T. Rasheed, P. Long, A. S. Roos, and S. Caro, "Optimization based Trajectory Planning of Mobile Cable-Driven Parallel Robots," in *IEEE International Conference Intelligent Robots Systems*, 2019, pp. 6788–6793.

[34] A. Sharifi and H. D. Taghirad, "Online Time-Optimal Trajectory Planning in Dynamic Workspace of Cable Suspended Robots," in *2nd RSI/ISM International Conference Robotics Mechatronics, ICRoM*, 2014, pp. 239–244.

[35] S. Lahouar, E. Ottaviano, S. Zeghoul, L. Romdhane, and M. Ceccarelli, "Collision Free Path-Planning For Cable-Driven Parallel Robots," *Rob. Auton. Syst.*, vol. 57, no. 11, pp. 1083–1093, 2009, [Online]. Available: http://dx.doi.org/10.1016/j.robot.2009.07.006.

[36] N. Zhang, W. Shang, and S. Cong, "Dynamic Trajectory Planning For a Spatial 3-DoF Cable-Suspended Parallel Robot," *Mech. Mach. Theory*, vol. 122, pp. 177–196, 2018, doi: 10.1016/j.mechmachtheory.2017.12.023.

[37] A. B. Alp and S. K. Agrawal, "Cable suspended robots: Feedback controllers with positive inputs," in *Proceedings American Control Conference*, 2002, vol. 1, pp. 815–820.

[38] J. H. Bak, J. H. Yoon, S. W. Hwang, and J. H. Park, "Sliding-Mode Control of Cable-Driven Parallel Robots with Elastic Cables," in *International Conference Control, Automation Systems, ICCAS*, 2016, pp. 1057–1060.

[39] J. P. Merlet, "Simulation of Discrete-Time Controlled Cable-Driven Parallel Robots on a Trajectory," *IEEE Trans. Robot.*, vol. 33, no. 3, pp. 675–688, 2017.

[40] D. Guo and K. K. Leang, "Image-Based Estimation, Planning, and Control of a Cable-Suspended Payload for Package Delivery," *IEEE Robot. Autom. Lett.*, vol. 5, no. 2, pp. 2698–2705, 2020.

[41] F. Sharifi and M. Sharifi, "Robust Control of Translational Cable-driven Robots," in *IEEE 4th International Conference on Knowledge-Based Engineering and Innovation, KBEI*, 2017, pp. 0667–0672.

[42] S. Cao, Z. Luo, and C. Quan, "Passive Velocity Field Control of a Redundant Cable-Driven Robot with Tension Limitations," in *IEEE International Conference Robotics Biomimetics, ROBIO*, 2016, pp. 131–136.

[43] L. Zhang, L. Li, Y. Zou, K. Wang, X. Jiang, and H. Ju, "Force Control Strategy and Bench Press Experimental Research of a Cable Driven Astronaut Rehabilitative Training Robot," *IEEE Access*, vol. 5, pp. 9981–9989, 2017.

[44] P. S. R. Kawamura s., Choe w., Tanaka S., "Development of an Ultrahigh Speed Robot FALCON using Wire Drive System," in *IEEE International Conference, Robotics Automation*, 1965, pp. 215–220.

[45] H. R. Fahham and M. Farid, "Optimum Design of Planar Redundant Cable-Suspended Robots For Minimum Time Trajectory Tracking," in *International Conference Control, Automation Systems*, 2010, pp. 2156–2163.

[46] A. Frank, "Optimization of Actuator Forces in Cable-Based Parallel Manipulators Using Convex Analysis," *Hist. Econ. Soc. Bull.*, vol. 6, no. 2, pp. 16–25, 1985.

[47] A. Nikoobin, M. R. Vezvari, and M. Ahmadieh, "Optimal Balancing of Planar Cable Robot in Point to Point Motion using the Indirect Approach," in *3rd RSI International Conference Robotics Mechatronics, ICROM*, 2015, pp. 499–504.

[48] D. Song, L. Zhang, and F. Xue, "Configuration Optimization and a Tension Distribution Algorithm for Cable-Driven Parallel Robots," *IEEE Access*, vol. 6, pp. 33928–33940, 2018.

[49] M. fmincon O. Toolbox, "MATLAB Documents," 2020. https://www.mathworks.com/help/optim/ (accessed Jun. 25, 2020).

[50] MATLAB, "fmincon Example," 2015. https://www.mathworks.com/help/optim/ug/fmincon.html (accessed Jul. 01, 2020).

[51] D. Lau, J. Eden, Y. Tan, and D. Oetomo, "CASPR: A Comprehensive Cable-Robot Analysis and Simulation Platform for the Research of Cable-Driven Parallel Robots," in *Intelligent Robots and Systems (IROS)*, 2016, pp. 3004–3011, [Online]. Available: http://ieeexplore.ieee.org/document/7759465.

[52] M. A. Khosravi and H. D. Taghirad, "On the Modelling and Control of Fully Constrained Cable Driven Robots with Flexible Cables," in *Proceedings - 2nd International Conference Control, Instrumentation Automation, ICCIA*, 2011, pp. 1030–1035.

[53] R. L. Williams and P. Gallina, "Planar Cable-Direct-Driven Robots, Part I: Kinematics and Statics," in *Proceedings of the ASME Design Engineering*

*Technical Conference*, 2001, vol. 2, no. 740, pp. 1233–1240.

[54] R. L. Williams and P. Gallina, "Journal of Intelligent and Robotic Systems," *J. Intell. Robot. Syst. Theory Appl.*, vol. 37, no. 1, pp. 69–96, 2003.

[55] H. Wang, T. Gao, J. Kinugawa, and K. Kosuge, "Finding Measurement Configurations for Accurate Robot Calibration: Validation with a Cable-Driven Robot," *IEEE Trans. Robot.*, vol. 33, no. 5, pp. 1156–1169, 2017.

[56] A. Pott and V. Schmidt, "On the Forward Kinematics of Cable-Driven Parallel Robots," in *International Conference Intelligent Robots Systems (IROS)*, 2015, pp. 3182–3187.

[57] R. Mersi and S. Vali, "Design and Control of a Suspended Cable-Driven Parallel Robot with Four Cables," in *International Conference on Robotics and Mechatronics (IcRoM)*, 2018, no. IcRoM, pp. 470–475.

[58] Y. Shen, H. Osumi, and T. Arai, "Set of Manipulating Forces in Wire Driven Systems," in *IEEE/RSJ/GI International Conference Intelligent Robots Systems*, 1994, vol. 3, pp. 1626–1631.

[59] C. C. R. Laboratory, "CASPR Tutorial 1: Installing CASPR on your computer," 2017. https://www.youtube.com/watch?v=b_24t_j1uQo (accessed Jul. 05, 2020).

[60] ROBOTIS, "DYNAMIXEL MX-64AT," 2020. http://www.robotis.us/dynamixel-mx-64at/ (accessed Jul. 21, 2020).

[61] H. Bayani, M. T. Masouleh, and A. Kalhor, "An Experimental Study on the Vision-Based Control and Identification of Planar Cable-Driven Parallel Robots," *Rob. Auton. Syst.*, vol. 75, pp. 187–202, 2016, [Online]. Available: http://dx.doi.org/10.1016/j.robot.2015.10.002.

[62] M. Kassem, "Experimental results," 2019. https://drive.google.com/drive/folders/1E8-WLINgPKDQKzeJOXclb0l61nu07XLd?usp=sharing (accessed Jul. 15, 2020).

[63] MATLAB, "Choosing the Algorithm," 2020. https://www.mathworks.com/help/optim/ug/choosing-the-algorithm.html (accessed Jul. 15, 2020).

# Vita

Mohamad Kassem was born in 1993, in Saida, Lebanon where he received his primary and secondary education. He received his B.Sc. degree in Mechanical Engineering from Near East University in Northern Cyprus in 2015 with the "First Honors" Academic Standing.

In February 2016, he joined the Mechatronics Engineering master's program in the American University of Sharjah as a full-time student and as a recipient of Al Ghurair Foundation for Education fully covered scholarship. During his master's study, he co-authored "Experimental verification of UAS based battery terminal voltage collapse detection on a simple embedded platform" paper which he presented at the 2018 11th International Symposium on Mechatronics and its Applications (ISMA).